A MODIFICATION OF THE $\bar{\phi}$,f-chart METHOD FOR SOLAR DOMESTIC WATER HEATING SYSTEMS WITH NO MIXING

by

MARC PAGNIER

A thesis in partial fulfillement of the
requirements for the degree of

MASTER OF SCIENCE

(Mechanical Engineering)

at the
UNIVERSITY OF WISCONSIN-MADISON
1986

Pour ceux qui m'aident et qui m'aiment mais que je ne vois pas

ACKNOWLEDGEMENTS

I would like to thank Professor Sandy Klein for his guidance through this thesis and for putting up with my convoluted "french writing style". I know I could not have had a better advisor. I would also like to thank Professor Jack Duffie for his many suggestions. He succeeds in making the solar lab a very enjoyable place to work.
There are many people I would also like to thank for the good times I had here, basically the solar lab staff and some members of the Cross-Cultures organization... Lots of them would deserve to be french.
The financial help provided by CERTED-TOTAL under the directorship of Mr. Manse is sincerely acknowledged.
Last but not least, acknowledgements are not sufficient to express my gratitude for the love I received from my family, particularly my mother and Cathy.

All the grammar and spelling mistakes in this thesis have been purposely introduced to entertain the reader and do not therefore reflect the author's actual knowledge of English.

ABSTRACT

The importance of stratification to the performance of Solar Domestic Hot Water (SDHW) systems has been emphasized in the last several years. For a long time, the use of high collector flow rates (about 70 kg/hr-m^2) was thought to be the part of the optimum strategy for SDHW systems. Recent studies based on experiments and simulations have shown, however, that the performance of these systems may be improved significantly by reducing the collector flow rate to about 10 kg/hr-m^2. High flow rates permit higher collection efficiencies but prevent stratification in the storage tank. In addition to the gains in thermal performance due to improved stratification, a low flow strategy has other advantages such as a reduction in piping materials and parasitic power requirements. The preceding factors explain the increasing interest in designing SDHW systems to operate at low collector flow rates.

Stratification can also be induced in the storage tank by the use of properly designed diffusers. The diffuser for the tank inlet flow is an important component since well designed diffusers prevent the momentum of the incoming fluid from destroying the stratification.

In anticipation of the development of better stratified systems, a design method is needed to evaluate SDHW systems for different designs. Present methods (like the f-chart and the $\bar{\phi}$,f-chart methods) were developed with the assumption of no stratification (fully-mixed tank), which is reasonable but conservative when high flow rates are used in common systems. Comparisons with experimental results show that these design methods may significantly underestimate the solar fraction when low collector flow rates are used.

Mixing in the storage tank is the main cause of the gains resulting from a decrease in the collector flow rate. A design method, based on the utilizability concept, has been developed to estimate the performance of SDHW Systems when there is no mixing in the tank. For this case, comparisons of the yearly solar fraction predicted by TRNSYS and by this new version of the $\bar{\phi}$,f-chart method result in a rms error of 1.5 % . The method provides an upper bound for the performance of the systems studied and the original $\bar{\phi}$,f-chart method developed by Braun provides a lower bound. The actual performance of the system could be determined from the ASHRAE-95 standard test results.

TABLE OF CONTENTS

LIST OF TABLES

LIST OF FIGURES

NOMENCLATURE

Symbols used in this thesis which do not appear below are defined locally in the text.

A	surface area
A_0	amplitude of the diurnal variation (peak to peak)
b_0	incidence angle modifier coefficient
CDD_b	cooling degree-days in a month for the base temperature
C_L	ratio of the daily load volume to the tank volume
C_p	specific heat of water
C_s	storage capacity per unit collector area of storage
C_s^*	C_s divided by 350 kJ/m^2-°C
F_R	collector heat removal factor
$F_R(\tau\alpha)_n$	intercept of the collector efficiency vs. $(T_{in,c} - T_{amb})/G_T$ curve at m_c|test, at normal incidence of solar beam radiation
$F_R U_L$	negative of the slope of the collector effciency vs. $(T_{in,c} - T_{amb})/G_T$ curve, at m_c|test
f	solar fraction
g	gravitational constant
h^*	dimensionless number for the cooling degree-days correlation
G	instantaneous incident radiation on the collector surface per unit area
hr	hour
H_T	total incident radiation on the collector surface per unit area
$I_{T,c}$	critical radiation level
k	clearness index
K_T	ratio of the solar radiation on a horizontal surface to the extraterrestrial radiation on a horizontal surface
$K_{\tau\alpha}$	incidence angle modifier
L	depth of fluid
lit	liter
m	meter

M	total daily mass
M_t	mass of fluid in the tank
N	number of nodes in the tank
N_m	number of days in the month
N_{on}	number of hours in the month the collector is operating
N^0	number of hours in the month when $T_{amb} > T_{mains} + \Delta T_{off}$
q_u	rate of useful energy gains
Q	monthly energy quantity
Q_{boil}	energy of the water when the temperature is above 100°C
Q_{max}	maximum useful energy gains (defined by Braun)
$Q_{max}(tot)$	maximum useful energy gains (defined in Chapter III)
$Q_{max}(rad)$	maximum useful energy gains from solar radiation (including losses)
$Q_{max}(therm)$	maximum thermal gains to the collector
Q_u	monthly useful energy gains
R	ratio of the total radiation on a tilted surface to that on a horizontal surface
t	time
t^*	dimensionless time for the ambient temperature correlation
T	temperature
$T_{a,h}$	hourly ambient temperature
T_{amb}^*	dimensionless parameter in the useful energy correlation
T_b	base temperature
T'_{min}	lower limit on the monthly-average collector inlet temperature
T_{tank}^*	dimensionless tank temperature
U	fluid inlet velocity
U_t	tank loss coefficient
UA_t	overall loss coefficient
V	volume
X	parameter for the f-chart and $\bar{\phi}$,f-chart correlations
X_c	monthly-average critical radiation level
X_m	parameter of the correlation for the utilizability (Clark)
Y	parameter for the f-chart correlation
Z	parameter for the $\bar{\phi}$,f-chart correlation

ΔT_t	top-to-bottom temperature difference
Δt	number of hours in a month
ΔT_{off}	controller lower deadband (to turn the pump off)
ΔT_{on}	controller upper deadband (to turn the pump on)
β	fluid volumetric thermal expansion coefficient
β	collector slope
δ	declination
ϕ	utilizability
θ	incidence angle
σ_m	standard deviation of the monthly-average temperature
σ_{yr}	standard deviation of the monthly-average temperature from the annual average temperature
τ	simulation timestep
τ_c	critical simulation timestep
$(\tau\alpha)$	transmittance-absorptance product

Superscript

–	monthly-average daily
~	monthly-average hourly
#	under test conditions
•	rate

Subscript

amb	ambient
aux	auxiliary
B	beam radiation
c	collector
corr	correction term
D	diffuse radiation
env	storage tank environment
FM	fully-mixed tank
G	ground radiation
HF	high collector flow rate

in	inlet
L,load	load
LF	low collector flow rate
los	tank losses
max	maximum
mains	mains supply water
min	minimum
NM	no mixing in the tank
off	when the pump does not operate
on	when the pump is operating
out	outlet
rad	radiation
set	auxiliary storage tank thermostat set point
stor	stored energy
t	tank
T	incident on collector surface
therm	thermal gains
ltest	test conditions
luse	actual conditions

CHAPTER I: INTRODUCTION

I.1 Introduction

The importance of stratification on the performance of Solar Domestic Hot Water (SDHW) systems has been emphasized in the last several years.

For a long time, the use of high collector flow rates (about 70 kg/hr-m^2) was thought to be the part of the optimum strategy for SDHW systems. Recent studies mainly based on experiments [1-3] and simulations [1,4] have shown, however, that the performance of these systems may be improved significantly by reducing the collector flow rate to about 10 kg/hr-m^2. High flow rates enable higher collection efficiencies but destroy the stratification in the storage tank. In addition to the gains in thermal performance due to improved stratification, a low flow strategy has other advantages such as a reduction in piping materials and parasitic power requirements. The preceding factors explain the increasing interest in designing SDHW systems to operate at low collector flow rates

Improved stratification can also result if proper diffusers are used in the storage tank. The diffuser for the tank inlet flow is an important component since well designed diffusers prevent the momentum of the incoming fluid from destroying the stratification [3].

In addition to evaluating the performance of a solar system, a prediction method can be used for designing a system to meet a designated part of the load with solar energy. Therefore, a performance prediction method is also commonly referred as a design method.

In anticipation of the development of better stratified systems, a design method is needed to evaluate SDHW systems for different designs. Present methods (like the f-chart and the $\bar{\phi}$,f-chart methods) were developed with the assumption of no stratification (fully-mixed tank), which is reasonable but conservative when high flow rates are used in common systems.

This chapter discusses factors affecting stratification. Reviews of of both f-chart and $\bar{\phi}$,f-chart methods are presented and the limitations of these methods will be treated. Chapter II deals with the present difficulties in accounting for the phenomenon of internal mixing in TRNSYS and introduces the proposed method to correct the $\bar{\phi}$,f-chart method. Chapter III details this method and presents some comparisons

between the new version of the $\bar{\phi}$,f-chart and simulation results. The limitations of the new version of the $\bar{\phi}$,f-chart design method are studied in Chapter IV.

I.2 Effects of Stratification

I.2.1 Physical Aspect of Stratification

Thermal stratification is characterized by the existence of a top-to-bottom temperature difference in a reservoir. It is a physical phenomenon by which cold fluid stays at the bottom of a tank and hot fluid stays at the top. Buoyancy forces are responsible for the circulation of the fluid since the driving force for the stratification is the density difference between hot and cold fluid.

The following temperature profile may be present in the tank when there is some stratification:

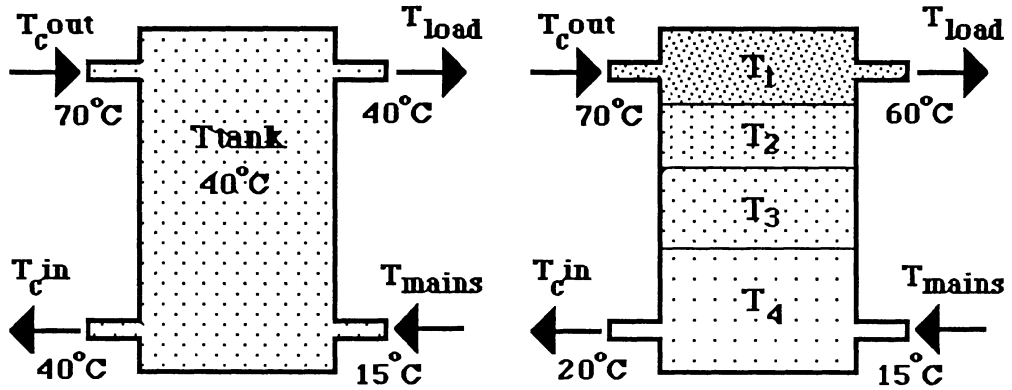

Figure 1.1: Example of a set of temperatures encountered for a fully-mixed tank and a stratified tank

$T_{c,out}$ = collector outlet temperature
T_{load} = temperature of the water delivered to the load
$T_{c,in}$ = collector inlet temperature
T_{mains} = water makeup temperature

Two phenomena affect stratification: mixing and recirculation through the collector.

I.2.1.1 Mixing

Hot fluid coming from the collector outlet and cold water provided by the mains (load side) enter the tank with a momentum that can overcome the buoyancy forces and destroy the stratification. The higher the flow rate, the larger the inlet momentum and the larger is the tendency of the fluid to mix. This phenomenon is called internal mixing and is treated in Section II.1. Internal mixing is dependent upon system characteristics like inlet diffusers and tank geometry.

The Richardson number, as defined by equation (1.1) is the ratio of the buoyancy force to the inlet momentum.

$$R_i = g\ \beta\ L\ \Delta T_t\ /\ U^2 \qquad (1.1)$$

where:

- g = gravitational constant [m/s^2]
- β = fluid volumetric thermal expansion coefficient [K^{-1}]
- ΔT_t = top-to-bottom temperature difference [K]
- U = inlet velocity [m/s]
- L = depth of the fluid [m]

Experiments [2,5] have shown that this number plays an important role in the formation and growth of the thermocline. There is a theoretical value for a critical Richardson number of 0.25 below which rapid mixing occurs which causes the destruction of the stratification. Experiments give a similar value since the critical R_i is found to be about between 0.3 and 0.5. With a conventional collection strategy (high flow and no diffuser), the Richardson number falls below its critical value, mixing occurs to some extent in the tank and the system fails to fully stratify. To prevent this, the flow rate has to be lowered or stratification-enhancing devices have to be used (axial flow diffuser).

I.2.1.2 Recirculation

This phenomena is caused by the fact that water that has already been warmed up by the collector may be recirculated through the collector. The higher the flow rate, the larger the recirculation. This causes a lower top-to-bottom temperature difference since the whole tank may be recirculated a few times during the day. Recirculation is mainly

dependent upon the collector flow rate, the load draw and the storage size. The influence of recirculation is treated in Chapter IV.

I.2.2 Effects of Stratification on the Collector

I.2.2.1 Modeling the Collector Performance

The collector performance is characterized by the Hottel-Whillier [6] equation (1.2).

$$q_u = A_c [F_R(\tau\alpha)_n K_{\tau\alpha} G_T - F_R U_L (T_{in,c} - T_{amb})]^+ \quad (1.2)$$

q_u = instantaneous useful energy gain

A_c = collector area

$F_R(\tau\alpha)_n$ = intercept of the collector efficiency vs. $(T_{in,c} - T_a)/G_T$ curve at $\dot{m}_c$/test, at normal incidence of solar beam radiation

$K_{\tau\alpha}$ = incidence angle modifier

G_T = instantaneous incident radiation on the collector surface per unit area

$F_R U_L$ = negative of the slope of the collector efficiency vs. $(T_{in,c} - T_a)/G_T$ curve, at $\dot{m}_c$/test

$T_{in,c}$ = collector inlet temperature

T_{amb} = ambient temperature

The parameters $F_R U_L$ and $F_R(\tau\alpha)_n$ are characteristic of the collector and determined from the ASHRAE 93-77 test procedure.

The incidence angle modifier [6] is a function of the solar incidence angle and can be approximated by:

$$K_{\tau\alpha} = 1 - b_0 [1/\cos\theta - 1] \quad (1.3)$$

where:

b_0 = incidence angle modifier coefficient from ASHRAE 93-77 test (b_0 is positive for a flat-plate collector)

θ = incidence angle, angle between beam radiation on a surface and the normal to that surface

For angles between 60° and 90°, equation (1.3) is no longer valid and a linear decrease to zero is often recommended (equation 1.4). This approach is used in

TRNSYS.

$$K_{\tau\alpha} = (1 - b_0)\ (90 - \theta) / 30 \quad \text{for} \quad \theta > 60° \tag{1.4}$$

One way to evaluate $K_{\tau\alpha}$ is to treat beam, diffuse, and ground-reflected radiation independently and to use (1.5) such as TRNSYS does:

$$K_{\tau\alpha} = (K_{\tau\alpha,B} G_{BT} + K_{\tau\alpha,D} G_D + K_{\tau\alpha,G} G_G) / G_T \tag{1.5}$$

where:

$K_{\tau\alpha,B}$ = incidence angle modifier for beam radiation
G_{BT} = beam component of G_T
$K_{\tau\alpha,D}$ = incidence angle modifier for diffuse radiation
G_D = diffuse component of G_T
$K_{\tau\alpha,G}$ = incidence angle modifier for ground-reflected radiation
G_G = ground-reflected component of G_T

The estimate of the monthly useful gains (Q_u) can generally be done with equation (1.6).

$$Q_u = A_c\ F_R(\overline{\tau\alpha})\ N_m\ \overline{H}_T\ \bar{\phi} \tag{1.6}$$

where:

$\bar{\phi}$ = monthly-average daily utilizability
N_m = number of days in the month
$\overline{H}_T$ = monthly-average daily radiation on a tilted surface per unit area

The presence of a bar above a symbol indicates a monthly-average value.

$\bar{\phi}$ is a solar radiation statistic [7-9] that may be calculated from the knowledge of the critical radiation level of the system and with the use of an algorithm presented by Clark et al. [8]. The critical radiation level ($I_{T,c}$) is the radiation level below which no useful energy is delivered by the collector because of the collector thermal losses.

I.2.2.2 Influence of Stratification

The presence of some stratification in the tank results in a lower collector inlet temperature (compared to a fully-mixed tank), which causes lower collector losses.

The collector efficiency is thus improved when internal mixing is decreased (e.g., use of a proper diffuser). The sensitivity of a system to the stratification is directly related to the collector losses. A "thermally perfect" collector with a loss coefficient of zero would not be affected by a change in the collector inlet temperature.

Enhancing stratification by lowering the flow rate produces two opposite effects in addition to reduced internal mixing. It first decreases the collector heat removal factor F_R (Figure 1.2) which lowers the collector efficiency thus decreasing the collected energy. On the other hand it decreases recirculation, thus decreasing $T_{in,c}$ and lowering the collector losses. The two phenomena above are working in opposite directions. Although the influence of each effect on the performance of the system can not be individually determined, the resultant of the combined effects can be obtained independently from the phenomenon of mixing by simulations (Chapter IV).

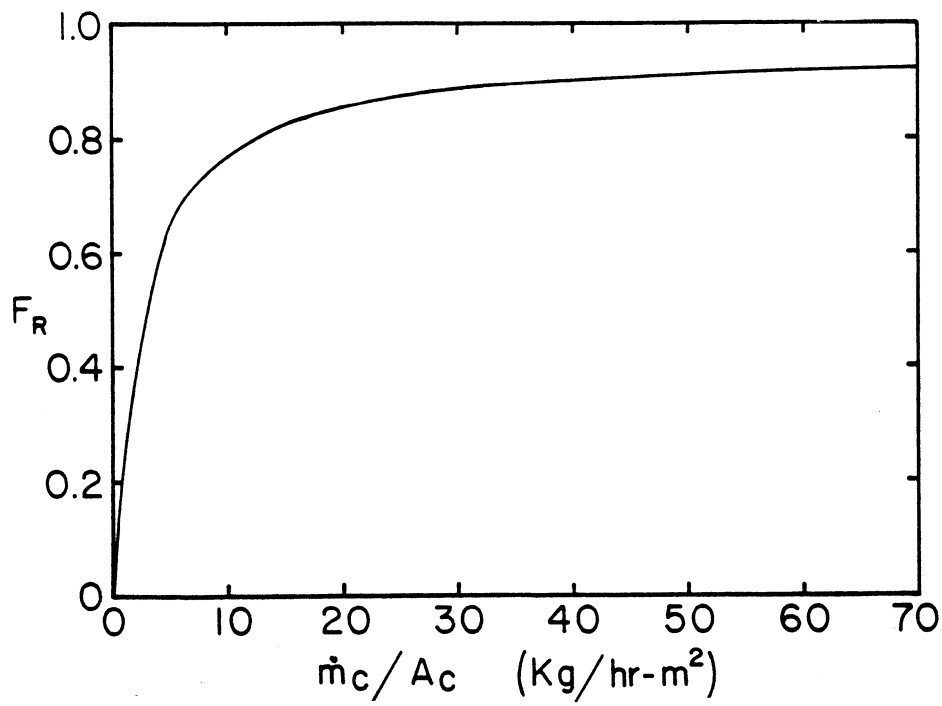

Figure 1.2: Dependence of Collector Heat Removal Factor on Collector Fluid Flow Rate per Unit Area for a Typical Flat Plate Collector

Lunde [10] states that the collected energy for a fully-mixed tank and for a stratified system are the same. A major limitation to his study, however, is that this

result applies only if both systems are evaluated for the same external conditions, for the same system characteristics (such as the tank volume) and after one turnover time (time after which the entire amount of water in the tank has been circulated once through the collector). The problem is that the high flow rate system has a much larger number of turnovers during a day, which prevents this kind of comparison. Another limitation of his study is that load draws are ignored in the evaluation of the performance of the system.

I.2.3 Effects of Stratification on Tank Losses

The demand for hot water is actually a demand of energy. A given amount of water at a fixed temperature (called the set temperature) is needed. Consider an example to understand the combined effect of load characteristics and stratification on the performance of the system.

A fully-mixed tank and a stratified tank (Figure 1.1) are compared for the same external conditions. It is presumed that the same amount of energy has been stored in both tanks. The temperature of the water delivered to the load is, however, higher when there is stratification. A mixing valve is used if the water delivered at the tank outlet is above the set temperature. Several cases may occur:

- If the temperature of the water delivered to the load is higher than the set temperature, no auxiliary is needed for either the stratified or the fully-mixed tank. But for a fully-mixed tank, more hot water at a lower temperature is needed and less water from the mains needs to be added to decrease the temperature to the set temperature (T_{set}).
- The difference is more sensitive if the stratified system delivers the water at a temperature above T_{set} while the fully-mixed tank delivers the water at a temperature below T_{set}. In one case, some auxiliary is needed to make up the temperature difference to Tset while in the other no energy has to be provided by the auxiliary.
- If both systems deliver water at a temperature below Tset, the amount of solar energy delivered by the stratified system is higher for the same volume of water drawn. More auxiliary is thus needed for the fully-mixed system.

In the last two cases, it has been shown that stratification results in a decrease in the amount of auxiliary needed on an instantaneous basis. The stronger the gradient separating cold and hot water, the better the performance.

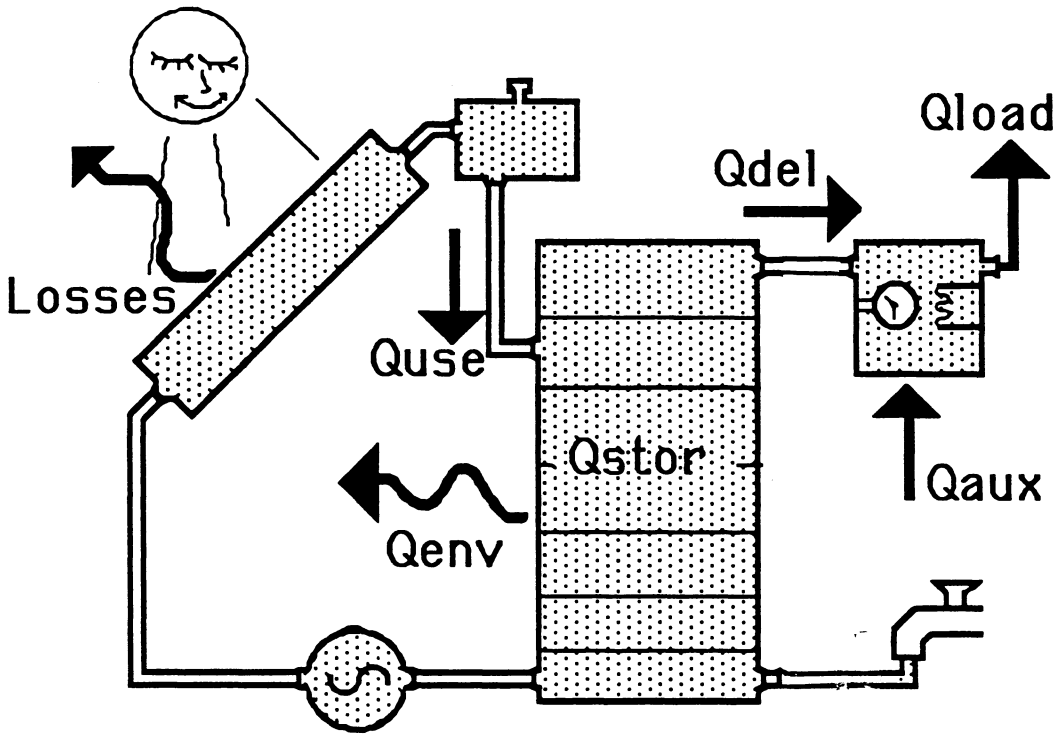

Figure 1.3 Fluxes of Energy in an Open-Loop System

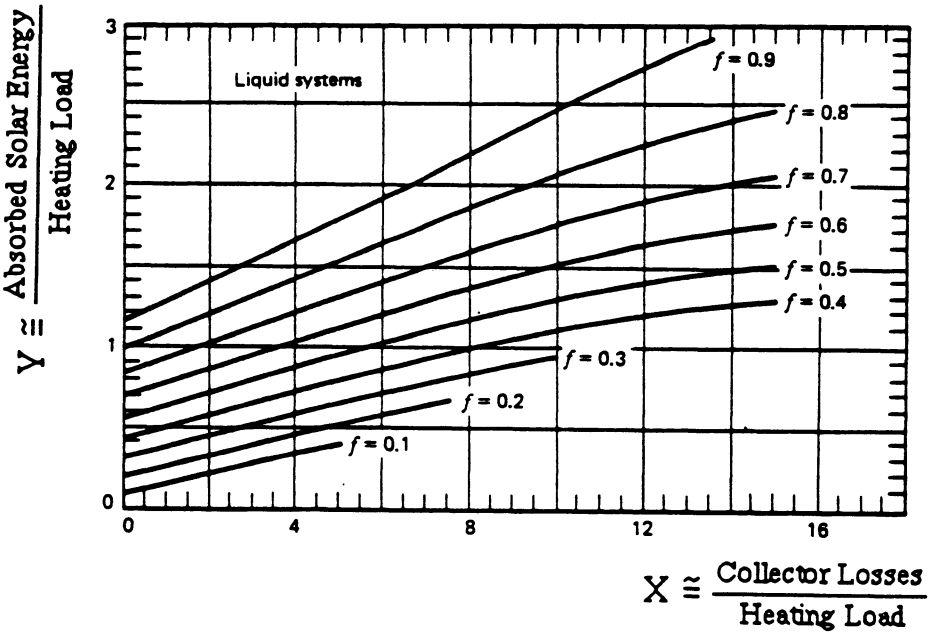

Figure 1.4 The f-chart for systems using liquid heat transfer and storage media. From Beckman *et al* [11]

There would be, however, no difference between both types of systems if there were no losses in the system. The energy that is not collected at a first draw would circulate through the collector and eventually be stored in the tank until a later use. On a long term basis (month and perhaps even day), the performance of both systems would be the same. Figure (1.3) shows the fluxes of energy. The losses being the causes of the difference between a stratified and a non-stratified system, the two driving forces of the difference are the tank loss coefficient (UA_t) and the collector loss coefficient ($F_R U_L$).

I.2.4 Increase in Performance with the Stratification

Relatively recent experiments [1-3] have shown an improvement by up to 20 percent for the performance of a system if low flow rates are used. The evaluation of the performance of a solar system is important for the economics of a potential buyer. Low flow rate strategies have proved to be interesting and are likely to expand whenever the SDHW sales expand. No existing design method however accounts for stratification. Commonly employed methods such as the f-chart and $\bar{\phi}$,f-chart methods can underestimate the performance by as much as 20 percent for low flow rates. The goal of this thesis is thus to develop a design method that takes into account stratification.

I.3 Design methods

Duffie and Beckman [6] categorized the design methods according to the assumptions upon which they are based and the ways in which the calculations are done. All these methods give estimates of the long-term (monthly and yearly) useful outputs of solar processes, but do not provide detailed information on process dynamics.

The first category applies to systems in which collector operating temperature is calculated. The critical radiation level (i.e., radiation levels above which useful energy can be collected). This category includes the $\bar{\phi}$,f-chart method which is described in detail in Section I.3.2.

The design methods in the second category are based on direct correlations of the results of a large number of detailed simulations. The f-chart method is the best known example of this type of methods and is described in Section I.3.1.

The third category is based on short-cut simulations. Long term estimates are

deduced from simulation results using representative days of meteorological data.

I.3.1 The f-chart method

The purpose of the f-chart method [6,11] is to provide an estimate for the fraction of total heating load that will be supplied by solar energy for a given solar heating system. The monthly-average solar fraction is called f and is defined by:

$$f = 1 - Q_{aux} / Q_{load} \tag{1.7}$$

where:

Q_{aux} = auxiliary energy provided by the system (monthly-average value)

Q_{load} = total heating load (monthly-average value)

The method is a correlation of the results of many hundreds of thermal performance simulations of solar heating systems. The conditions of the simulations were varied over ranges of parameters of practical systems designs [6]. The resulting correlations give f, the fraction of the monthly heating load (space and/or hot water) supplied by solar energy as a function of two dimensionless parameters X and Y defined by equations (1.8) and (1.9). Since this paper only deals with Solar Domestic Hot Water systems (SDHW), the description of the f-chart method is for this case.

$$X = \frac{A_c \; F_R U_L \; (11.6+1.8 \; T_{set}+3.86 \; T_{mains}- 2.32 \; \overline{T}_{amb}) \; \Delta t}{Q_{load}}$$

$$\cong \frac{\text{Collector Losses}}{\text{Heating Loads}} \tag{1.8}$$

$$Y = \frac{A_c \; F_R(\overline{\tau\alpha}) \; H_T \; N_m}{Q_{load}} \cong \frac{\text{Absorbed Radiation}}{\text{Heating Loads}} \tag{1.9}$$

where:

F_R = collector-heat exchanger efficiency factor

U_L = collector overall loss coefficient [W/m^2-°C]

Δt = total number of seconds in the month

N_m = number of days in the month

$(\overline{\tau\alpha})$ = monthly-average transmittance-absorptance product

$\overline{T}_{amb}$ = monthly-average ambient temperature (°C)

T_{mains} = mains water supply temperature (°C)

T_{set} = minimum acceptable hot water temperature (°C)

The calculation of monthly water heating load is the following:

$$Q_{load} = M_{load}\ N_m\ C_p\ (T_{set} - T_{mains}) \qquad (1.10)$$

where:

C_p = specific heat of water

M_{load} = daily hot water requirements

To account for heat losses from the auxiliary hot water tank, an additional term has to be used for the calculation of the load: $Q_{losses} = (UA)_t\ (T_{set} - T_{env})$, since the auxiliary tank is always assumed to be at the temperature T_{set}.

The determination of the solar fraction f supplied by the system is made using Figure 1.4 or a curve fit to the information in this figure.

There are certain limitations on the f-chart method:

- the f-chart method was developed for a storage capacity of 75 liters of water per square meter of collector area and no modification is possible to account for other storage tank sizes.

- the f-chart method is based on the assumption of a well insulated solar preheat tank (0.42 $W/m^2°C$). This loss coefficient is below the values generally used in the design of storage tanks as it is shown in Section II.2.The f-chart method would thus tend to overestimate the performance of a solar system.

- the simulations on which f-chart is based do not account for stratification. Even for high flow rates, there is actually some stratification which gives better performance than if the tank were truly fully mixed.

Both effects seem to have about the same influence on the performance of systems with high flow rates and tend to negate each other. The f-chart method gives good results in the estimate of the solar fraction in conventional systems [12]. For low flow rates however, the effect of stratification overwhelms the error made on tank losses

and the f-chart method causes the solar fraction to be underpredicted by up to 20% (Chapter IV).

I.3.2 The $\bar{\phi}$,f-chart method

The f-chart method is not applicable to many process water heating systems where makeup water enters the system above 20°C and/or the desired set temperature lies above 70°C. To overcome these limitations, a more "general and fundamental" design procedure called the $\bar{\phi}$,f-chart method method [13,14] has been developed. The $\bar{\phi}$,f-charts are similar to the f-charts with the exception that the effect of the collector inlet temperature is considered through the use of utilizability (or $\bar{\phi}$) concept [7-9]. The $\bar{\phi}$,f-chart design method, which in its original form was limited to closed-loop systems (description in Figure 1.5) has been extended to open-loop water heating systems by Braun et al. [15]. The main difference of the open-loop systems (description in Figure 1.6) with respect to closed-loop systems is the fact that high temperatures for the delivered water are required and relatively low temperatures of makeup water are received. Braun developed the correlations used in this method with the data from hundreds of TRNSYS simulations assuming that the storage tank is always fully-mixed. The following description of the $\bar{\phi}$,f-chart method is limited for open-loop systems. The different steps of this iterative method are:

- step 1: Initial guess of the solar fraction
- step 2: Q_{max} ,the maximum energy that could be collected by the solar system is calculated from equation (1.11).

$$Q_{max} = A_c \; F_R(\overline{\tau\alpha}) \; N_m \; \overline{H}_T \; \bar{\phi}_{max} \qquad (1.11)$$

where:

A_c = collector area

$(\overline{\tau\alpha})$ = monthly-average transmittance absorptance product

N_m = number of days in the month

$\overline{H}_T$ = monthly-average daily radiation on the collector per unit area

$\bar{\phi}_{max}$ corresponds to the monthly-average utilizability of the system if the collector always runs at a constant collector inlet temperature equal to T'_{min}. T'_{min} is defined for a fully-mixed tank as the lower limit on the monthly-average collector inlet temperature for a particular solar fraction f (equation 1.12). T'_{min} would be the

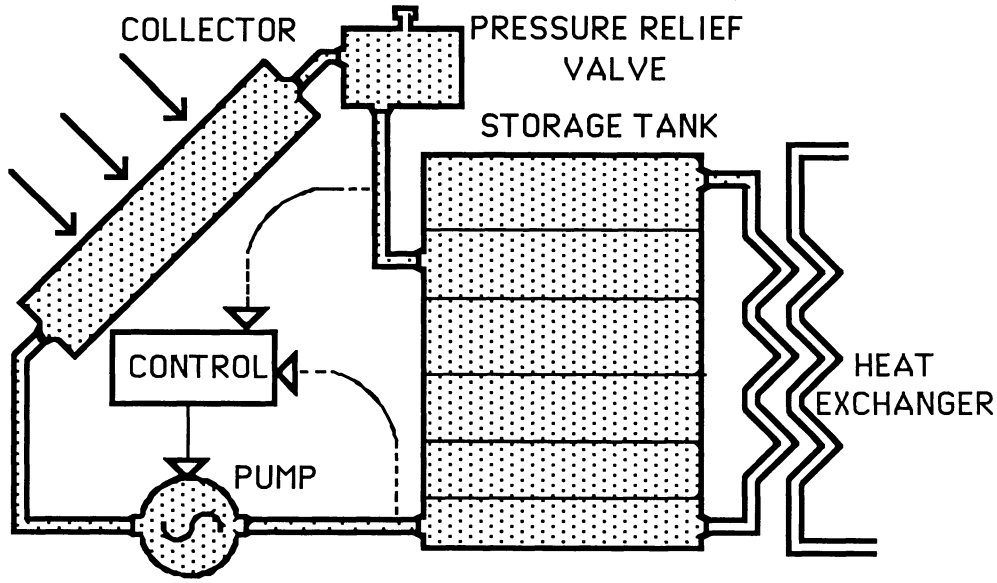

Figure 1.5 Closed-Loop System Schematic

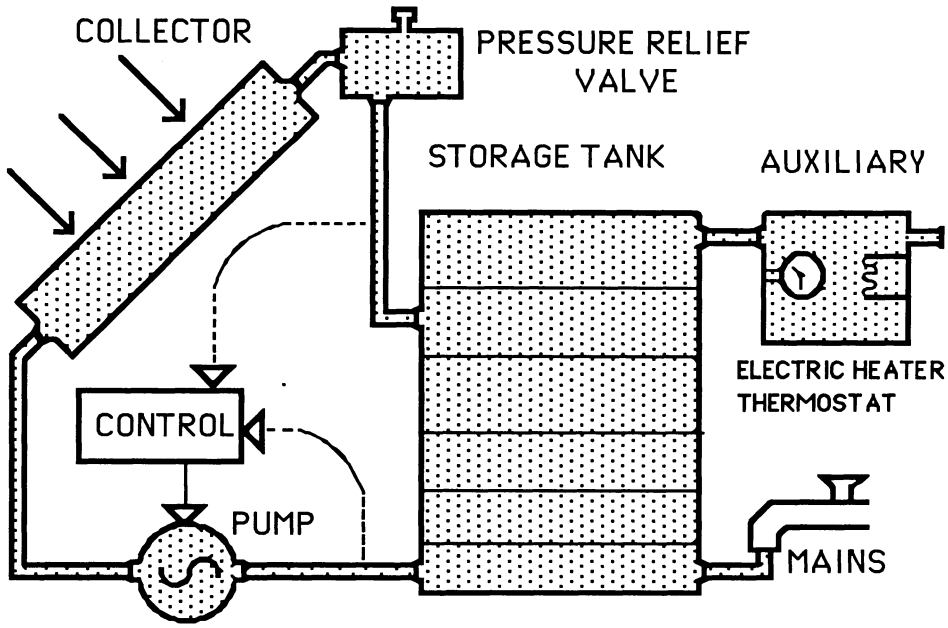

Figure 1.6 Open-Loop System Schematic

temperature of the tank if the solar energy collection and load were both distributed evenly throughout each hour of every day of the month.

$$T'_{min} = T_{mains} + f\ (T_{set} - T_{mains}) \qquad (1.12)$$

The minimum value of the monthly critical radiation level of the system corresponds to T'_{min}, the lowest possible collector inlet temperature.

$$I_{T,c\ min} = F_R U_L / F_R(\overline{\tau\alpha})\ (T'_{min} - \overline{T}_{amb}) \qquad (1.13)$$

$\bar{\phi}_{max}$ is then calculated with the utilizability method from the minimum critical level $I_{T,c\ min}$. An algorithm $\bar{\phi} = \bar{\phi}(I_{T,c})$ is needed for this calculation and the present $\bar{\phi}$,f-chart method uses the one developed by Clark et al. [8]. This algorithm evaluates the monthly average hourly radiation utilizabilities to determine $\bar{\phi}_{max}$ and is described in Section III.4.

Since neither the load nor the energy collection are evenly distributed during the month, the monthly average collector inlet temperature is higher than T'_{min} and subsequently $\bar{\phi}$ is lower than $\bar{\phi}_{max}$. A correction has thus to be made on Q_{max} to determine Q_u.

- step 3: The useful gains from the collector are calculated as following:

$$Q_u = Q_{max} - a\ (\exp(bf) - 1)\ (1 - \exp(cX))\ \exp(dZ)\ Q_{load} \qquad (1.14)$$

where:

$a = 0.015\ (C_s/(350\ kJ/m^2{}^\circ C))^{-0.76} = 0.015\ (C_s{}^*)^{-0.76}$

$b = 3.85$

$c = -0.15$

$d = -1.959$

and

$$X = A_c\ F_R U_L\ (100^\circ C)\ \Delta t\ /\ Q_{load} \qquad (1.15)$$

$$Z = Q_{load}\ /\ M_{load}\ N_m\ C_p\ (100^\circ C) \qquad (1.16)$$

C_s = storage capacity per unit collector area of storage

Δt = number of hours in the month

- step 4: the estimation of the tank losses is made using the equation (1.17).

$$Q_{los} = (UA)_t \ (T_t - T_{env}) \qquad (1.17)$$

where:

Q_{los} = losses (or gains) to the environment of the tank (at the temperature T_{env})
$(UA)_t$ = overall tank loss coefficient
T_t = monthly-average average tank temperature

The monthly-average tank temperature originally was estimated as the average of $T_{in,c}$ (collector inlet temperature) and T'_{min}. The error could be significant for poorly insulated tanks or for systems dealing with high temperatures. A correlation (1.18) has been found by Braun et al. [15] to improve the estimate of the losses.

$$T_t = T'_{min} + g \ (\exp (kf) - 1) \exp (hZ) \qquad (1.18)$$

where:

$g = (0.2136°C) \ (C_s/(350 \ kJ/m^{2}°C))^{-0.704} = 0.015 \ (C_s^{*})^{-0.704}$
$h = - 4.002$
$k = 4.702$

- step 5: a new solar fraction is determined from energy balance (1.19)

$$Q_u + Q_{aux} = Q_{los} + Q_{load} \qquad (1.19)$$

$f = 1 - Q_{aux} / Q_{load} = (Q_u - Q_{los}) / Q_{load}$ where all the energies are calculated in the preceding steps. The new solar fraction is used as an initial guess in step one until the convergence.

Unlike the f-chart method, the $\bar{\phi}$,f-chart method described above accounts for any storage loss coefficient and does no longer underestimate the storage losses. Since it still does not account for stratification, the results are underestimated and do not agree with experiments even for high flow rates. Comparisons of the solar fraction between experimental results and estimates by design methods are made in Chapter IV. The use

of the $\bar{\phi}$,f-chart design method described in this section results in underestimates of the solar fraction by up to 10 % for a system with a conventional flow rate of 72 kg/hr-m^2 and by up to 25 % for a system with a flow rate of about 10 kg/hr-m^2.

I.3.3 Improvement of the Design Methods

It has been shown that both existing design methods will underestimate the performance of a stratified system. A scheme has thus to be found to extend the results of the existing methods to systems with various amounts of mixing and recirculation. Whatever the solution, it has to be found from simulations. The reliability of the proposed correction depends obviously on the accuracy of the simulation program. Chapter I.4 deals thus with TRNSYS [16], the program available for this research.

I.4 Stratification in TRNSYS

TRNSYS is a transient systems simulation program with a modular structure. Two different tank models give the user the option of introducing some stratification in a system: the multi-node tank model (TYPE 4) and the plug-flow model (TYPE 38).

I.4.1 Multi-Node Storage Tank Model

This model represents thermal stratification by dividing the tank into a user specified number of fully-mixed segments or nodes whose sizes may be specified. Mass and energy balances are performed individually on each node. The resulting system of dependent differential equations is then solved.

A one-node tank simulates the behavior of a tank with a maximum amount of mixing since the hot water from the collector outlet is mixed with the rest of the tank at each timestep. No stratification is allowed in this case. The larger the number of nodes however, the smaller the mixing. Theoretically, an infinite number of nodes means no mixing but Wuestling [4] and Hirsch [17] have shown that increasing the number of nodes beyond ten does not significantly affect the results. This result may depend on the system since Veltkamp [18] found that 64 nodes were required to accurately represent thermal stratification in the system he studied.

To accurately model the performance of a stratified system [17], the timestep of the simulation (τ) has to conform to the inequality (1.20).

$$\tau < V_t \ (N \ \dot{V}_c)^{-1} \qquad (1.20)$$

where:

V_t = storage tank volume [m^3]

N = number of nodes in the tank

$\dot{V}_c$ = (collector) volume flow rate [m^3/hr]

For a low flow rate, a highly stratified system is thus expensive to simulate since the timestep of the simulation can be very small (on the order of one minute). This model may be useful for a comparison of different flow rates for the same number of nodes but the computer time required is the main reason why this model was not used in this research.

I.4.2 Plug-Flow Storage Tank Model

This model uses a variable number of variable segments of fluid to model stratification [4,16]. At each timestep, a given amount of fluid, which is at a uniform temperature equal to the collector outlet temperature, is inserted into the tank at the appropriate location (step 1 in figure 1.7). Its volume is determined by the product of the collector flow rate times the timestep. All segments below are thus shifted downwards. Another segment representing the load is then inserted (at the mains water temperature in the case of an open-loop system) at the appropriate location in the tank temperature profile (step 2 in figure 1.7). The segments and/or fractions of segments whose position falls outside the bounds of the tank are returned to the collector and/or load.

Two modes are available to determine the appropriate location at which the segment must be inserted. In mode 1, the tank has a fixed inlet position and any temperature inversions are eliminated by mixing with appropriate adjacent nodes. In mode 2, segments are inserted in the tank profile so that no temperature inversion is created. This mode is necessary if no mixing is assumed. Choosing the second mode is however not sufficient to obtain maximum stratification (largest top-to-bottom temperature difference).

As the timestep increases, the segments that are inserted in the tank increase in volume. Since the temperature of each one of those segments is uniform, choosing a small timestep causes a large number of small segments with different temperatures to be created instead of a large one. Therefore, increasing the timestep implicitly

introduces some mixing of the nodes in the tank model, which is analogous to what happens with actual mixing in the storage tank of the system. This phenomenon is thus called mathematical mixing. The minimum amount of mathematical mixing is obtained with a timestep as small as possible. Other restrictions for stratification in the present model are the limit on the number of nodes in the tank (50) and the fact that adjacent nodes with a temperature difference less than 0.5 °C are mixed together (to reduce the computational effort due to the handling of a large number of nodes). The influence of these constraints on the degree of mathematical mixing in the tank is studied in Chapter IV.

There is a similarity between this tank model and the multi-node model. The variable that determines the amount of mixing in the tank is either the timestep (Type 38) or the number of nodes (Type 4). Neither of those models however accounts explicitly for actual internal mixing.

Chapter II presents the physical aspect of internal mixing and shows the influence of mathematical mixing on the simulation results.

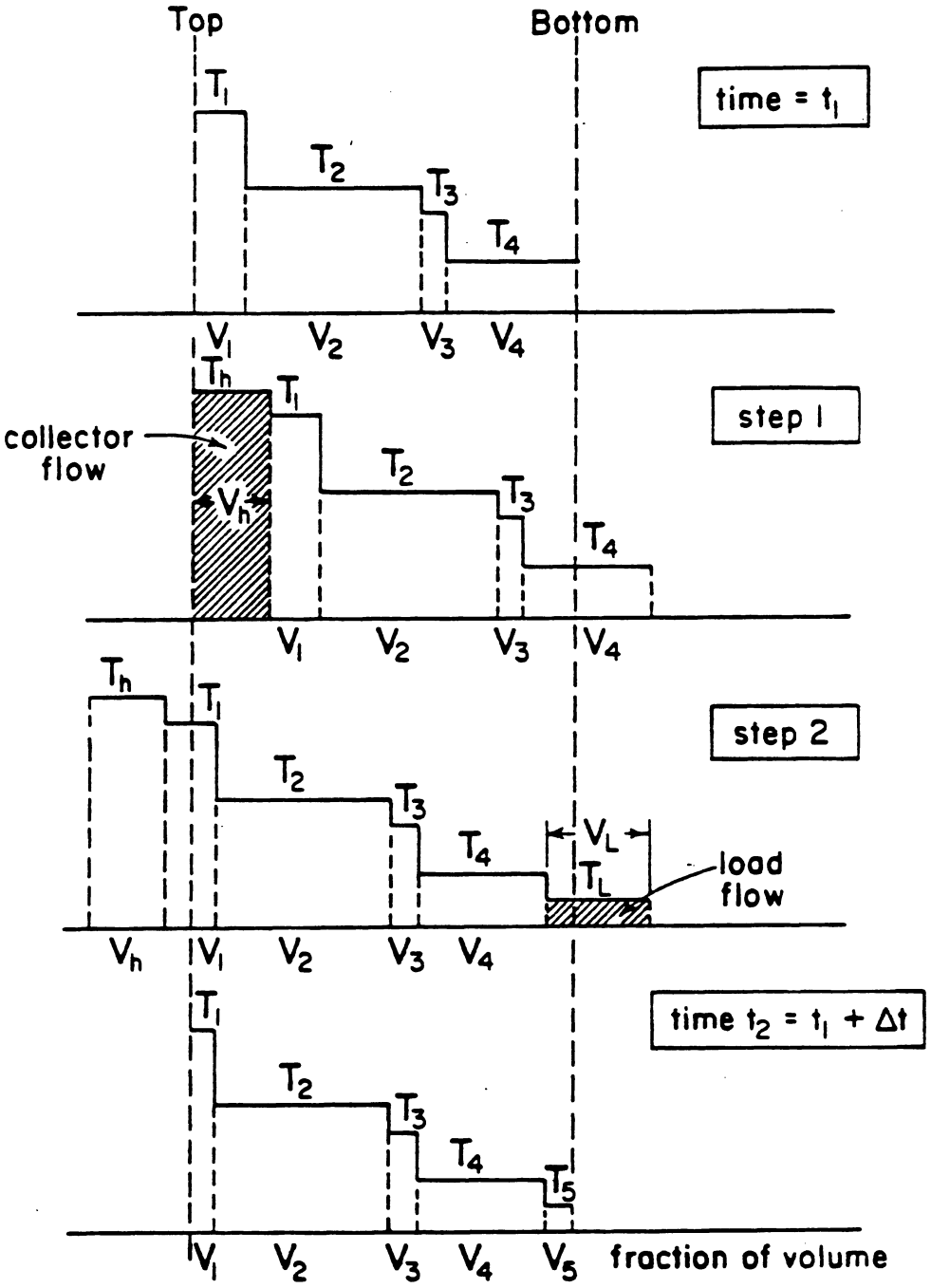

Figure 1.7 Operation of Plug-Flow Storage Tank Model. From Klein et al. (15).

CHAPTER II: EFFECTS OF DIFFERENT VARIABLES

II.1 Influence of Internal Mixing

II.1.1 Presentation

In addition to the velocity at which the fluid enters the tank (Section I.2), there are many parameters contributing to internal mixing in the storage tank.

First of all, the manner in which the fluid is introduced into the storage tank influences the degree of stratification. Fanney [18] tested different models of diffusers and showed a significant increase in stratification resulting from the use of an axial-flow diffuser. Further experiments [3] indicate that this type of diffuser may improve the performance of a system when a high flow rate (72 kg/hr-m^2 in the experiments) is used. For a low flow system however, the use of an axial-flow diffuser may not enhance the stratification or improve performance because of the larger surface of contact between the inlet fluid and the tank content. The combined effect of flowrate and diffuser is thus not well defined at this stage of the research.

Secondly, the influence of the tank design is of importance to improve the stratification. Lavan and Thompson [20] found that stratification increases with the height-to-diameter ratio. Because of tank losses, the optimum ratio is in the range between 3 and 4.

Thirdly, the height at which the water is introduced into the storage tank is a variable affecting mixing. A fixed inlet position causes temperature inversions and decreases stratification. Multiple inlet positions may be used to increase the performance of a system.

The combined effect of all the foregoing parameters is included in the definition of the Richardson number (equation 1.1) through the term ΔT_t, the tank top-to-bottom temperature difference (Section I.2.1.1).

$$R_i = g\ \beta\ L\ U^2\ \Delta T_t \qquad (1.1)$$

ΔT_t is, however, not a consequence of only internal mixing but it can also result from a larger rate of recirculation through the collector (Section I.2) even if no mixing is occurring. The definition of the Richardson number is also limited to instantaneous values and can not be extended to long term values. Equation (2.1) for example,

includes only the effect of the flowrate and not the other effects.

$$R_i = g\ \beta\ L\ U^2\ (T_{set} - T_{mains}) \qquad (2.1)$$

Klein and Fanney [3] compared results from experiments with TRNSYS and found a strong dependence of the number of nodes (for the multi-node tank model) or timestep (for the plug-flow model) on the performance of a simulated system when high flow rates are used. They explained this dependence with a phenomenon called mathematical mixing because of its analogy to the internal mixing in the tank. Mathematical mixing in the plug-flow model is increased when the timestep of the simulation is increased (Section I.4.2). The results that led to the better agreement with experiments for the high flow rate system were obtained for a timestep of 15 minutes (plug-flow model) or for 3 nodes (multi-node model). This number of 3 nodes shows that the assumption of a fully-mixed tank (one node) results in too much mathematical mixing to get a good agreement with the experiments. For other systems and other flow rates however, the timestep that characterizes the amount of stratification may be different.

Too little is presently known about the influence of mixing. Cole and Bellinger [2] accounted for mixing in their simulation by including an empirical constant derived from the experiment. This approach can not be generalized to other systems as long as this constant is not defined according to the characteristics of any system studied. At this stage of the research, it does not seem possible to explicitly incorporate mixing in a computer model like TRNSYS knowing only the characteristics of a system. Experiments and subsequently the development of a theory about mixing are needed before improving the model.

II.1.2 Consequences of Mixing on Previous Research

II.1.2.1 Promising Control Alternatives by Wuestling

Wuestling [4] studied several control alternatives with the use of TRNSYS. He found thus that reducing the collector flow rate to approximately 20 percent that of conventional collector flow rates could result in improvements in annual system performance from 10 to 15 percentage points. The limitations to his study are discussed in this section.

Even for conventional flow rates in usual systems (no stratification-enhancing devices), a certain amount of stratification is present in the tank. Assuming the storage tank to be fully-mixed as he did in his comparisons leads to underestimates of the performance of a system. It will be shown for a particular set of experiments in Chapter IV that the assumption of a fully-mixed tank causes a 10 % underestimate of the solar fraction by the $\bar{\phi}$,f-chart method compared to the experimental results.

Wuestling also used the plug-flow model with a variable inlet mode to simulate the behavior of a highly stratified tank. The influence of the timestep on the results, as noted by Klein for the system he studied, might cause Wuestling's results to be biased. There is no mention in his thesis about the timestep used in the simulations except in a sample of a TRNSYS deck [4], in which a half-hour timestep is used. Simulation results are not directly provided for any system in Wuestling's thesis. It is thus not possible to find out the timestep used in the simulation except by estimating it from graphic results. It has been estimated that Wuestling used a 15 minute timestep in Figure 3.4 in his thesis [4] and a 30 minute timestep in Figure 3.6 [4]. It is not possible to find the timestep used in other cases.

The base case as chosen by Wuestling [4] and described in Table 2.1, has been simulated for a range of simulation timesteps varying between one minute and one hour, for three different collector flow rates (10, 50 and 72 kg/hr-m^2) and for the month of March in Madison, WI. The result is shown in Figure 2.1. The timestep has no influence on the performance of a low flow rate. For a flow rate of 72 kg/hr-m^2, however, the influence is small for timesteps below 30 minutes but the change in the slope causes a more dramatic drop in the performance of the simulated system for timesteps between 30 minutes and one hour. For this system, the choice of either 15 or 30 minutes (or lower) does not affect consequently the results. Another system (collector area doubled) has been simulated (Figure 2.2) and it can be noted that the knee in the curve happens for a timestep of around 15 minutes. The solar fraction levels off for timestep between 45 minutes and 60 minutes, which suggests that the tank may have reached a full-mixed state. It is shown with this figure that the dependence of the timestep may be strong and may thus lead to biased conclusions for high flow rates if the influence of the timestep is not thoroughly investigated beforehand.

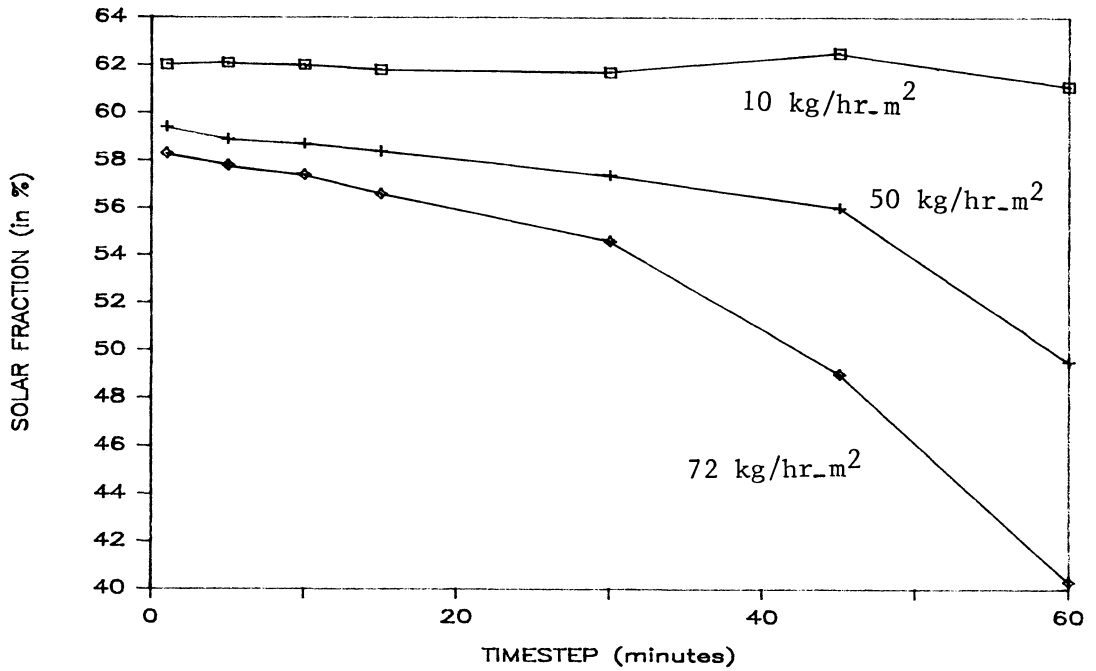

Figure 2.1 Influence of the Timestep on the Solar Fraction for three Collector Flow Rates (Collector Area = 4.2 m^2)

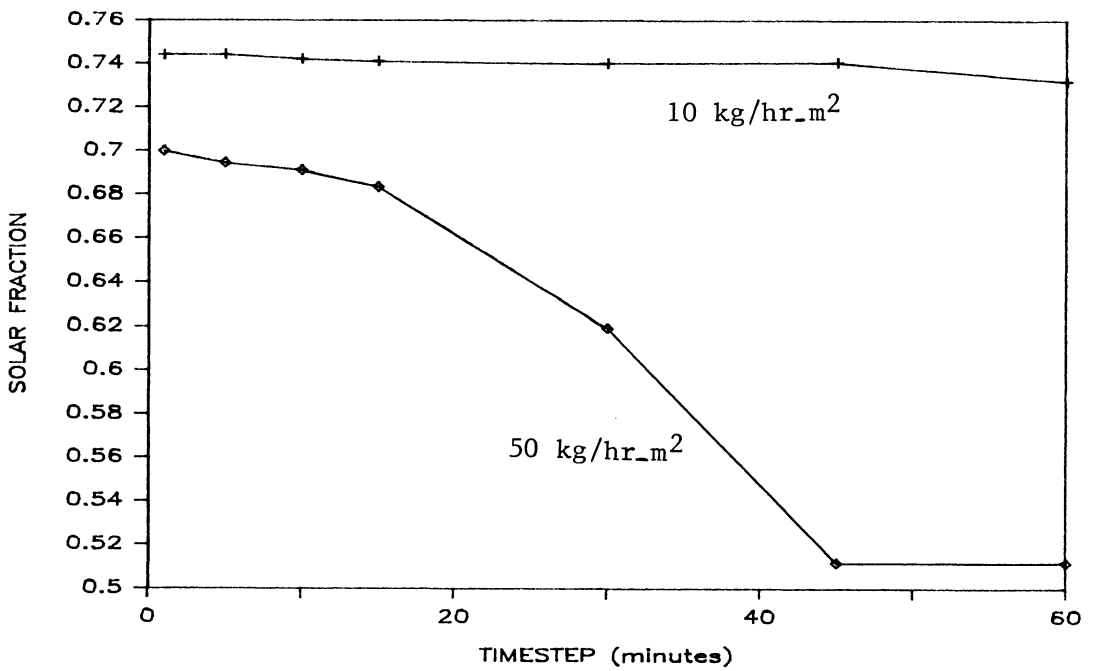

Figure 2.2 Influence of the Timestep on the Solar Fraction for two Collector Flow Rates (Collector Area = 8.4 m^2)

TABLE 2.1

DESCRIPTION	VALUE
COLLECTOR	
Area	4.2 m^2
$F_R(\tau\alpha)_n$ test	0.805
$F_R U_L$ test	4.73 W/m^2-°C
m_c test	72 kg/hr-m^2
b_o	0.1
PREHEAT TANK:	
Volume	303 liters
Loss Coefficient	1.08 W/m^2-°C
T_{env}	21°C
AUXILIARY TANK:	
Volume	151 liters
Loss Coefficient	1.047 W/m^2-°C
LOAD	
Volume (Distributed over Rand Profile)	300 liters/day
T_{set}	60°C
T_{mains}(March)	10.4°C

Table 2.1 System Specifications for the Simulations in Chapter II. From Wuestling [4]

According to Klein et al. [16], the timestep of a simulation with TRNSYS has to be chosen sufficiently small to meet stability conditions. Analytical divergence may occur when solving the differential equations encountered in the storage tank model. A largest possible value of the timestep for which the integration algorithm is stable is:

$$\tau_c = M_t / (\dot{m}_c + \dot{m}_L) \qquad (2.1)$$

where:

τ_c = critical timestep [hour]

$\dot{m}_c$ = hourly collector flow rate [kg/hr]

$\dot{m}_L$ = hourly load flow rate [kg/hr]

M_t = mass of fluid in the tank [kg]

Neglecting the effect of the load flow rate, $\tau_c = M_t / \dot{m}_c$. τ_c corresponds to the timestep at which the amount of water entering the tank during each timestep is larger than the mass of water present in the tank.

As noted earlier, the solar fraction in Figures 2.1 and 2.2 decreases linearly with an increase in the timestep until a certain timestep when the slope of the curve decreases more sharply. The timestep where the performance falls off is found to be about half of the critical timestep defined in equation (2.1). In the example of Figure 1.2, the drop off in the curve is around 15 to 20 minutes and equality (2.1) leads to τ_c equal to 15 minutes (M_t = 303 kg). Equality (2.1) seems to provide a good idea of the position of the critical timestep above which mathematical mixing increases more dramatically. The influence of the timestep should be studied more in detail for different systems (tank volumes, collector flow rates and load flow rates) to confirm equality (2.1). The critical timestep is only a quantitative notion to get an idea of the order of magnitude of the timestep needed for a simulation when a maximum amount of stratification is required.

Use of equality (2.1) to determine the critical timestep for a low flow leads to 105 minutes for the system simulated in Figure 2.2. This number is smaller than timesteps usually used (1 to 60 minutes). Being so far below τ_c, the performance of the system does apparently not change anymore with the timestep because the influence of mathematical mixing has became very small for these timesteps. It is found that the use of a low flow rate combined with timesteps less than 1 hour results in little mathematical mixing in the model in the same manner as a smaller timestep implies no mixing for a higher flow rate.

The fact that the solar fraction of a low flow rate system is independent of the timestep could also result from a limit on the stratification in the tank due to numerical restrictions in the tank model. A minimum limit on mixing is actually due to the assumptions built in the plug-flow model, i.e. a maximum of 50 nodes is allowed in the tank and adjacent nodes with a temperature difference less than 0.5°C are mixed. Those limits will be extended later (Chapter IV) to investigate the influence of mixing

at very small timesteps and it will be shown that the solar fractions of the systems studied do not change substantially.

Even if it is not possible to define the number of nodes present in the plug-flow model at a given time, an idea of the minimum number of nodes in the tank is provided by the ratio of the tank volume to the product ($\dot{m}_c \tau_c$). This approach considers only the collector side of the system. For a timestep of 15 minutes, a tank volume of 300 liters, a collector area of 4 m^2 and a low flow rate of 10 kg/hr-m^2, the assumption of no load leads to about seven nodes. The number of nodes in the tank, however, is actually larger because of the effect of the load flows.

A variable inlet mode has been chosen in the simulations used to obtain figures 2.1 and 2.2. The behavior may be different for a fixed inlet mode where more mixing is assumed for every timestep but the decrease in performance with an increase of the timestep (increase in mixing) remains.

Wuestling [4] uses the plug-flow model only to determine the performance of a stratified system at low collector flow rates. In this case, the timestep has no effect on the result since the tank is implicitly assumed to be highly stratified, which results in overestimates of the solar fraction. Wuestling modeled the conventional flow rate case with the assumption of a fully-mixed tank, which is conservative. The increase in performance when using a low flow strategy is thus overestimated on both sides by Wuestling.

II.1.2.2 Correction of f-chart anf $\bar{\phi}$,f-chart by Copsey

The influence of the timestep used is more important on Copsey's results [22] than it was with Wuestling [4]. The only indication Copsey provides about storage tank stratification is that he used the plug-flow model with the fixed inlet position mode. No indication of the timestep used is provided and no samples of TRNSYS decks are presented.

Copsey compared the performance at different flowrates for the same simulation timestep. It was shown in the preceding section that the results of the comparison are dependent on the timestep and on the system. From Figure 2.2, a timestep of 15 minutes results in a gain of 6 % when low flow rates are used instead of a high flow rate but a timestep of 45 minutes leads to an increase in performance of 22 % for the same system and same flow rates. For a fixed inlet mode, the difference is not as

important since some mathematical mixing is already present, independent of the timestep but the timestep still has an important effect on the performance of the system. An arbitrary choice of a timestep and the decision of using a fixed inlet mode introduce some mathematical mixing in the tank for each system and for each flow rate simulated. This artificial mixing is not based on experimental results and is unreliable. The consequence is the discrepancy of the results stemming from the choice of different timesteps (Figure 1.1 and 1.2). The proposed correction for f-chart to account for any flow rate by Copsey [22] is thus dependent upon the timestep chosen.

II.1.3 How to Account for Mixing in a Design Method

There is presently no way to simulate the actual amount of mixing in a tank for a given system and for a given flow rate. Because of the lack in knowledge about mixing, the only accurate simulation results at this time are obtained either when the tank is truly fully-mixed or when no mixing occurs in the tank . A fully-mixed tank is a conservative assumption, even for systems operated at high flow rates. A tank with no mixing gives an upper bound for the performance of a system and is closer to the behavior of systems with low flow rates.

The f-chart and $\bar{\phi}$,f-chart methods have been developed with the assumption of a fully-mixed tank. The development of a design method to account for stratification has to use the assumption of no mixing to get an upper bound for the performance of a system. The real performance of a system (with some internal mixing) will lie in between the performance of a fully-mixed system and the performance of a system with no mixing. The exact position can only be found either with experimental data about the considered system (such as from the standard test ASHRAE 95-1981) or with the help of a correlation defining mixing as a function of certain characteristics of the system. The first possibility is studied in Chapter IV.

II.2 Influence of Parameters on the Performance of a SDHW System

There are two possibilities to develop a correction for systems with no mixing. Either the f-chart or the $\bar{\phi}$,f-chart methodology may be used. In the first case, a correction factor has to be introduced for parameters like the tank volume and for the tank loss coefficient since they are not accounted for in the definitions of X (equation 1.8) and Y (equation 1.9). In addition to these tank characteristics, the influence of the controller

deadbands should be considered. The influence of all the parameters cited above may also depend upon the flowrate chosen. In this chapter, the simulations have been run with the system described by Wuestling for March in Madison, WI. This month has been chosen because previous results [4] showed that the system performance in March nearly resembles the annual performance. Table 2.1 shows the characteristics of the system studied as a base case.

II.2.1 Storage Size

The f-charts are based upon the assumption of the use of a standard storage tank size (75 liters of water per unit of collector area). The method to account for a different storage size has been developed for liquid space heating systems, but has been used for SDHW systems [11].

The study of the influence of the volume on the solar fraction requires the tank losses to be the same during the comparison. Otherwise the change in the losses will interfere with the effects of the tank storage size. A loss coefficient of zero has thus been chosen in this chapter. Tank volumes for SDHW systems usually vary between 150 and 500 liters,but tank volumes may be as high as a few thousand liters when space heating has to be provided at the same time. Tank volumes 0 to 500 liters of stored water per square meter of collector area have been simulated to study the general trends of the systems.

Figure 2.3 compares the performance of two systems with different flow rates (10 kg/hr-m^2 and 50 kg/hr-m^2) for a wide range of tank volumes. Both systems have been simulated with the plug-flow tank model and a small timestep (one minute), resulting in little mathematical mixing in the tank. It is seen that the difference between the flow rates gets smaller when the storage tank size increases. The performance increases sharply for small tanks and then levels off. The recirculation of the water through the collector decreases with an increase in the volume, i.e., hot water from the collector outlet is less and less likely to reach the bottom of the tank even for high flow rates. The collector inlet temperature decreases at the same time until the point when only water from the mains is sent through the collector. For a very large tank, the difference between the performance of both systems is difficult to predict since the collector heat removal factor is higher for a high flowrate but the stratification is still better for low flowrates (segments of hot water are larger for high flowrates). The

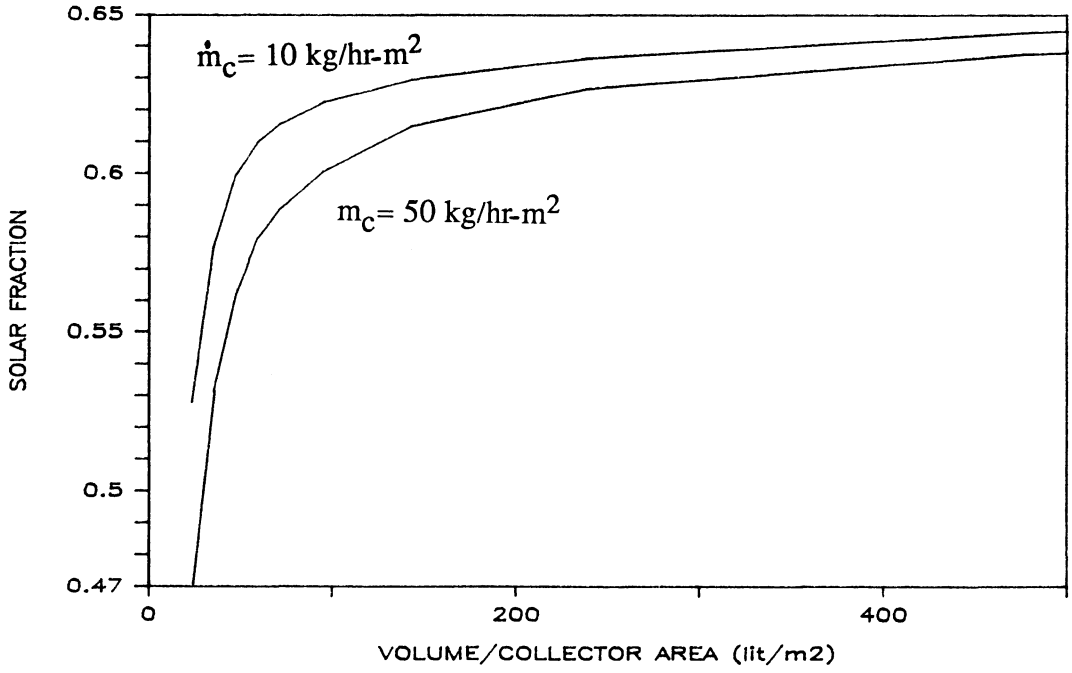

Figure 2.3 Dependence of the Solar Fraction on the Tank Volume per Unit of Collector Area for Two Different Collector Flow Rates (m_c)

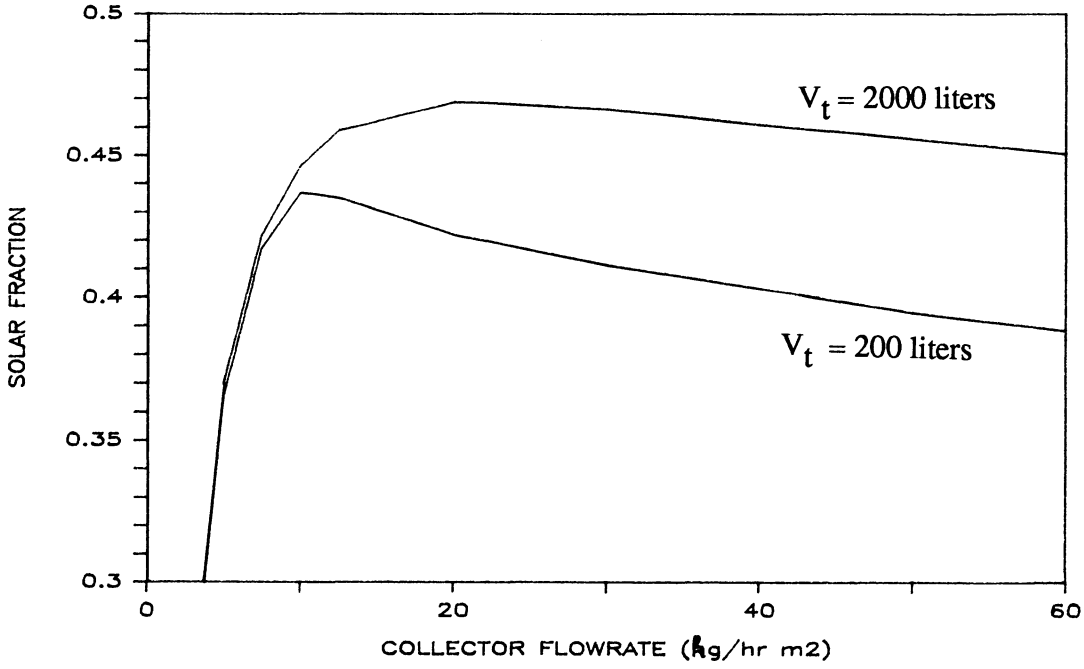

Figure 2.4 Dependence of the Solar Fraction on the Collector Flow Rate for Two Different Storage Tank Sizes and a Daily Load Equal to 450 liters.

performance of the systems should, however, both reach a different limit when there is no recirculation. The main conclusion from this graph is that the gains due to the use of a larger tank level off above 100 liters per square meter of collector area. This result is slightly dependent upon the load (300 liters for a collector area of 4.2 m^2 in the case of Figure 2.3).

Figure 2.4 compares the performance of two tanks (50 kg/m^2 and 500 kg/m^2) at different flow rates for a daily load of 450 liters. It is seen that the optimum flow rate varies according to the tank size and that the influence of the flow rate is more sensitive on small tanks than on larger tanks. The circulation number (collector flow rate divided by the tank volume) seems thus to be an important parameter. This parameter is, however, not sufficient to determine the optimum collector flow rate. In the case of Figure 2.4, the optima for the two systems simulated are for different circulation numbers (about 0.23 and 0.05).

II.2.2 Storage Tank Loss Coefficient

The f-chart method does not allow any correction for the preheat tank losses. The simulations that this design method is based upon, have been done with a loss coefficient equal to 0.42 W/m^2-°C.

A survey among different commercially available storage tanks [23] show that the tank insulation is between R-4 (1.5 W/m^2-°C) and R-24 (0.24 W/m^2-°C) according to the manufacturers' data. There is a correction factor to apply to these values when the tanks are used in real life. Fanney [24] used different tanks and experimentally measured the overall tank loss coefficients for each of them. The ratio of the measured tank loss coefficient to the loss coefficient obtained directly from the thickness of insulation is found to be about 1 and 1.6. The measured tank loss coefficients used by Fanney are between 0.8 and 1.2 W/m^2-°C, which is two to three times as much as the value assumed in f-chart.

The value of the overall tank loss coefficients obviously depends of the surface area of the tank (for example: a 300 liter cylinder tank has a surface of about 3 m^2) as well as the linear loss coefficient (U_t). UA_t is however likely to be in the range between 1.0 W/°C and 5.0 W/°C for usual SDHW systems (Fanney's measurements of the overall tank loss coefficient are between 2.0 W/°C and 4.6 W/°C).

Tank losses will modify the dependence of the volume on the solar fraction as

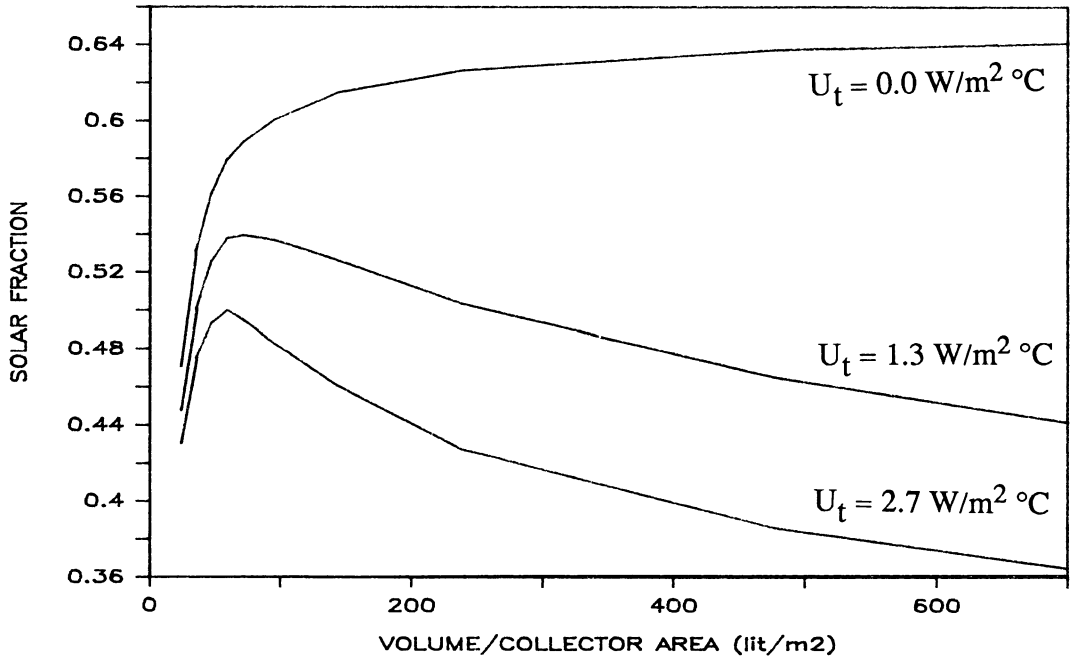

Figure 2.5 Dependence of the Solar Fraction on the Tank Volume per Unit of Collector Area for a High Flow System (50 kg/hr m^2) with Different Tank Loss Coefficients (U_t)

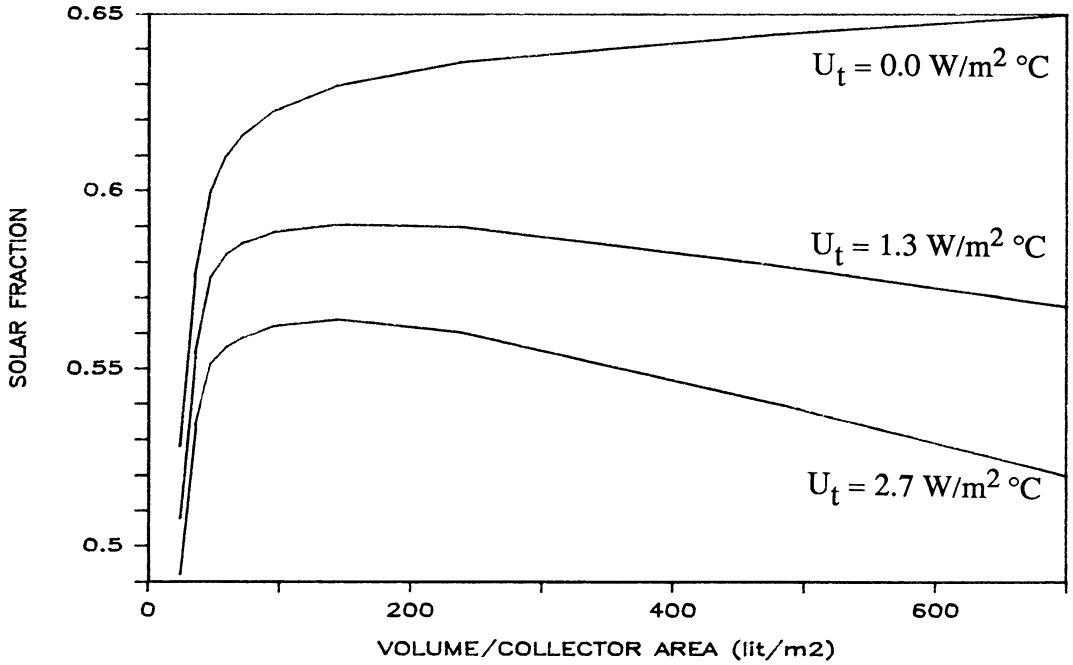

Figure 2.6 Dependence of the Solar Fraction on the Tank Volume per Unit of Collector Area for a Low Flow Rate System (10 kg/hr m^2) with Different Tank loss Coefficients (U_t)

seen in the preceding section since an increase in the tank size for a given insulation (R-value) increases the surface area of the tank and thus the losses. The gains due to a lower collector inlet temperature (Section II.2.1) outweigh the increase in the tank losses for small volumes but further increases produce only little gains (foregoing chapter) and the tank losses are predominant. Figure 2.5 and 2.6 respectively show this phenomenon for a low flow rate and a high flow rate. The particular shape of the curves is dependent upon the way the surface area increases when the volume increases. In the simulations it was assumed that the tank has the shape of a cylinder of fixed height (1.6 meter).

It can be seen from these figures that the optimum storage size is higher for a low flow system (about 150 kg/m^2) than it is for a high flow rate (about 75 kg/m^2). These optima depend slightly on the load (300 liters per day for these simulations) since larger tanks give better results for higher loads. The influence of the tank volume however is a more sensitive parameter for the high flow rate system than for the low flow rate system. In the latter case, varying the storage size between 50 and 250 kg/m^2 does not significantly change the results. The tanks used for conventional systems are thus well suited for low flows.

The influence of the overall tank loss coefficient (UA_t) has been investigated for a flow rate of 10 kg/hr-m^2. It can be seen in Figure 2.7 that the solar fraction of the system increases with an increase in the tank volume. First of all, when the tank volume is increased, the collector inlet temperature decreases because the recirculation rate of the water in the tank is smaller. Therefore, the collector losses decrease. Secondly, an increase in the tank volume for a constant overall tank loss coefficient results in a lower average tank temperature since more cold water from the mains is stored in the tank. Consequently, the tank losses decrease.

II.2.3 Controller Deadbands

The most common type of thermostat is the differential controller. Two sensors measure the temperature at the collector inlet and at the tank inlet (see figures 1.5 and 1.6 for the schematic of a SDHW system). Whenever the temperature difference is above a specified value (ΔT_{on}), the controller turns the pump on and the fluid circulates through the collector. When the temperature difference falls below another specified value (ΔT_{off}), the pump is turned off. ΔT_{on} and ΔT_{off} are either fixed or

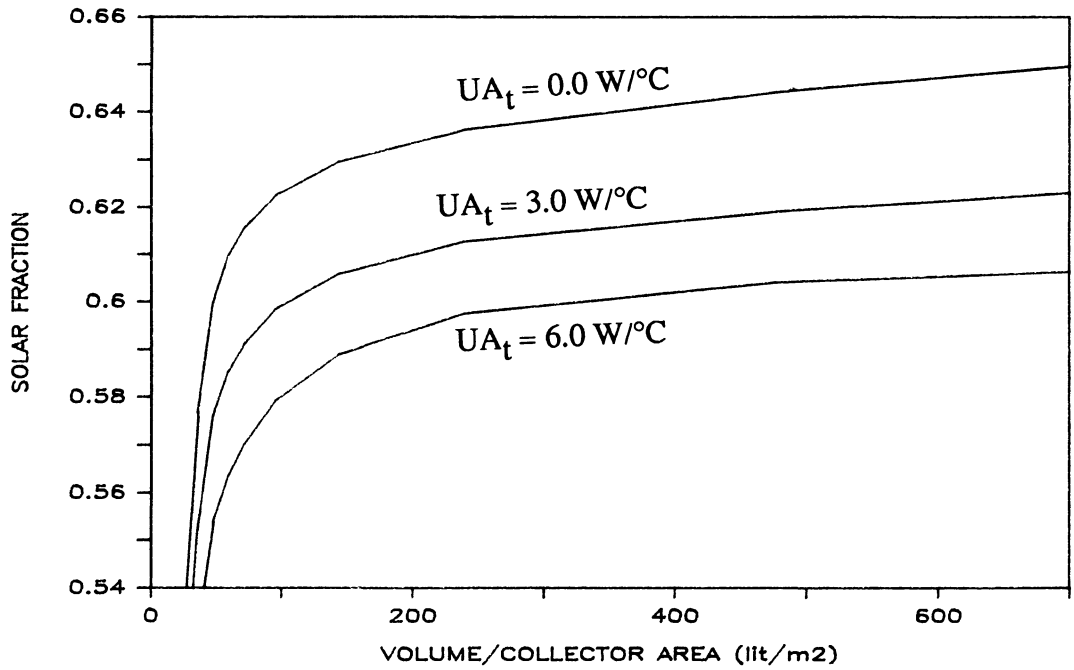

Figure 2.7 Dependence of the Solar Fraction on the Tank Volume per Unit of Collector Area for a Low Flow Rate System (10 kg/hr-m^2) with Different Overall Tank loss Coefficients (UA_t)

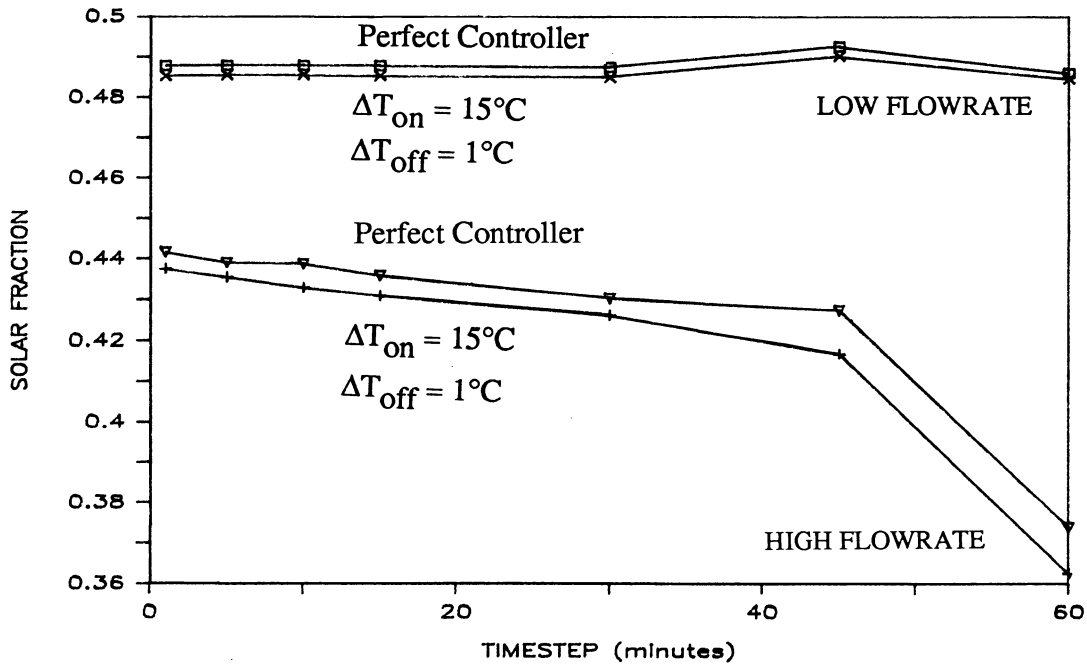

Figure 2.8 Dependence of the Solar Fraction on the Timestep of the Simulation for a Low Flow System (10 kg/hr-m^2) and a High Flow System (50 kg/hr-m^2) and two Different sets of controller Deadbands.

user adjustable and are called controller deadbands. A survey of commercial controllers [23] shows that the range for ΔT_{on} is from 5 to 25 °F (2.5 to 14°C) while the range for ΔT_{off} is from 1 to 6°F (0.5 to 3.4°C).

The controller deadbands have been shown [24] to have little influence on the performance of solar systems when high flow rates are used, due to the relatively high collector inlet temperatures involved in this case. Whenever the solar radiation stops, the collector outlet temperature is actually the ambient temperature because the collector is assumed to have zero capacitance. Since the temperature at the bottom of the tank is relatively high (due to large recirculation of the water in the case of high flow rates in addition to mixing), the controller turns the pump off.

For a low flow, however, the collector inlet temperature is much lower and may be as low as the mains temperature. In this case, thermal gains from the ambient to the collector can be important. Figure (2.9) shows the detail of the influence of the low collector inlet temperature, which increases the amount of solar radiation collected as well as the amount of thermal gains from the ambient temperature. The dynamic variations of several temperatures are plotted versus the time of the day in two cases. For the sake of simplicity, the collector inlet temperature has been assumed to be a constant and thermal gains have been exaggerated compared to solar gains. The nomenclature for Figure 2.9 is:

$T_{c,in}$ = collector inlet temperature (assumed to be constant in the figure)
$T_{c,out}$ = collector outlet temperature
$T_{ambient}$ = ambient temperature
t_{on} = time at which the pump turns on
t_{off} = time at which the pump turns off

The bottom part of Figure 2.9 shows the amount of solar radiation ($T_{c,out}$ - $T_{c,in}$) that would be collected by a system, chosen so that it can not take advantage of the benefits due to a warm ambient temperature. The top figure shows the influence of the ambient temperature on the collection of the energy. Not only thermal energy is gained but a part of the solar radiation that was not possible to collect in the first case is collected.

The thermal gains may be divided in two parts depending on if they occur at the same time than solar radiation. When the pump is running, thermal gains happen whenever the collector inlet temperature is below the ambient temperature. Thermal

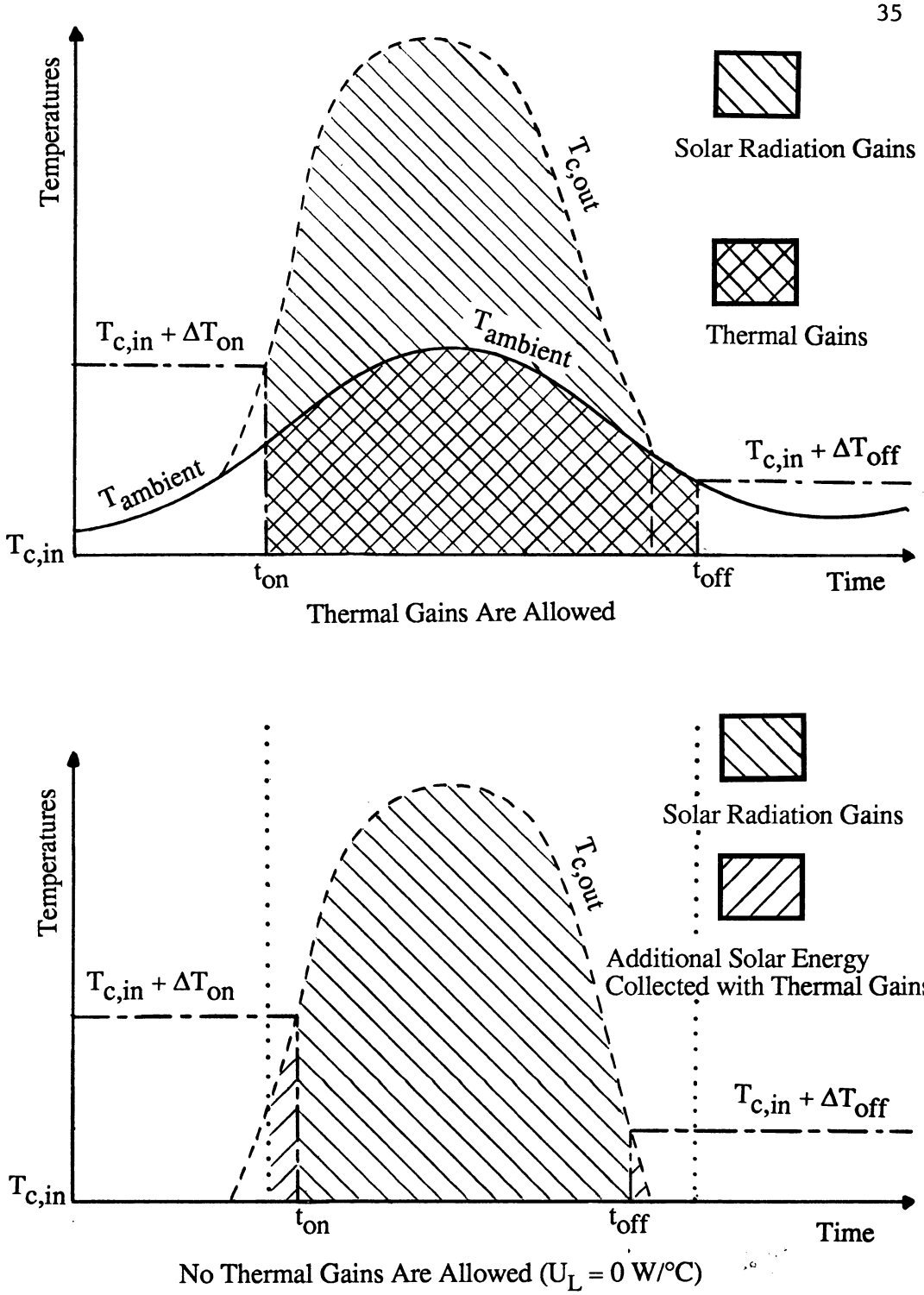

Figure 2.9 Influence of the Thermal Gains on the Collected Energy

gains may also happen when radiation ends in the evening. If the temperature difference between the ambient and the collector inlet is above ΔT_{off} then the pump remains on and some gains occur even during the night. Thermal gains during the night are typically smaller than the thermal gains during the day for two reasons:
- ambient temperature is obviously higher during the day (especially for clear skies)
- the collector has usually run a few hours before the evening, thereby warming the water in the tank and increasing the temperature at the bottom of the tank. A study of the thermal gains from simulation results is presented in Chapter III.

The pump running time is a parameter that has been used by Wuestling [4] and Copsey [22] to determine the degree of recirculation of the tank through the collector. From the analysis above, it is clear that the pump running time is a sensitive parameter dependent upon the controller deadbands. Thermal gains during the night may slightly improve the performance of a solar system but the pump running time will be greatly increased thus biasing the studies using the pump running time as a parameter and increasing pump energy consumption.

Another drawback of the nightly thermal gains in actual systems is the resultant destruction of the stratification. The pump turns on during a warm night, water goes through the collector, collects a little energy and comes back in the tank destroying the thermal stratification that was beforehand present in the tank. The same phenomenon may be noticed in certain cases with the simulations. Two systems with different flow rates (10 kg/hr-m^2 and 50 kg/hr-m^2) have been simulated with two different sets of controller deadbands (Figure 2.8). For a high flow rate, the performance of the system with ΔT_{on} = 15°C and ΔT_{off} = 1°C is higher than the performance of a controller with both deadbands equal to zero (called perfect controller). This paradox is explained by the fact that running the collector at night or times of low radiation produces some mathematical mixing in the plug-flow model. If the amount of water needed to go through the collector during one timestep ($\dot{m}_c \tau$), exceeds the size of the bottom segment in the tank, several segments (and/or fractions of segments) are lumped together to obtain one segment at a uniform temperature. This segment is subsequently heated up in the collector before being reintroduced into the tank. With a perfect controller, the pump is turned on even if very little energy may be gained. It results in some segments being mixed together, thereby decreasing the stratification without adding significant energy in the tank.

Two simultaneous effects influence the performance of the system when the controller deadbands are lowered, the additional gains at night (or times of low radiation) and the decrease in the top-to-bottom temperature difference. In the simulations, the result of these combined effects depends on the timestep and the flow rate used, since a reduction in one of these parameters decreases the size of the segments and the influence of mathematically-induced mixing. Decreasing the timestep is a solution to eliminate this type of mixing for high flow rates but the timestep needed would result in significant computation in the simulations.

II.3 Development of a New Version of $\bar{\phi}$,f-chart

Copsey [12] developed a modification to the f-chart and $\bar{\phi}$,f-chart methods to account for the effect of the flow rate. As shown in Section II.1.2.2, an arbitrary choice of the timestep and the use of a fixed inlet mode introduce some mathematical mixing in the simulation depending on the flow rate and the system characteristics. This strategy leads to good estimates of the solar fraction only if the amount of mathematical mixing in the simulations is the same as the actual amount of mixing in the tank. The estimate of the performance of systems with stratification-enhancing devices, among others, is not possible with Copsey's correction. On the other hand, this correction requires the knowledge of the parameter ($\tau\alpha$), the absorptance- transmittance product, which is usually not available.

The goal of this research is primarily to improve the estimate of the performance of a system using low flow rates. Even if the development of the design method has to assume no mixing (Section II.1.2.2), this assumption does not significantly affect the results because mixing is usually small at low flow rates. It will be shown in Chapter IV that the method developed is also applicable to any system provided there is no mixing in the tank.

The choice is to develop either the f-chart method or the $\bar{\phi}$,f-chart method. The main advantage of the use of a method based on utilizability is its flexibility. The influence of the volume, the tank loss coefficients and the controller deadbands has to be introduced in the method. Since their influence is also dependent on the flow rate, the use of a correction factor like in the f-chart method is complicated. The $\bar{\phi}$,f-chart method has therefore been chosen. The parameters cited above may thus be introduced at any level in the $\bar{\phi}$,f-chart iterative process and especially in the two correlations used

to calculate the useful energy (equation 1.14) and the tank temperature (equation 1.18). The different steps of the method may have to be modified to account for the characteristics of a system with no mixing. The two correlations may also have to be changed since they were obtained with a regression analysis from simulations on TRNSYS with a fully-mixed tank [15]. A high number of simulations has to be run with negligible mathematical mixing to get a data base to determine the correlations needed with enough accuracy. A reasonable range of parameters has to be investigated and some assumptions have to be made in the simulations.

II.3.1 Collector Flow Rate

The systems in the data base have been simulated with a collector flow rate equal to 10 kilograms of water per hour per square meter of collector. According to Wuestling [4] and Hirsch [17], this flow rate is optimum for usual SDHW systems. It will be shown in Chapter IV that the performance of a system with no mixing is not very dependent on the flow rate. The particular flow rate chosen is therefore not important as long as no mathematical mixing is produced in the simulations.

The main reason in choosing a flow rate as low as 10 kg/hr-m^2 is actually to simulate no mathematical mixing. The timestep chosen has then little influence on the results since the simulations deal with reasonable tank sizes. A five minute timestep is sufficiently below the critical timestep τ_c (Equation 2.1) for any system studied to avoid the problems encountered in Section II.1. Results in Chapter IV will confirm that, for the systems studied, mixing is negligible at this flow rate.

II.3.2 Influence of Boiling

This effect is usually treated with the use of a relief valve that discards energy, whenever the outlet temperature is above 100°C. The method developed in this paper is intended to give an upper bound for the performance of a stratified system. Boiling has thus been treated differently since water above the boiling point was mixed in the tank with the upper nodes until the temperature of the upper segment falls below 100°C. No energy was thus discarded in the simulation. To determine the influence of boiling, the energy that would have been discarded has been registered in the simulations by counting the amount of water exiting the collector with temperatures above the boiling point. This influence is expected to be small and is checked in

Chapter III.

II.2.3 Range of parameters

The range of parameters investigated is comparable to the range used by Braun et al. [15]. Some modifications are the following:

- the range for $F_R(\overline{\tau\alpha})$ has been extended to [0.50 - 0.80] since the range given in Braun's paper is characteristic for high flow systems. The correction for low flows [6] results in a decrease in F_R and thus in $F_R(\overline{\tau\alpha})$. The range for F_RU_L has also been extended to [2.0 W/m^2-°C - 8.6 W/m^2-°C] for the same reason.
- the mains temperature, the set temperature and the daily water usage ranges have been reduced because this paper only deals with SDHW systems.
- the room temperature has been allowed to vary in the range [18°C - 22°C].

TABLE 2.2

PARAMETERS	LOWER BOUND	UPPER BOUND
Collector:		
$F_R(\overline{\tau\alpha})$	0.50	0.80
F_RU_L	3.6 W/m^2-°C	8.6 W/m^2-°C
Slope	Latitude	Latitude
Storage:		
C_s	175 kJ/m^2	700 kJ/m^2
UA_t	1.0 W/°C	4.0 W/°C
T_{env}	18°C	22°C
Load:		
T_{mains}	5°C	20°C
T_{set}	40°C	80°C
Water Usage	20 liters/day-m^2	250 liters/day-m^2

Table 2.2 Range of parameters for the simulations on TRNSYS and for the design method

A summary of the range of parameters used may be found in Table 2.2. Different locations are simulated: Madison, WI, Albuquerque, NM, Seattle, WA and Miami, FL. A total of 210 yearly simulations has been run with TRNSYS for Madison to get the data base necessary to correlate the useful energy and the tank temperature. Fourteen different systems have been simulated for each of the other cities to check the influence of the location on the results. A listing of a TRNSYS simulation deck is included in Appendix A.

CHAPTER III: A NEW VERSION OF THE $\bar{\phi}$,f-chart METHOD

III.1 Methodology

The only useful weather data available to the user of a design method are the monthly-average ambient temperature ($\overline{T}_{amb}$) and the monthly-average daily radiation on a horizontal surface ($\overline{H}$). The development of the $\bar{\phi}$,f-chart method relies on several algorithms to calculate the variables needed from the data cited above. The calculation of Q_{max}, the maximum useful energy that could be collected by the system, requires the knowledge of three different variables, $\overline{H}_T$, $(\overline{\tau\alpha})$ and $\bar{\phi}$, which can be obtained with the following algorithms:

- Determination of the monthly-average daily radiation on a tilted surface such as given by Klein and Theilacker [25] using the algorithm for estimation of diffuse radiation developed by Erbs et al. [26].
- Determination of the monthly-average transmittance-absorptance product, Klein [27].
- Determination of the monthly-average daily utilizability, Clark and Klein [8].

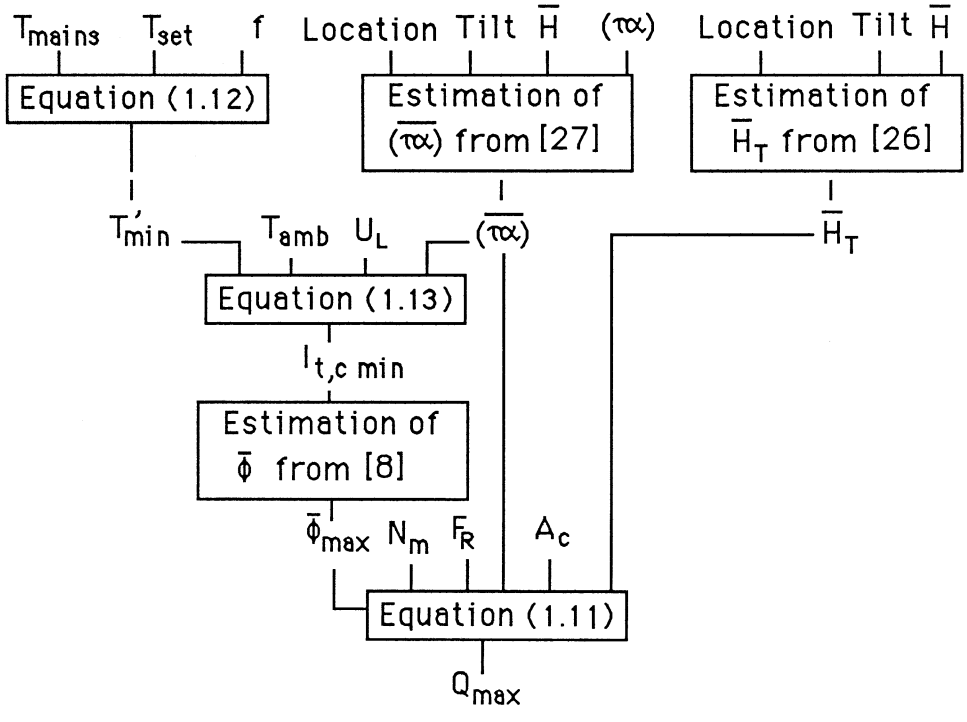

Figure 3.1 Schematic of the calculation of Q_{max}

As seen in Figure 3.1, the calculation of the maximum monthly useful energy that could be collected by the system (equation 1.11) requires the use of different algorithms. The weather variables $\overline{T}_{amb}$ and $\overline{H}$ are directly calculated from monthly averages of the particular weather data used in the simulations, i.e. the Typical Meteorological Year (TMY) for each city studied.

The algorithms used are based on correlations for different locations and periods of the year. There is an error resulting in their use for the particular weather data and location used in the simulations. The simulations on TRNSYS are based upon values of $\overline{H}_T$ and $(\overline{\tau\alpha})$ that are respectively calculated by the radiation processor and by the collector model. The same parameters have therefore to be used when establishing the correlations for the monthly-average tank temperature and the monthly useful energy gains in order to have results independent from the algorithms used. The determination of $\bar{H}_T$ and $(\overline{\tau\alpha})$ is made with equations (3.1) and (3.2) from TRNSYS outputs for each month of the year and for each location.

$$\overline{H}_T = \frac{\int \bar{I}_T \, dt}{N_m} \tag{3.1}$$

$$\frac{(\overline{\tau\alpha})}{(\tau\alpha)} = \frac{\int K_{\tau\alpha} \, \bar{I}_T \, dt}{\int \bar{I}_T \, dt} \tag{3.2}$$

The monthly-average daily utilizability is a characteristic of the distribution of the solar radiation. The curve $\bar{\phi} = \bar{\phi}\,(\bar{I}_{T,c})$, characteristic of the distribution of the solar radiation data used in the TRNSYS simulations, may be directly found with equation (3.3) from outputs of the hourly radiation on the collector surface, for each value of the critical radiation level $(\bar{I}_{t,c})$ and for each month.

$$\bar{\phi} = \frac{\int (\bar{I}_T - \bar{I}_{T,c})^+ dt}{\int \bar{I}_T \, dt} \tag{3.3}$$

Figure 3.2 shows the monthly-average daily utilizability plotted versus the critical

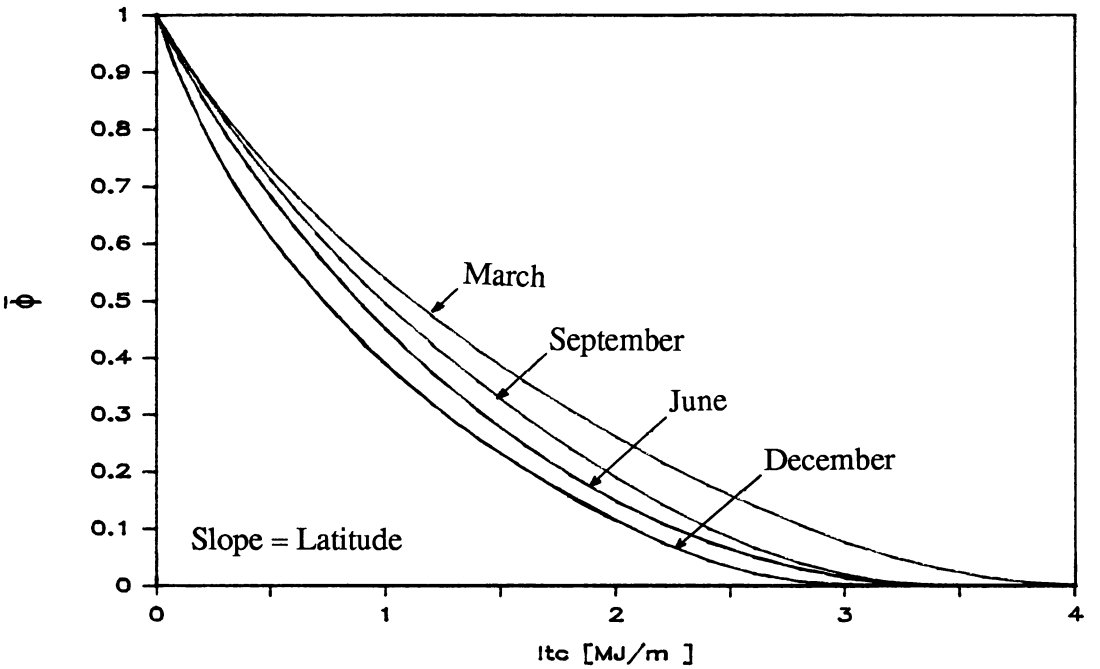

Figure 3.2 Dependence of the Monthly-Average Utilizability on the Critical Radiation Level for Four Different Months in Madison (from TMY Weather Data)

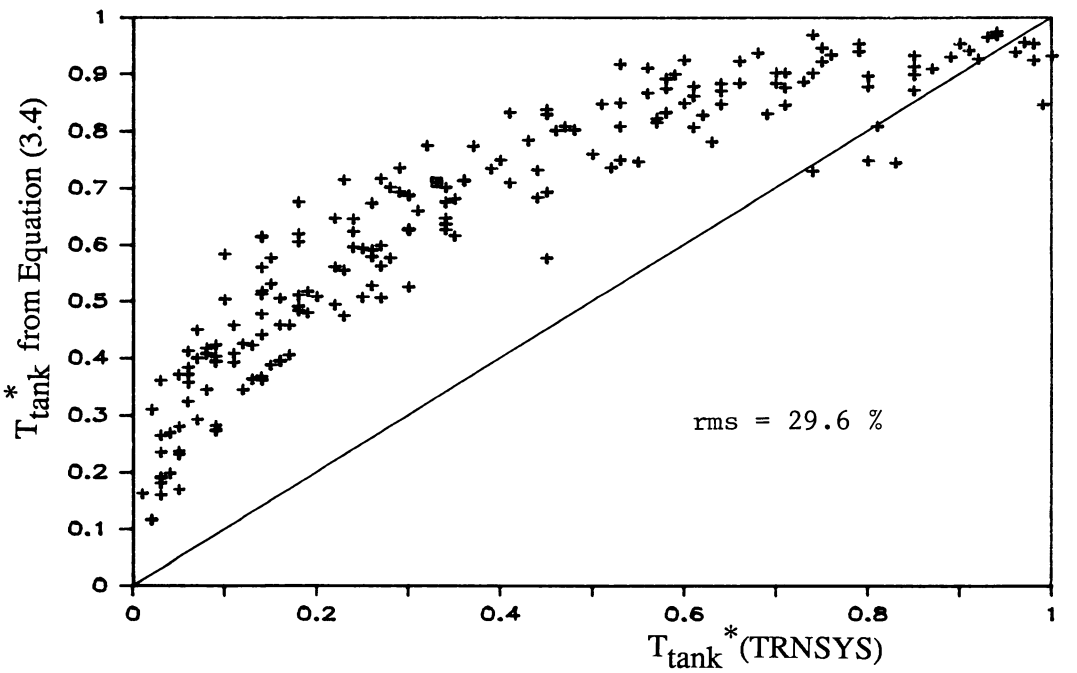

Figure 3.3 Comparison of the Dimensionless Monthly-Average Tank Temperature (T_{tank}^*) between TRNSYS and Equation (3.4) developed for a fully-mixed tank

radiation level for four months in Madison.

The error in the prediction of any variable by a method is affected by the various errors introduced by all the algorithms used in the method. The correlations developed in the next two sections only use the variables $\overline{H}_T$, $(\overline{\tau\alpha})$ and $\overline{\phi}$ obtained directly from the TRNSYS simulations. The error obtained when combining the correlations developed in Sections III.2 and III.3 and the algorithms calculating $\overline{\phi}$, $(\overline{\tau\alpha})$ and $\overline{H}_T$ is then presented in Section III.4.

III.2 Correlation for the Monthly-Average Tank Temperature (Ttank)

III.2.1 Modification of the Equation for a Stratified System

The original equation for the monthly-average of the average tank temperature is given by:

$$T_{tank} = T'_{min} + g\,(\exp(kf) - 1)\ \exp(hZ) \qquad (3.4)$$

where:

$$T'_{min} = T_{mains} + (T_{set} - T_{mains}) \qquad (3.5)$$

The coefficients g,k,h as well as the variable definitions are given in Section I.3.2. Equation (3.4) may be written in a dimensionless form:

$$T_{tank}^{*} = \frac{T_{tank} - T_{mains}}{T_{set} - T_{mains}} = f + g\,(\exp(kf) - 1)\ \exp(hZ)\ (100.\,Z)^{-1} \qquad (3.6)$$

For a fully-mixed system, T'_{min} is the minimum collector inlet temperature (or tank temperature) necessary to meet the fraction f of the load (Section I.3.2). T'min would be the temperature of the tank in the ideal case of a continuous draw and an evenly distributed solar energy collection. For a system without a heat exchanger, T'_{min} is defined by equation (3.5). For a stratified system, T'_{min} no longer has this significance since the collector inlet temperature, the average tank temperature and the temperature of the load are generally different. The temperature at the bottom of the tank may be as low as the mains temperature and the system may still provide a significant fraction of the load. There is, however, a relationship between the monthly-average tank temperature and the monthly solar fraction as it will be shown in

TABLE 3.1 Different Models for the Average Tank Temperature and rms Errors

	Different Models for $\frac{T_{tank} - T_m}{T_{set} - T_m}$	r.m.s. in percent
(0)	$f + 0.2136\ (C_s^*)^{-0.704}\ [\exp(4.702\ f) - 1]\ \exp(-4.002\ Z)\ (100\ Z)^{-1}$	29.63
(1)	$f + 8.907\ (C_s^*)^{-0.49}\ [\exp(-16.0\ f) - 1] \exp(-10^{-3}\ Z)\ (100\ Z)^{-1}$	20.44
(2)	$(C_s^*)^{-0.19} \{0.494\ f^2 + 3.82\ 10^{-2} f\ [\exp(3.54 f) - 1]\ [1 - \exp(-0.81\ Y/f)]^2\}$	9.86
(3)	$(C_s^*)^{-0.26} \{0.441\ f^2 + 5.19\ 10^{-3} f\ [\exp(4.04\ f) - 1]\ Z^{-1}\}$	8.15
(4)	$(C_s^*)^{-0.19} \{0.334\ f + 8.65\ 10^{-4}\ [\exp(6.21\ f) - 1]\ [1 - \exp(-1.73\ Y/f)]^2\ Z^{-1}\}$	7.46
(5)	$(C_s^*)^{-0.21} \{0.555\ f^2 + 3.88\ 10^{-3} f\ [\exp(4.60\ f) - 1]\ [1 - \exp(-1.09\ Y/f)]^2\ Z^{-1}\}$	7.07

(0) is the equation of the temperature from a fully-mixed tank

Section III.2.2.

The correlation for the tank temperature (3.6) was developed for a fully-mixed tank and it is not necessarily applicable to stratified systems. Figure 3.3 shows a comparison between the dimensionless monthly-average tank temperatures provided by the TRNSYS simulations and those calculated using equation (3.6). The discrepancy is large as shown by a rms error for T_{tank}^* equal to 29.6 percent.

Three different variables are used to characterize the tank temperature in equation (3.4). When the system collects more energy, the solar fraction f increases as well as the monthly-average tank temperature T_t. The influence of the load demand is included in the coefficient Z, which is defined by the difference between the set temperature and the mains temperature for an open-loop system (equation 1.16). The tank capacity (C_S^*) is also of importance since the average temperature of the storage tank generally decreases with an increase in the tank volume (Section II.2.1).

Equation (3.4) has been used to correlate the monthly-average tank temperature with the variables described above. A curve fitting of the coefficients g,k and h leads to a rms error of 20.4 % (Table 3.1). The lowest rms error obtained for an equation using the same variables f, Z and C_S^* is 8.2 %.

To improve the correlation, another variable is needed to account for the influence of the time of the year on the monthly-average tank temperature. The variable Y defined by equation (3.7) has therefore been introduced. Y is defined by Beckman and Klein [11] in the f-chart method and is related to the ratio of the total energy absorbed on the collector plate surface to the total heating load during the month.

$$Y = \frac{N_m \overline{H}_T F_R(\overline{\tau\alpha}) A_c}{Q_{load}} \approx \frac{\text{Energy absorbed}}{\text{Load}} \qquad (3.7)$$

Different forms were tested and the one that represented the influence of Y the best is: $\{ 1 - \exp (a Y / f) \}^2$. The reason is that the ratio Y / f includes the influence of the ambient temperature through the term of the collector losses (or gains) as shown in equation (3.9).

$$f = \frac{Qu - Losses}{Q_{load}} = \frac{\text{Energy absorbed - Collector losses - Tank Losses}}{\text{Load}} \qquad (3.8)$$

$$\frac{Y}{f} = 1 - \frac{\text{Collector losses + Tank Losses}}{\text{Energy absorbed}} \qquad (3.9)$$

Different models have been tested to correlate the monthly-average tank temperature for the systems simulated with the variables f, Z, C_s^* and Y/f. Some models are shown in Table 3.1. The best rms error obtained was 7.07 % for equation (3.10). Figure 3.4 shows the comparison between the tank temperature obtained from TRNSYS and the tank temperature calculated with equation (3.10).

$$T_{tank}^* = (C_s^*)^a \{b\ f^2 + c\ f\ [\exp(d\,f) - 1]\ [1 - \exp(e\ Y/f)]^2\ Z^{-1}\} \qquad (3.10)$$

where:

a = - 0.21

b = 0.555

c = $3.88\ 10^{-3}$

d = 4.60

e = - 1.09

The largest limitation on the result of the proposed correlation comes from the remaining scatter when considering the variations of the tank temperature versus the solar fraction. Other variables than Y (ambient temperature...) would have to be introduced to improve the correlation if it is needed.

During an iteration step in the $\bar{\phi}$,fchart method, correlations provide Q_u and Q_{los}, which gives the value of Q_{aux} from the energy balance (3.11). An error on Q_{los} introduces an error on Q_{aux} and subsequently on f because the definition of the solar fraction (3.12) is used at each iteration to establish the value of f from Q_{aux}. The consequences of the combined errors in the correlations (losses, useful energy) on the solar fraction is investigated in Section III.4.

$$Q_u + Q_{aux} + \Delta Q_{stor} = Q_{load} + Q_{los} \qquad (3.11)$$

$$Q_{aux} = (1 - f)\ Q_{load} \qquad (3.12)$$

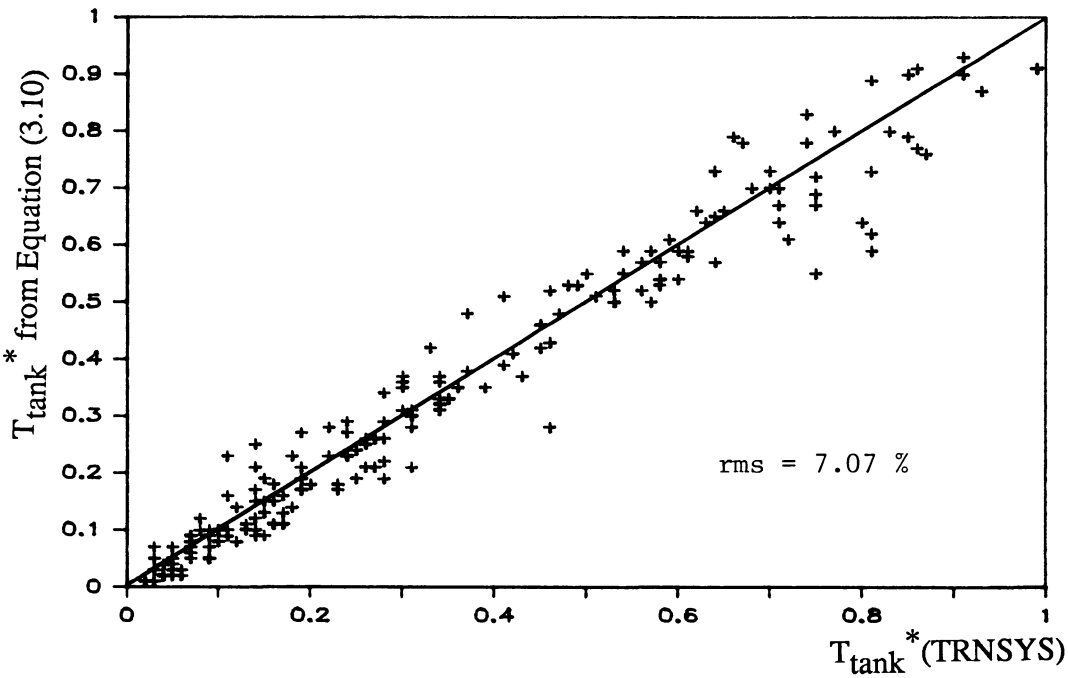

Figure 3.4 Comparison of the Dimensionless Monthly-Average Tank Temperature (T_{tank}^*) between TRNSYS and Equation (3.10)

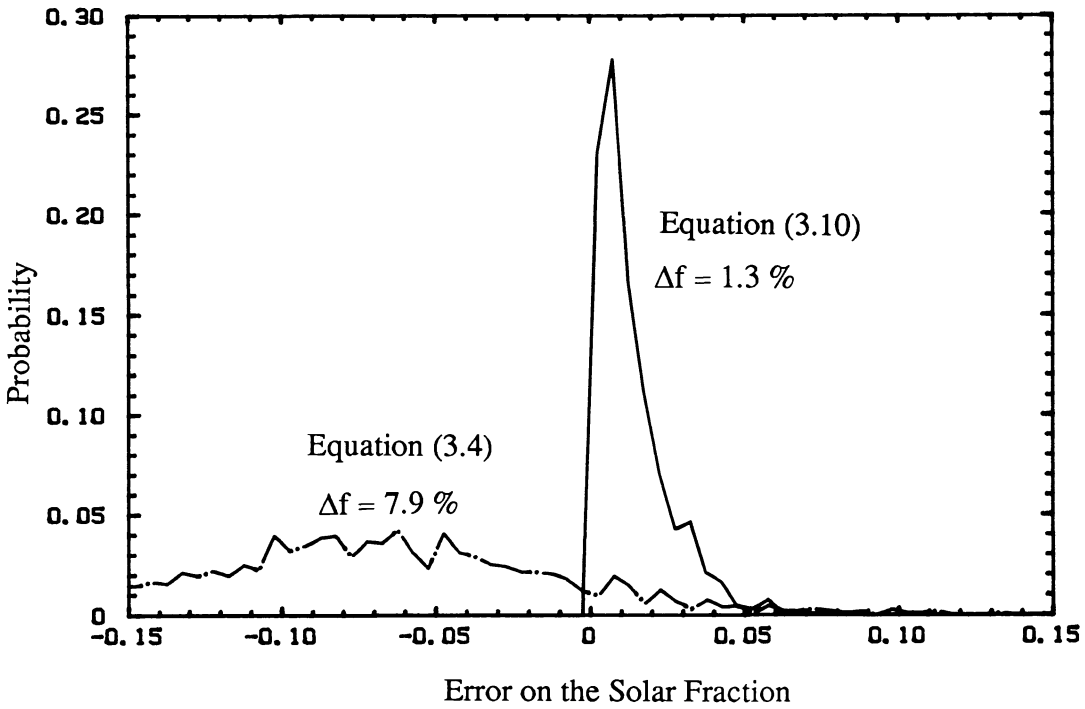

Figure 3.5 Probability Function of the Error on the Solar Fraction due to an Error on the Monthly-Average Tank Temperature when Using Equation (3.10)

The error made on the estimation of the tank temperature will result in errors on the tank losses. Since the losses generally represent a small fraction of the other energy quantities (solar radiation, load, auxiliary), the influence on the solar fraction of an error in the estimated tank temperature should be relatively small.

The error made on the losses and the resulting error on the solar fraction have then been investigated to determine the minimum level of accuracy needed for the correlation of the tank temperature. Figure 3.5 gives an idea of the probability distribution of the error induced on the solar fraction when using a correlation of the tank temperature. This figure results from comparisons made to determine $[Q_{los}(TRNSYS) - Q_{los}(Correlation)] / Q_{load}(TRNSYS)$ for a large number of systems simulated. Since the energy balance is verified both for TRNSYS and $\bar{\phi}$,fchart, ΔQ_{los} is equal to ΔQ_{aux} and furthermore equal to $\Delta f\ Q_{load}$. The number of occurrences in a given range of error was then divided by the total number of simulation to get an approximation of the probability distribution. Two correlations have been studied: the original equation for a fully-mixed tank (3.4), generated by Braun et al. [15] for a fully-mixed tank, and the proposed equation (3.10). The average error on the solar fraction resulting from this figure is 7.9 % for the original equation and 1.3 % for the new equation. This result is limited to systems with a tank loss coefficient of 1.5 W/C. If the loss coefficient is doubled, the error on Q_{aux} is doubled.

It was expected that the tank temperature be dependent on the tank loss coefficient. The direct influence was found to be small. Equation (3.10) was curve fitted for systems with different tank loss coefficients and the final rms error was 7.07 %. If the sample of simulations is reduced to systems with a same tank loss coefficient (1.5 W/C), the improvement remains limited (0.2%), which is the reason why no further modifications have been made to equation (3.10) to account for the tank loss coefficient. Even if the tank loss coefficient does not appear directly in the correlation for the tank temperature, it is implicitly already included in the solar fraction (Equations 3.11 and 3.12).

III.2.2 Final Correlation for the Monthly-Average Tank Temperature

The large rms error (7.07 %) found in the preceding chapter is partially explained by

the fact that no restrictions have been made on the data available from the simulations. After studying systems with solar fractions higher than 99% (stand-alone photovoltaic systems), Klein and Beckman [28] showed that systems with such solar fractions are very dependent upon the distribution of solar radiation and, as a result, have performance that can vary greatly from one ten year period to the next. Realistic performance estimates for these systems on this period were therefore not possible. It may be estimated from his study that monthly predictions for systems with solar fractions above 90% are illusive. The same equation as (3.10) has been curve fitted for a new set of data with systems whose monthly solar fraction is below 90%. The final rms error is 5.07 %. The correlation (3.13) is proposed to estimate the monthly-average temperature of a system with a flow rate of 10 kg/hr-m^2 and no mixing.

$$T_{tank}^{*} = (C_s^{*})^{a} \{b\ f^2 + c\ f\ [\exp(d\,f) - 1]\ [1 - \exp(e\ Y/f)]^2\ Z^{-1}\} \qquad (3.13)$$

where:

a = - 0.27

b = 0.542

c = $1.263\ 10^{-2}$

d = 3.40

e = - 0.922

The determination of the correlation for the useful energy gains in the next section will also be limited to solar systems with solar fractions lower than 90 %. Comparisons of the solar fraction predicted by TRNSYS and by the $\bar{\phi}$,f-chart method are made in Section III.4 for all solar fractions.

III.3 Correlation for the Monthly Useful Energy Gains (Qu)

III.3.1 Modification of the Equation for a Stratified System

The original equation for the monthly-average useful energy gain, Q_u, is given by:

$$Q_u = Q_{max} - a\ (\exp(b\,f) - 1\ )\ (\ 1 - \exp(c\ X)\ )\ \exp(d\ Z)\ Q_{load} \qquad (3.14)$$

where:

$$Q_{max} = A_c F_R(\overline{\tau\alpha}) N_m \bar{H}_T \bar{\phi}_{max} \quad \text{with} \quad \bar{\phi}_{max} = \bar{\phi}(I_{T,c\,min}) \tag{3.15}$$

$$I_{T,c\,min} = \frac{F_R U_L}{F_R(\overline{\tau\alpha})} (T'_{min} - \bar{T}_{amb}) \tag{3.16}$$

Coefficients a,b,c,d as well as the parameters X and Z are defined in Section I.3.2. For a stratified system, the definition of $\bar{\phi}_{max}$ has to be modified from the manner in which it was originally defined. The minimum collector inlet temperature to obtain a given solar fraction is no longer T'_{min} as it was the case for a fully-mixed tank. As stated in Section III.2, the collector inlet temperature may be as low as the temperature of the mains water if there is no recirculation. The lowest critical radiation level must thus be defined as:

$$I_{T,c\,min} = \frac{F_R U_L}{F_R(\overline{\tau\alpha})} (T_{mains} - \bar{T}_{amb}) \tag{3.17}$$

Another modification has to be included in the definition of Q_{max}. Comparisons were made between results of simulations for Q_u and calculated values of Q_{max} using equations (3.15) and (3.17). It was noted that the actual useful energy can be higher than the theoretical maximum calculated using equation (3.15) especially in the summer months.

The reason that Q_u can be greater than Q_{max} calculated using equation (3.15) results from the limiting value of $\bar{\phi}$. When the ambient temperature is higher than the mains temperature, $I_{T,c\,min}$ is negative and $\bar{\phi}_{max}$ is set equal to one. All the absorbed solar radiation is effectively collected since there are no thermal losses from the collector. But the temperature difference between the ambient air and the fluid in the collector can be a source of further gains. It is likely that the value of the collector loss coefficient U_L changes depending on the direction of the thermal energy flows because the thermal characteristics (convection loss coefficient...) on both sides of the collector glazing are asymmetrical. For simplicity it is assumed that U_L remains constant.

The thermal gains, called Q_u(therm), may occur during the night since the driving force is the temperature difference between the ambient air and the collector fluid. Q_{max}, as defined by equation (3.15), is only the maximum useful energy provided by the solar radiation and should thus better be called Q_{max}(rad). This correction was not really needed for a fully-mixed tank since T'_{min} is above the ambient temperature in

almost all cases.

Both energy terms are uncoupled since Q_{max}(rad) depends only on the solar radiation (including the thermal losses) and Q_{max}(therm) is the maximum amount of thermal energy gains. The form of the maximum useful energy is thus:

$$Q_{max}(tot) = Q_{max}(rad) + Q_{max}(therm) \qquad (3.18)$$

The first term, Q_{max}(rad) is defined in the same way as for the fully-mixed system; a form for the second term, Q_{max}(therm) is developed in the next section. An improved definition of Q_{max}, incorporating both the maximum possible radiation and thermal energy gains, improves the correlation of actual useful energy collection as shown later (Table 3.2).

III.3.2 Accounting for the Thermal Energy Gains.

The amount of thermal energy gains is a direct function of the collector loss coefficient. The less the collector is insulated from the outside, the higher the gains. When ambient temperatures lower than T_{mains} occur, the losses from the collector are already included in Q_u(rad) since $\bar{\phi}$ is determined from $I_{T,c\ min}$ which characterizes the amount of energy needed to overcome the losses.

$$Q_u(therm) = A_c\ F_R U_L \int_{month} (T_{amb} - T_{in,c})^+\ dN_{on} \qquad (3.19)$$

where N_{on} is the number of hours in the month when the collector is operating. N_{on} is a complex function of most of the internal parameters of the system as well as the external driving functions. The superscript "+" sign is used to indicate that only positive values of $(T_{amb} - T_{in,c})$ are considered; negative values are set to zero. The collector thermal losses are therefore not included in the definition of Q_u(therm).

The maximum possible value for Q_u(therm) is needed for the correlation of the useful energy. The collector inlet temperature may be as low as the mains temperature. Q_u(therm), defined by equation (3.19) is thus bounded on the upper side by:

$$\text{Upper Bound of } Q_u(therm) = A_c\ F_R U_L \int_{month} (T_{amb} - T_{mains})^+\ dN_{on} \qquad (3.20)$$

The next step in finding Q_{max}(therm) is to evaluate the integral in equation

(3.20). A first approach consists in considering that all the hours when T_{amb} is above T_{mains} are the source of possible gains. This method causes the gains to be overestimated because the effect of the controller deadbands is more sensitive to the amount of the thermal gains than it is for radiation gains. The reason is that the temperature difference involved (T_{amb} - $T_{in,c}$) is usually on the same order as the usual values of the controller deadbands. The effect of ΔT_{on} (Section II.2) is limited, but the effect of ΔT_{off} may be quite important as far as the as the thermal gains are concerned since this value determines how long the collector operates.

High values of ΔT_{off} force the pump to turn off when there is no solar radiation because the sum of the collector inlet temperature and ΔT_{off} becomes higher than the ambient temperature (which is the collector outlet temperature when there is no solar radiation). On the contrary, low values of ΔT_{off} may allow the pump to stay on during part or all of the night. As shown in Section II.2, the value of ΔT_{off} used in the data base (1.7 °C) is a medium value among existing differential controllers and ΔT_{off} has a limited effect on the performance of the system. Higher values than 1.7°C, however, may cause the useful energy gains to be overestimated by the design method if ΔT_{off} is not included in the equation for Q_{max}(therm).

An upper bound for the integral in equation (3.20) is equation (3.21) if we consider that the collector may be operating at all times when the ambient temperature is above the mains temperature plus ΔT_{off}. This approach depends on three assumptions since it does not account for:

- collector thermal capacitance effects
- the limitations in the pump-on time due to ΔT_{on} which causes overestimates of Q_{max}(therm)
- the thermal gains when the collector operates because of the solar radiation even if T_{amb} is lower than $T_{mains} + \Delta T_{off}$. This assumption causes Q_{max}(therm) to be underestimated especially when the ambient temperature is around the mains temperature, i.e. when thermal gains are not too important.

$$\text{Upper Bound of } Q_u(\text{therm}) = A_c \; F_R U_L \int (T_{amb} - T_{mains}) \; dN^0 \qquad (3.21)$$

where N^0 is the number of hours in the month when Tamb > Tmains + ΔT_{off}.

It is possible to directly evaluate the integral in equation (3.21) for the simulations

made with TRNSYS since the weather data are known hour by hour. This approach is used for the determination of Q_{max}(therm) along the process leading to the choice of a correlation for Q_u (i.e. in Section III.3). In this way, the influence of the method used to evaluate the integral (3.21) does not bias the correlation for Q_u.

A $\bar{\phi}$,fchart user has no access to hourly weather data and a method of estimating Q_{max}(therm) is needed. If the integral in equation (3.21) is broken in two parts (equation (3.22)), an existing correlation developed by Erbs [29] may be used.

$$Q_{max}(\text{therm}) = A_c F_R U_L \int (T_{amb}-T_{mains}-\Delta T_{off})^+ \, dN^0 + A_c F_R U_L \int \Delta T_{off} \, dN^0$$

$$= 24 \; A_c \; F_R U_L \; (CDD_b \; + \Delta T_{off} \; N^0) \qquad (3.22)$$

The significance of each one of the integrals developed in equation (3.22) may be visualized with Figure 3.6.

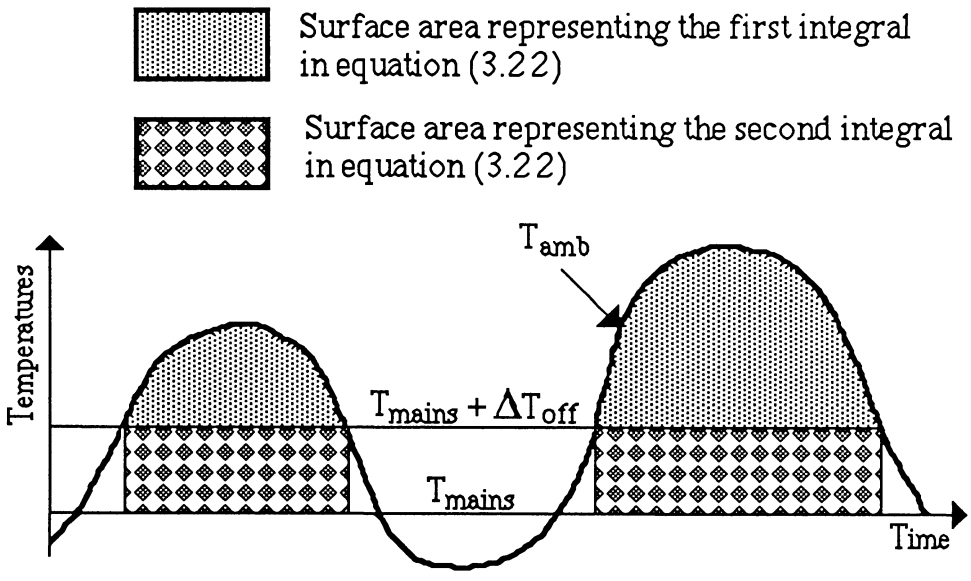

Figure 3.6 Physical significance of the integrals in equation (3.22)

The term CDD_b represents the cooling degree-days in a month for a base temperature of $T_{mains} + \Delta T_{off}$ and may be evaluated using the correlation (3.24)

developed by Erbs [29].

$$T_b = T_{mains} + \Delta T_{off} \tag{3.23}$$

$$CDD_b = \sigma_m \, (N_m)^{\frac{3}{2}} \left[\frac{h^*}{2} + \frac{\ln(\cos(1.698\, h^*))}{3.396} + 0.2041 \right] \tag{3.24}$$

where:

h^* is a dimensionless number defined by equation (3.25)

N_m is the number of days in the month considered.

σ_m is the standard deviation of the monthly-average temperature and is calculated with equation (3.26) using σ_{yr} the standard deviation of the monthly-average temperatures from the annual average temperature.

$$h^* = (\bar{T}_{amb} - T_b) / (\sqrt{(N_m)}\, \sigma_m) \tag{3.25}$$

$$\sigma_m = 1.45 - 0.0290\, \bar{T}_{amb} + 0.0664\, \sigma_{yr} \tag{3.26}$$

$$\sigma_{yr} = \sum_{i=1}^{12} [\, \bar{T}_{amb}(i) - \bar{T}_{amb}(year) \,] / 11 \tag{3.27}$$

N^0 is determined from Erbs' results with the following equation.

$$N^0 = N_m \, [\, 1 + \exp(-3.396\, h^*) \,]^{-1} \tag{3.28}$$

The final definition of Q_{max}(therm) that will be used in the proposed $\bar{\phi}$,f-chart method and in sections following Section III.3 is thus equation (3.29). This expression of Q_{max}(therm) is bounded between zero (as U_L approaches zero) and $M_c\, C_p / A_c$ (as U_L approaches infinity).

$$Q_{max}(therm) = A_c \; F_R U_L \; 24 \; (CDD_b + \Delta T_{off} \; N^0) \tag{3.29}$$

The values of Q_{max}(therm) from equation (3.22), i.e. from a direct calculation from the hourly weather data of TMY and equation (3.29) have been compared in Figure 3.7 for a collector area of 4 m^2 and a value of $F_R U_L$ equal to 4.7 W/m^2-°C.

The resulting rms error of 0.58 % shows the good agreement of the correlation used (Erbs [29]) in the evaluation of equation (3.22)

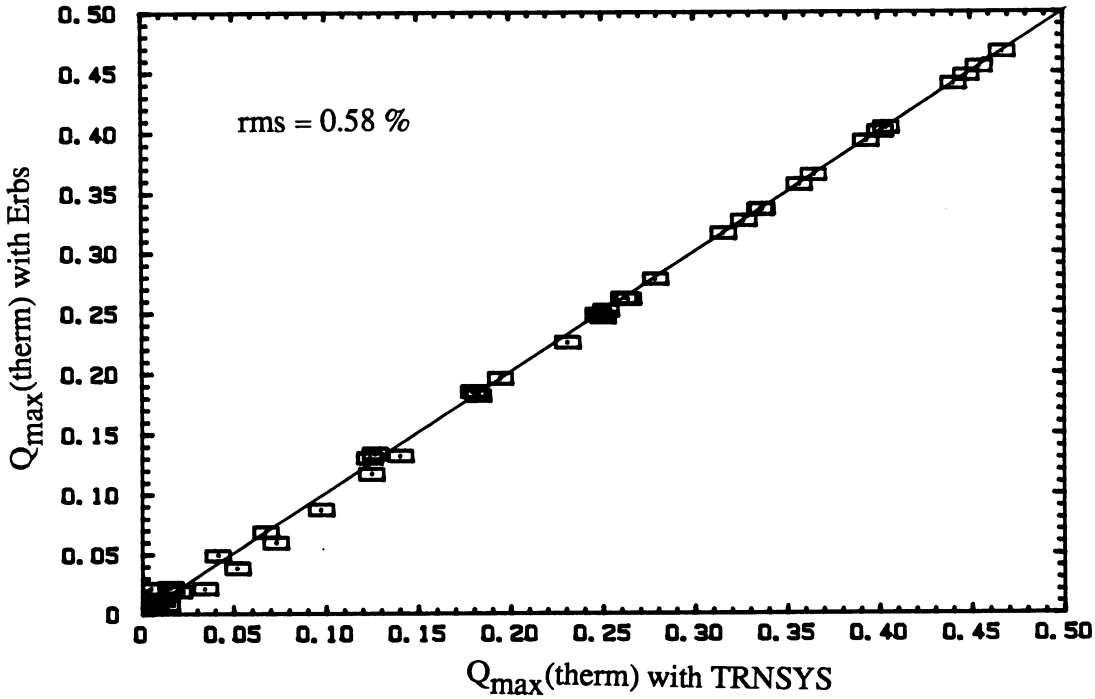

Figure 3.7 Comparison of Qmax(therm) predicted by Equation (3.22), i.e., Direct Calculation from TRNSYS and by Equation (3.29), i.e., with Erbs' Correlation, for Madison, Albuquerque, Seattle and Miami

III.3.3 Comparison between the Different Types of Useful Energy Gains

The relative importance of Q_{max}(therm) vs Q_{max}(rad) has been calculated for months where Q_{max}(therm) is positive, i.e. $\bar{\phi}_{max} = 1$ ($I_{T,c\ min} < 0$) thus:

$$\frac{Q_{max}(therm)}{Q_{max}(rad)} = \frac{F_R U_L}{F_R(\overline{\tau\alpha})} \frac{\int (T_{amb} - T_{mains})^{+} dN^{0}}{\int \bar{I}_T\, dt} \qquad (3.30)$$

To estimate the order of magnitude of the thermal gains, the ratio of the maximum energy gains defined in equation (3.30) has been calculated for two different collector types:

- "Low Quality" Collector, $F_R U_L$ = 8.6 W/m^2-°C and $F_R(\overline{\tau\alpha}) = 0.70$
- "High Quality" Collector, $F_R U_L$ = 3.6 W/m^2-°C and $F_R(\overline{\tau\alpha}) = 0.75$

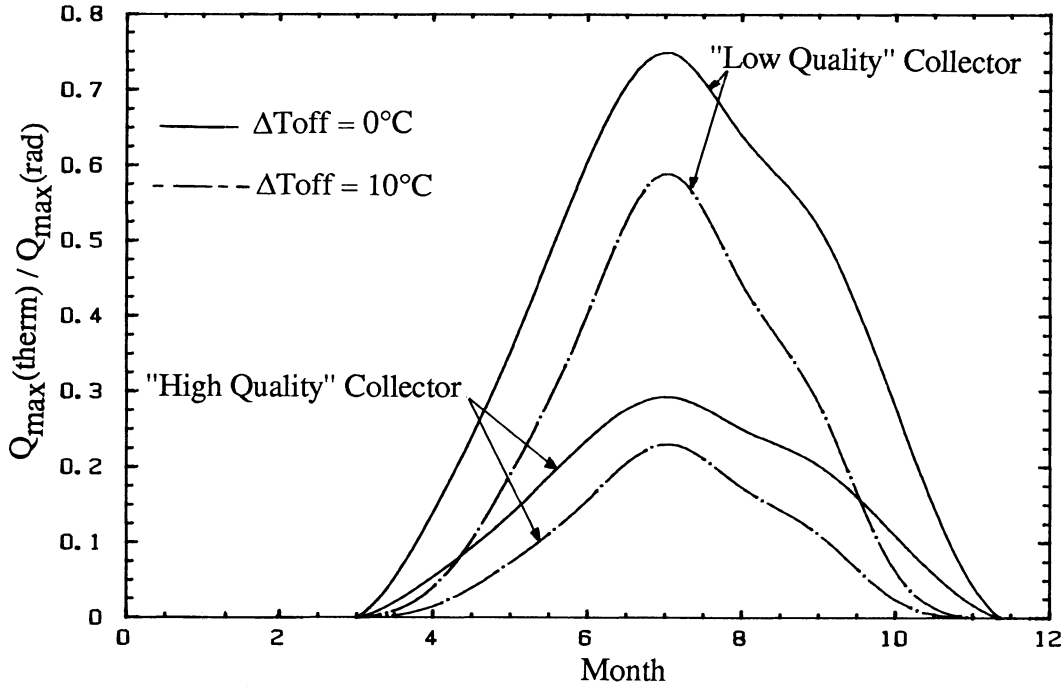

Figure 3.8 Dependence of the Ratio of the Maximum Thermal Gains Divided by the Maximum Radiation Gains on the Time of the Year in Madison, for Two Different Collectors and Two Different Turn Off Deadbands (ΔToff).

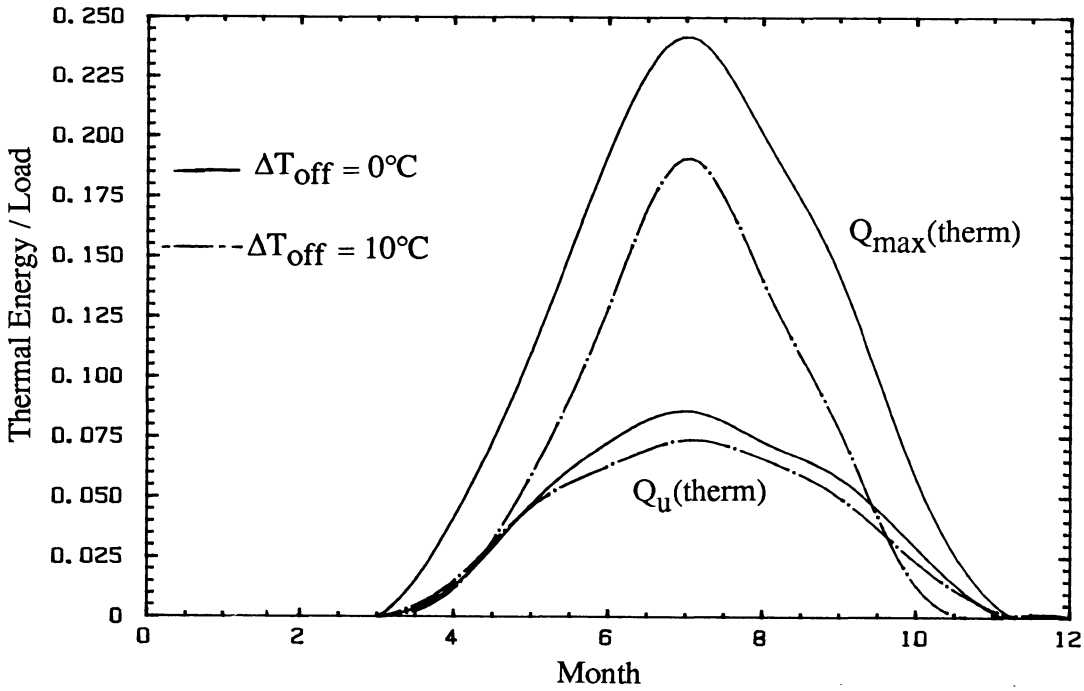

Figure 3.9 Comparison of the Maximum Amount of Thermal Gains and the Actual Thermal Gains for a "High Quality" Collector in Madison and Two Different Turn Off Deadbands.

and two radically different values of ΔT_{off}, 0°C and 10°C. The ratio of Q_{max}(therm) by Q_{max}(rad) has then been plotted in Figure 3.8 for each month of the year in Madison. Results from Figure (3.8) do not reflect the actual thermal gains since Q_{max}(therm), by definition, is only an upper bound for the thermal gains. When the ambient temperature is high, the actual radiation gains are close to the maximum value of Q_{max}(rad) but the actual thermal gains are only a fraction of Q_{max}(therm). The three approximations made in the definition of Q_{max}(therm) usually have a little effect on the collected energy, Q_{max}(therm) is therefore the amount of thermal gains that would be collected if the collector inlet temperature were equal to the mains temperature during all the month.

A system with the "High Quality" collector described above has been simulated for the same values of ΔT_{off}. Whenever the collector was operating in the simulation, the thermal gains to the collector ($A_c F_R U_L K_{\tau\alpha} (T_{amb} - T_{in,c})^+$) were summed, which allows a comparison between Q_{max}(therm) and the actual values of Q_u(therm) in Figure 3.9. It can be seen from this example that the value of Q_{max}(therm) provides an upper bound for the thermal gains. The actual thermal gains are even greater than Q_{max}(therm) for the month of October due to the approximation made, i.e. Q_{max}(therm) does not account for the thermal gains when the collector operates and when T_{amb} is lower than $T_{mains} + \Delta T_{off}$. This problem is however limited to certain months when the thermal gains are not important and for values of ΔT_{off} beyond the usual range.

III.3.4 Correlation for the Monthly Useful Energy Gains (Qu)

The general form of the correlation for the useful energy is the following:

$$Q_u = Q_{max}(tot) - Q_{corr} = Q_{max}(rad) + Q_{max}(therm) - Q_{corr} \quad (3.31)$$

The first term Q_{max}(tot) is the maximum energy that could be collected by the solar system. The second term Q_{corr} corrects for the fact that the energy is not always collected with a collector inlet temperature equal to the mains temperature. The correction also implicitly includes the influence of the assumptions made when establishing the definition of Q_{max}(therm), i.e., the small influence of the collector capacities and ΔT_{on} and the thermal energy not accounted for in Q_{max}(therm).

III.3.4.1 Parameters upon which Q_{corr} Depends

- The higher the fraction of the load that is met by solar energy, the higher the average collector inlet temperature and the larger the correction term.
- As the storage capacity increases, recirculation decreases, the collector inlet temperature approaches the mains temperature and the useful gain approaches a maximum.
- X, as defined by equation (3.32) is proportional to the collector loss coefficient and is a measure of the sensitivity of the system performance to the collector inlet temperature ($T_{in,c}$).

$$X = A_c \, F_R U_L \, (100°C) \, \Delta t \, / \, Q_{load} \qquad (3.32)$$

When thermal losses are considered, a correction has to be made on Q_{max}(rad). For X equal to zero, the correction term Q_{corr} must be equal to zero because the collection of solar radiation is independent of the collector inlet temperature and the thermal losses. As $F_R U_L$ increases, the correction increases.

The value of Q_{max}(therm) overestimates the thermal gains because the collector inlet temperature is above the mains temperature. A correction has thus to be included in Q_{corr} to account for this influence. The higher $T_{in,c}$, the lower the percentage of thermal energy collected. But an increase in the thermal energy collected causes an increase in $T_{in,c}$ since a part of this energy might be dumped and stored in the tank. A parameter needs to be introduced in the correlation to characterize the value of the actual thermal gains. This parameter is a function of both the collector loss characteristics and the ambient temperature. Using the monthly-average ambient temperature is not a good choice since the performance of the system depends on the ambient temperature only when the collector is operating. The dimensionless parameter T_{amb}^* defined in equation (3.33) is better because it is directly proportional to Q_{max}(therm) and does not depend on the collector parameters. The product (X T_{amb}^*) is equal to Q_{max}(therm) divided by the load and represents the amount of the thermal gains.

$$T_{amb}^* = (CDD_b + \Delta T_{off} \, N^0) \, / \, (N_m \, (100°C)) \qquad (3.33)$$

When more thermal gains are collected, T_{amb}^{*} (equation 3.33) and $T_{in,c}$ increase. The correction term must increase also.

- There are periods when the the temperature of hot water that can be delivered by the solar system is at a higher temperature than required by the load. During these periods, energy delivery must be tempered in some way. For a water heating system, the common solution is the use of a mixing valve (so that the water delivered remains at T_{set}). Energy tempering results in higher energy storage temperatures during the hours of energy collection than if the same amount of water were removed at the storage temperature. Especially for a system that meets a high fraction of the load, tempering results in an increase of the collector inlet temperature (for the same energy supplied to the load). The main parameter that determines the degree of tempering is the nature of the load requirement. For a particular solar fraction, the difference between Q_u and Q_{max}(tot) will be greater for a system that must temper delivered energy more often. To include this effect in the $\bar{\phi}$,fchart method and make the procedure general for both open-loop and closed-loop systems, a dimensionless parameter Z has been defined by Braun et al [15] as:

$$Z = Q_{load} / (C_L' (100°C)) = (T_{set} - T_{mains}) / (100°C) \qquad (3.34)$$

For an open-loop system water heating system, C_L' is the product of the monthly mass of water usage and the specific heat C_p. Z is thus equal to the second expression given in equation (3.34).

III.3.4.2 Equation for the Monthly Useful Energy Gains

The use of the original equations (3.14) through (3.16) with the coefficients developed for a fully-mixed tank results in a rms error of 28.7 % (Table 3.2) which gave the original incentive to improve the correlation for a stratified system. The same equation with the coefficients curve fitted by non-linear regression makes the rms error drop drastically down to 5.1 % on a monthly basis. The correlation can be improved further as illustrated in Table 3.2. In a first step, Q_{max} is replaced by Q_{max}(rad) (definition given in equations 3.8 and 3.10), which leads to a rms error of 5.7 %. The addition of Q_{max}(therm), whose definition is given in equation (3.29) improves the results of the

TABLE 3.2 Different Models for the Useful Energy Gains and rms Errors

Different Models for $\frac{Q_{useful}}{Q_{load}}$	r.m.s. in percent
(0) $Q^{0}_{max}(rad) - 0.015\,(Cs^{*})^{-0.76}[\exp(3.85\,f) - 1]\;[1 - \exp(-0.15\,X)]\;\exp(-1.959\,Z)$	28.64
(1) $Q^{0}_{max}(rad) - 0.082\,(Cs^{*})^{0.15}[\exp(1.307\,f) - 1]\;[1 - \exp(-1.53\,X)]\;\exp(1.70\,Z)$	5.10
(2) $Q_{max}(rad) - 2.742\,10^{-3}\,(Cs^{*})^{-1.33}[\exp(5.197\,f) - 1]\;\exp(-0.3577\,Z)\;X$	5.71
(3) $Q_{max}(tot) - 9.341\,10^{-5}\,(Cs^{*})^{-0.78}[\exp(5.895\,f) - 1]\;\exp(2.80\,Z)\;X$	4.21
(4) $Q_{max}(tot) - 2.825\,10^{-4}\,(Cs^{*})^{-0.67}[\exp(4.848\,f) - 1]\;\exp(2.06\,Z)\;X\;[1 + 1.30\,X\,T^{*}_{amb}]$	3.82
(5) $Q_{max}(tot) - 2.874\,10^{-4}\,(Cs^{*})^{-0.67}[\exp(4.653\,f) - 1]\;\exp(1.91\,Z)\;X\;[1 + (1.30\,X\,T^{*}_{amb})^{\frac{1}{4}}]$	3.16

(0) is the equation for the useful energy when the tank is fully mixed

correlation, the rms error dropping to 4.2 %. The addition of the parameter T_{amb}^* leads to a rms error of 3.16 %. The final equation is the following:

$$Q_u = Q_{max}(tot) - \alpha\ (Cs^*)^{\beta}\ [\exp(\gamma f) - 1]\quad \exp(\delta Z)\ [1 + (\varepsilon X T_{amb}^*)^{\lambda}] \qquad (3.35)$$

where:

$\alpha = 2.874\ 10^{-4}$

$\beta = -0.67$

$\gamma = 4.653$

$\delta = 1.91$

$\varepsilon = 1.30$

$\lambda = 0.25$

and

$$Q_{max}(tot) = Q_{max}(rad) + Q_{max}(therm) \qquad (3.18)$$

$$Q_{max}(rad) = A_c\ F_R(\overline{\tau\alpha})\ N_m\ \overline{H}_T\ \bar{\phi}_{max} \quad \text{with} \quad \bar{\phi}_{max} = \bar{\phi}\ (I_{T,c\ min}) \qquad (3.15)$$

$$I_{T,c\ min} = \frac{F_R U_L}{F_R(\overline{\tau\alpha})}\ (T_{mains} - \overline{T}_{amb}) \qquad (3.17)$$

$$Q_{max}(therm) = A_c\ F_R U_L\ 24\ (CDD_b + \Delta T_{off}\ N^0) \qquad (3.29)$$

Following the recommendations made in Section III.2.4, only systems with solar fractions lower than 90 percent have been taken into account for the curve fitting. The use of equation (3.34) to evaluate the energy collected for systems with a solar fraction between 90 and 100 percent leads to a rms error of 6.2 percent. Figures 3.10 (solar fraction below 90%) and 3.11 (solar fraction between 90 and 100 %) compare the monthly useful energy given by TRNSYS and calculated from equation (3.35).

III.3.5 Influence of the Location

A limited number of systems have been simulated in three other cities to investigate the influence of the location. The climates of Seattle, Albuquerque and Miami give a wide range of meteorological situations. Equation (3.35) leads to the following rms errors,

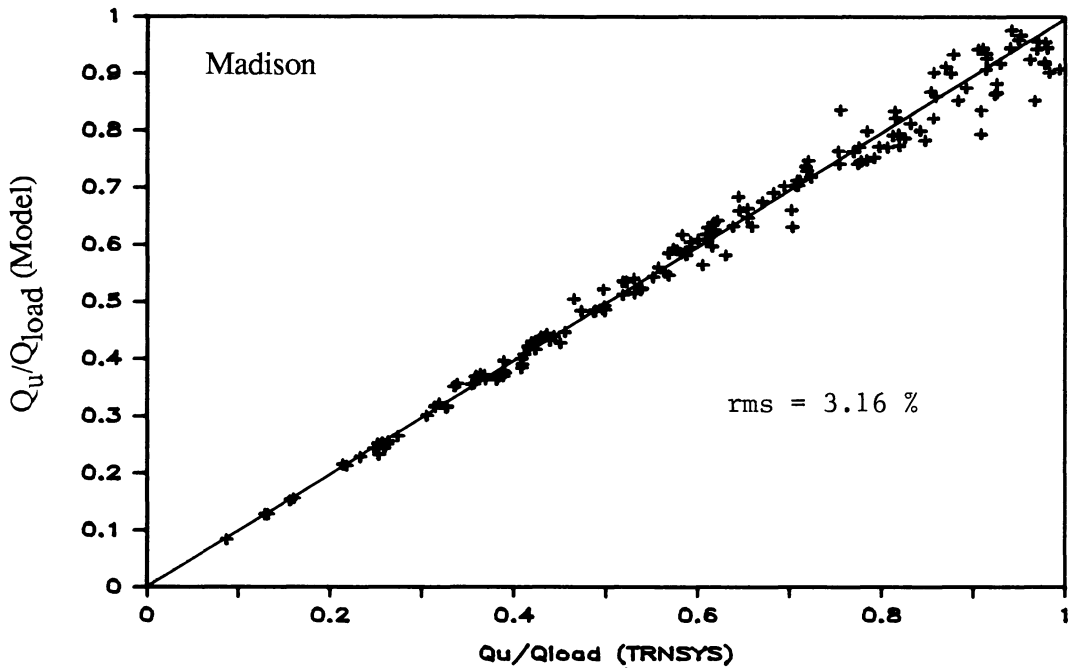

Figure 3.10 Comparison of the Dimensionless Monthly-Average Useful Energy Collected (Q_u/Q_{load}) between TRNSYS and the Proposed Model for Systems with a Solar Fraction Below 90 %

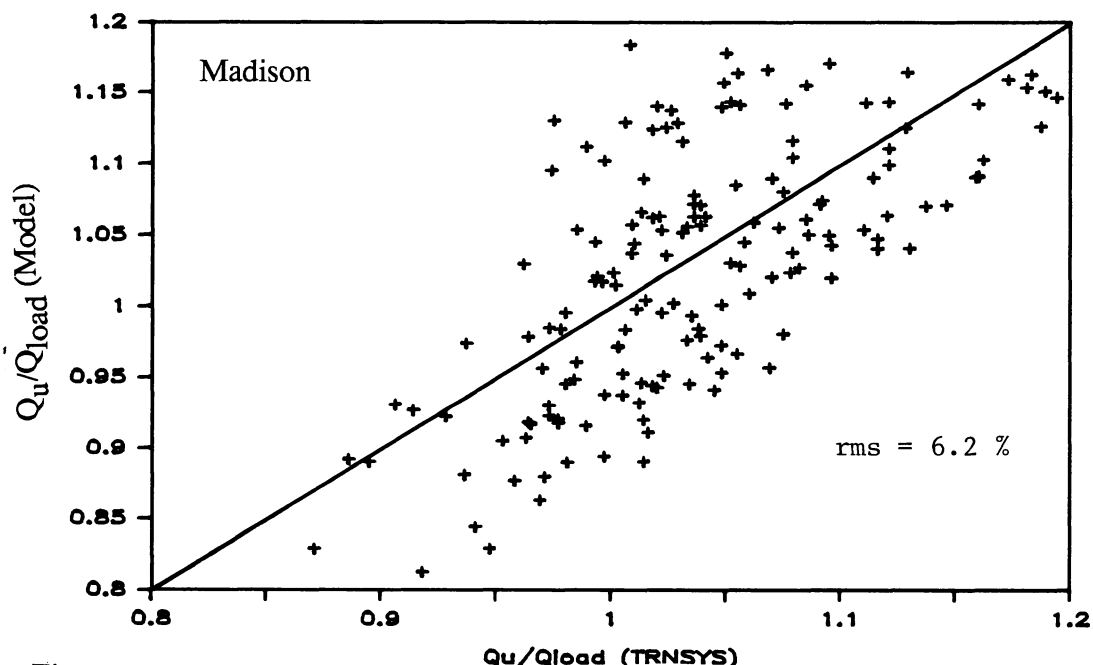

Figure 3.11 Comparison of the Dimensionless Monthly-Average Useful Energy Collected (Q_u/Q_{load}) between TRNSYS and the Proposed Model for Systems with a Solar Fraction Above 90 %

1.8% for Seattle, 4.1% for Albuquerque and 2.4% for Miami when compared to the useful energy from TRNSYS (Figure 3.12). The general trend for Albuquerque is to underestimate the useful energy. A constant ambient temperature is used in the determination of $\bar{\phi}_{max}$. In Albuquerque, the ambient temperature variations are actually large which results in higher ambient temperatures during the day than what has been assumed and therefore less collector losses. The hourly variations of the ambient temperature will be included in the algorithm to calculate Q_{max}(rad) in Section III.4. It will be shown that the error on the estimate of the solar fraction by the design method for Albuquerque is reduced and closer to the error of the solar fraction for Madison.

III.3.6 Influence of Boiling

The energy that would have discarded with a overheat prevention valve (Q_{boil}) has been summed for each month and for each system. It is found that for 96 % of the systems simulated, Q_{boil} is less than 0.5 % of the load. Boiling should therefore be neglected with respect to the other energy quantities.

III.4 Comparisons of the Solar Fraction Between TRNSYS and the Developed Procedure

The comparison of the solar fraction between the results of the simulation from TRNSYS and the results from the $\bar{\phi}$,f-chart method should be made before and after introducing each algorithm used in the $\bar{\phi}$,f-chart method. In this way, the error due to each algorithm can be individually determined.

III.4.1 Influence of the Correlations for the Monthly-Average Tank Temperature and the Monthly Useful Energy Gains on the Solar Fraction

Comparisons of the solar fraction are made between TRNSYS and the model when only the two correlations needed to calculate the monthly-average tank temperature and the useful energy gains are used in the $\bar{\phi}$,f-chart method. The determination of $\bar{\phi}$, H_T and $(\overline{\tau\alpha})$ is made with the methods used in the preceding sections and described in Section III.1. The monthly-average ambient temperature ($\overline{T}_{amb}$) and the monthly -average solar radiation on a horizontal surface ($\overline{H}$) are also directly determined from TRNSYS. The determination of the cooling degree days (CDD_b) and of the weather

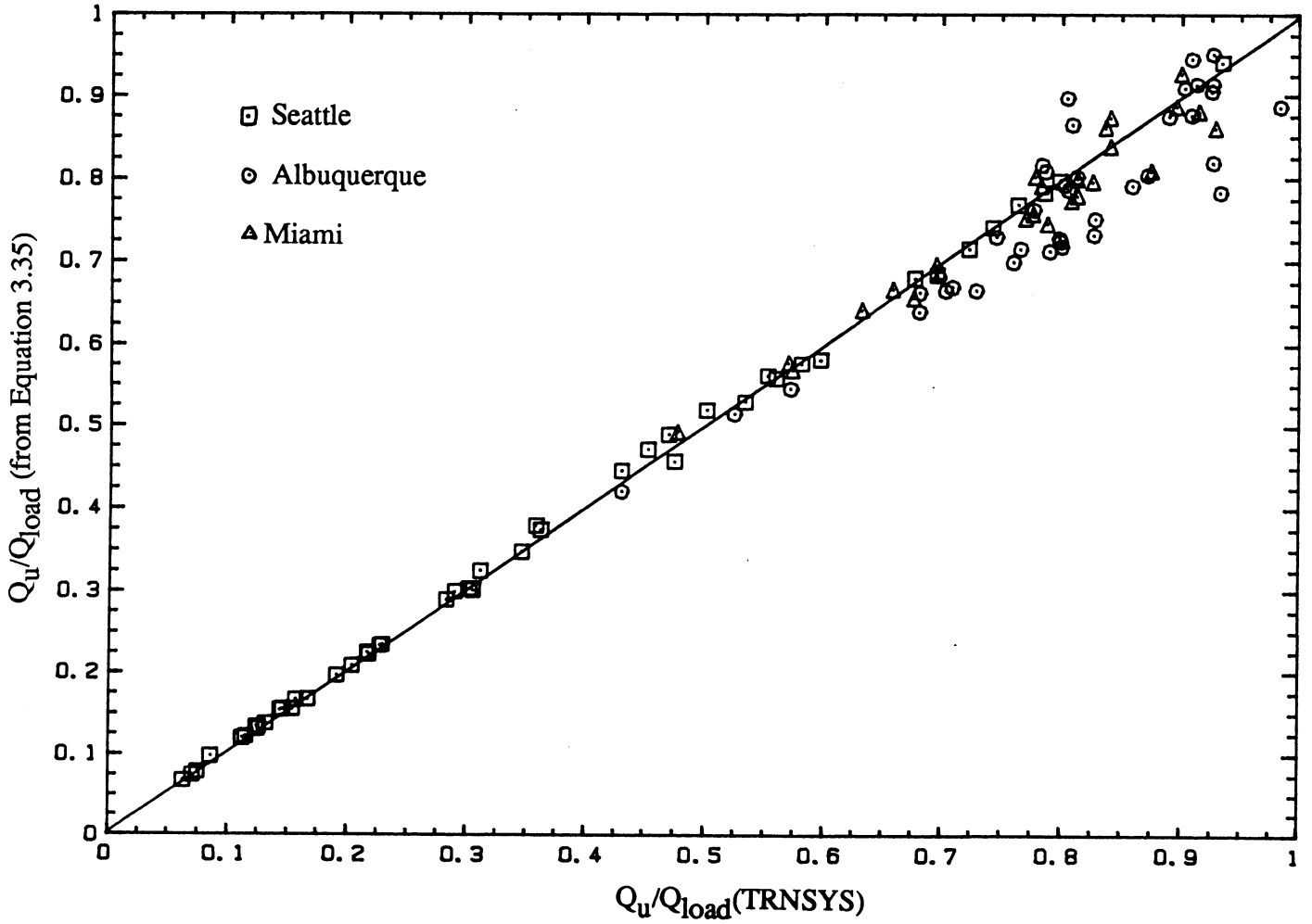

Figure 3.12 Comparison of the Monthly Useful Energy Gains predicted by TRNSYS and by Equation (3.35) in Madison for Different Locations

variable N^0 is made by directly using the TMY weather data.

The monthly and yearly solar fractions predicted by TRNSYS have been compared to the solar fractions predicted by the model developed in Chapter III for different locations. The results of the rms errors are indicated in Table 3.3 in column 3 (rms direct) and in Figures 3.13 through 3.19.

TABLE 3.3

LOCATION	PERIOD	rms (in %) direct	rms (in %) Clark	rms (in %) Final
Madison	month	2.07	2.21	3.37
	year	0.98	0.97	1.53
Seattle	month	1.71		3.76
	year	1.01		2.02
Albuquerque	month	4.12		4.08
	year	3.27		3.09
Miami	month	1.89		2.53
	year	1.39		1.53

Table 3.3 Values of the rms errors for the comparison of the solar fraction between TRNSYS and the Model

As a means of comparison, the yearly solar fraction has been calculated for Madison with the correlations used in the original $\bar{\phi}$,f-chart method (developed for a fully-mixed tank [15]). The result has been compared in Figure 3.17 with the solar fraction of the stratified system predicted by TRNSYS. The underestimate of the solar fraction by the original design method results in a rms error of 18.7 %.

III.4.2 Influence of the Correlation for the Cooling Degree-Days

The use of Erbs' correlations to determine Q_{max}(therm) (from Equation 3.29) and T_{amb}^* (from Equation 3.33) does not produce any changes in the estimates of the

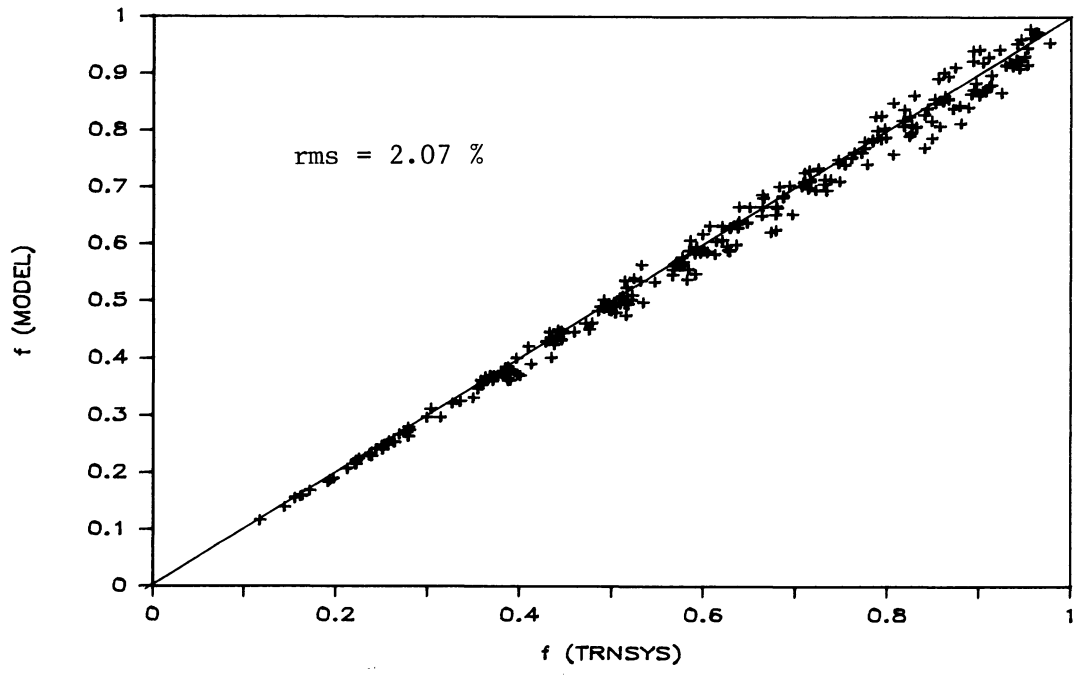

Figure 3.13 Comparison of the Monthly Solar Fraction predicted by TRNSYS and by the Model (Section III.4.1) in Madison, WI

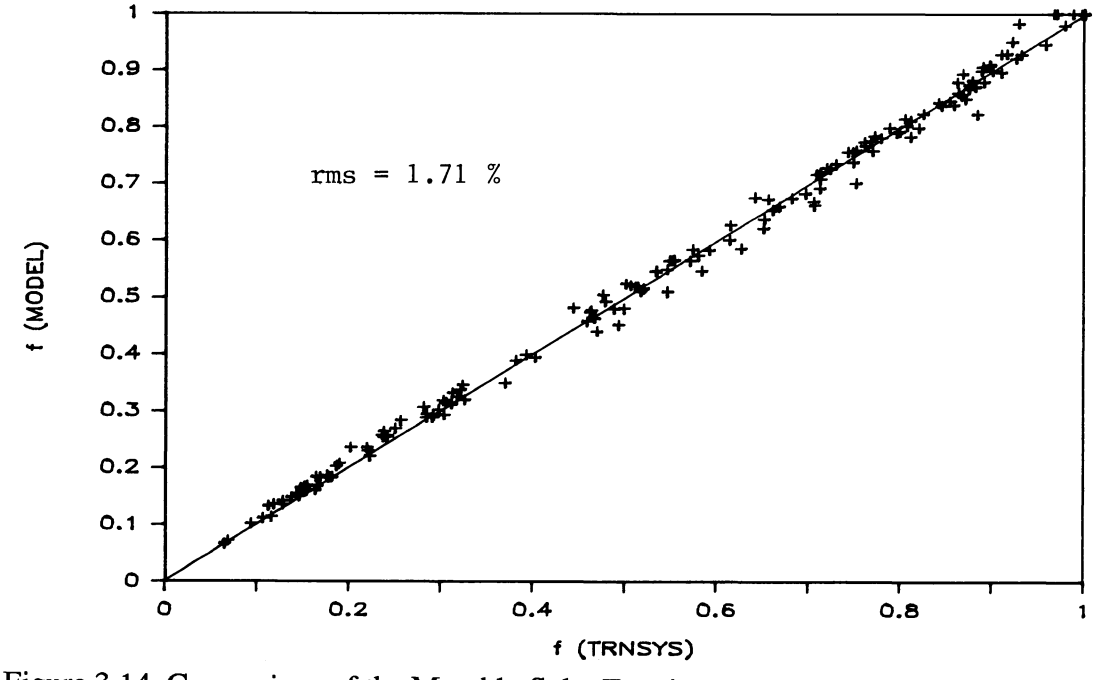

Figure 3.14 Comparison of the Monthly Solar Fraction predicted by TRNSYS and by the Model (Section III.4.1) in Seattle, WA

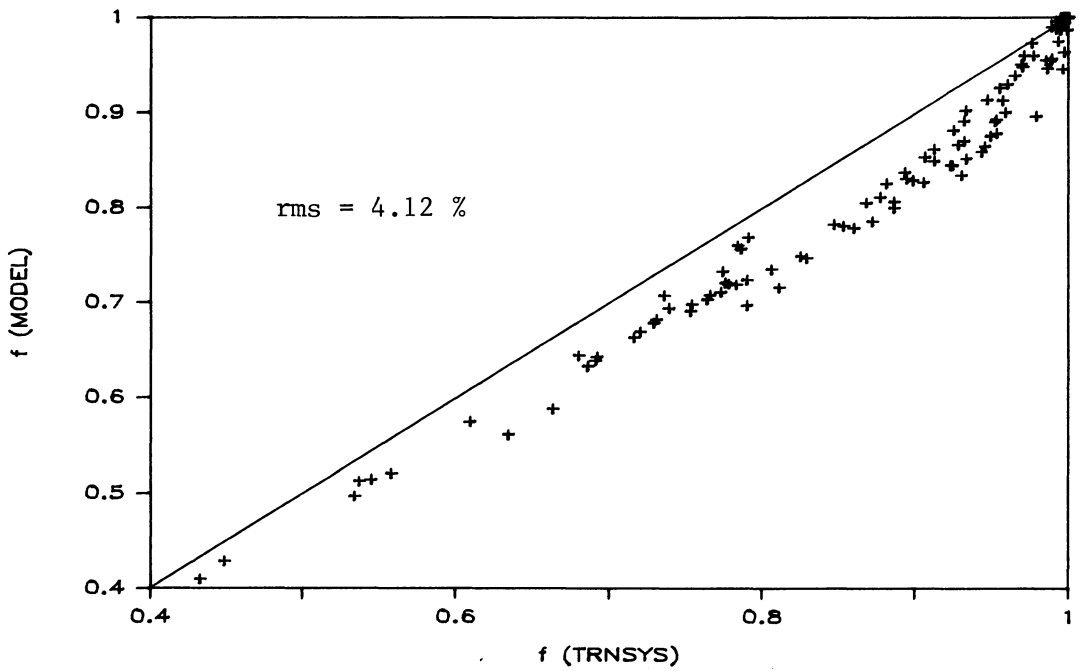

Figure 3.15 Comparison of the Monthly Solar Fraction predicted by TRNSYS and by the Model (Section III.4.1) in Albuquerque, NM

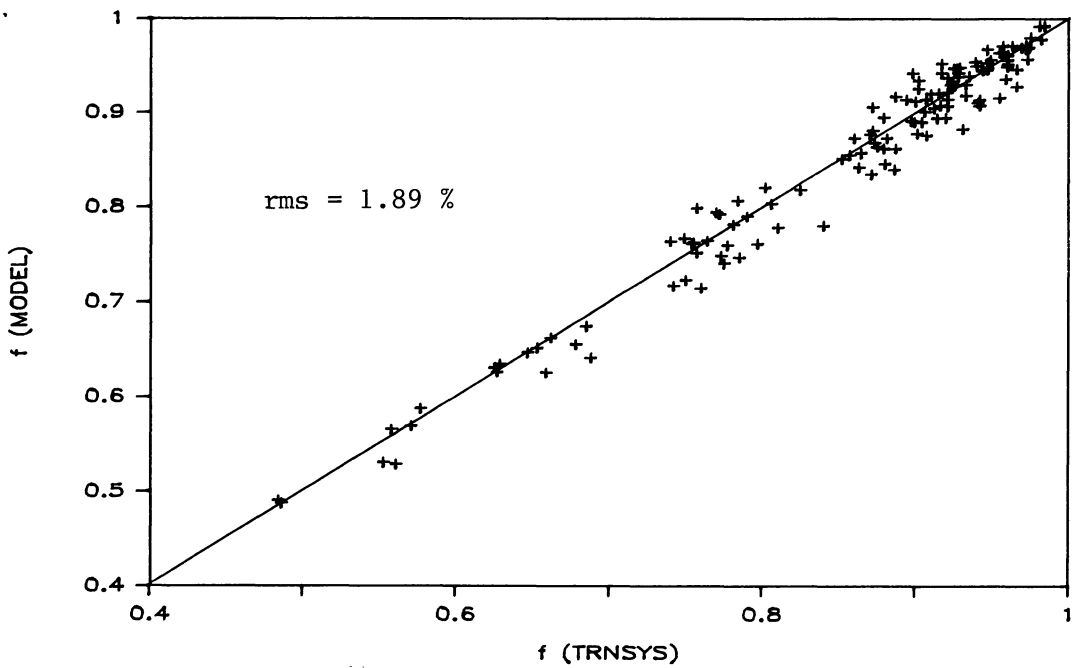

Figure 3.16 Comparison of the Monthly Solar Fraction predicted by TRNSYS and by the Model (Section III.4.1) in Miami, FL

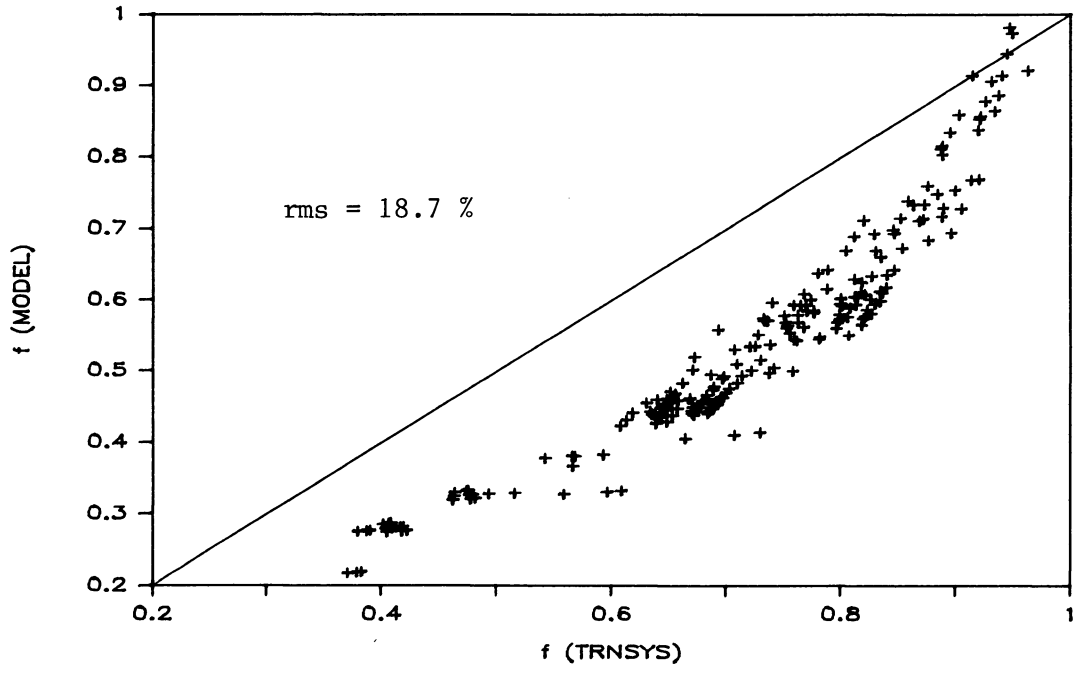

Figure 3.17 Comparison of the Yearly Solar Fraction predicted by TRNSYS and by the Original Model (Fully-Mixed Tank) in Madison

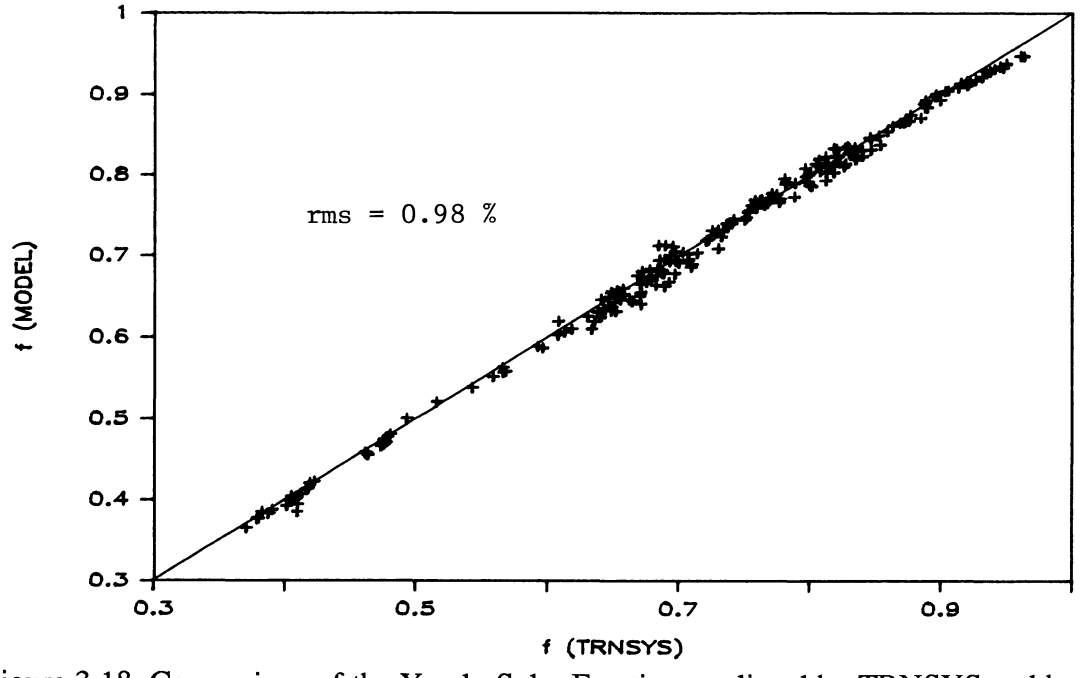

Figure 3.18 Comparison of the Yearly Solar Fraction predicted by TRNSYS and by the Model (Section III.4.1) in Madison

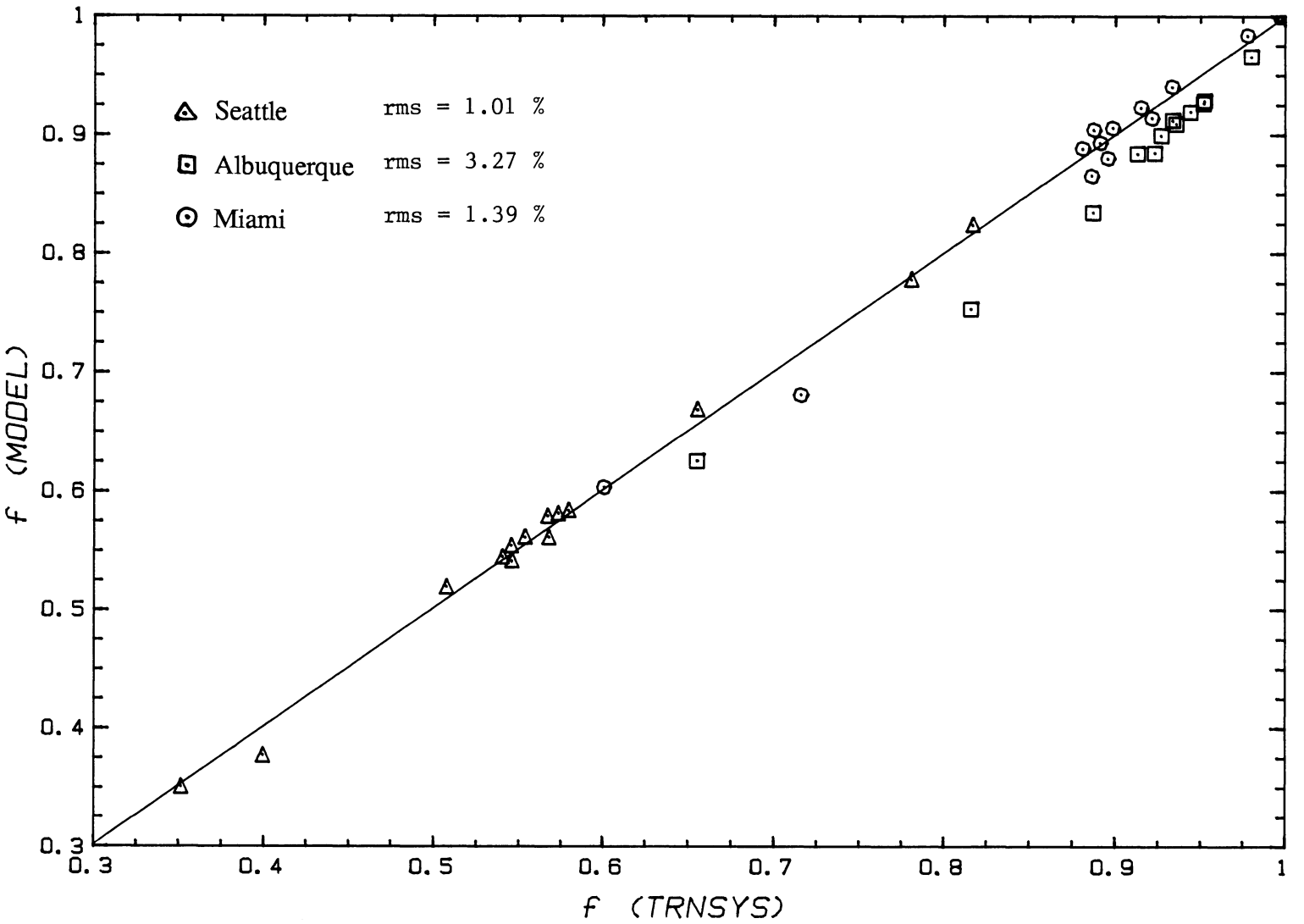

Figure 3.19 Comparison of the Yearly Solar Fraction predicted by TRNSYS and by the Model (Section III.4.1) for Different Locations

solar fraction by the $\bar{\phi}$,f-chart method when compared to a direct calculation of Q_{max}(therm) and T_{amb}^{*} from the weather data . The reason is the particularly good agreement of the correlation with the weather data used, as shown in Figure 3.7. The comparisons in the next sections are made with the algorithm developed by Erbs to calculate the cooling degree days (CDD_b) and N^0.

III.4.3 Influence of the Determination of $\bar{\phi}$

The monthly-average hourly utilizabilities $\tilde{\phi}$ are calculated with the following algorithm developed by Clark et al. [8].

$$\tilde{\phi} = \begin{cases} 0, X_c > X_m \\ (1-X_c/X_m)^2, X_m = 2 \\ | \, |a| - [a^2 + (1+2a)\,(1-X_c/X_m)^2]^{0.5} \, | \quad \text{otherwise} \end{cases} \tag{3.36}$$

and

$$a = (X_m - 1) / (2 - X_m) \tag{3.37}$$

$$X_m = 1.85 + 0.169\,\tilde{R}/\tilde{k}^2 - 0.0696\,(\cos\beta)/\tilde{k}^2 - 0.981\,\tilde{k}/(\cos\delta)^2 \tag{3.38}$$

where:

X_c = critical ratio (ratio of the critical radiation level ($I_{T,c}$) to the monthly-average hourly radiation on the collector)

$\tilde{k}$ = monthly-average hourly clearness index ($\bar{I}/\bar{I}_0$)

$\tilde{R}$ = $\bar{I}_T/\bar{I}$

δ = declination

β = slope of collector surface

$\bar{\phi}$, the monthly-average daily utilizability is then calculated from the monthly-average hourly utilizabilities $\tilde{\phi}$ with equation (3.39) .

$$\bar{\phi} = \frac{\sum_{Day} \bar{I}_T \tilde{\phi}}{\sum_{Day} \bar{I}_T} \tag{3.39}$$

The values of X_c, $\tilde{k}$, $\tilde{R}$ and $\bar{I}_T$ have been provided by TRNSYS. This avoids the need for other algorithms, which would result in additional errors independently of the method above. Using the correlations developed for the monthly-average tank temperature (T_t) and the monthly-average energy gains (Q_u), the solar fraction has then been determined for each system in Madison. A comparison with the results from TRNSYS leads to a rms error of 2.21 % for the monthly solar fraction and 0.97 % for the yearly solar fraction. These results are shown in column 4 (rms Clark) of Table 3.3. The influence of the algorithm to calculate $\bar{\phi}$ is small, the rms error of the monthly solar fraction increases by 0.14 % and the rms error of the yearly solar fraction is almost exactly the same (decrease by 0.01 %). This algorithm is therefore used to calculate the monthly-average utililizability in the design method developed in this chapter.

III.4.4 A New Version of the $\bar{\phi}$,f-chart Method

The last step of the analysis is to compare the solar fraction given by TRNSYS and the solar fraction obtained with the complete $\bar{\phi}$,f-chart method with no information provided from TRNSYS. The monthly-average temperature and the solar radiation on the horizontal surface are the only inputs to the method and they are part of a weather data file provided with the $\bar{\phi}$,f-chart method.

The rms error of the comparison TRNSYS - $\bar{\phi}$,f-chart in Madison is 2.6 % for the yearly values of the solar fraction and 4.3 % for the monthly values of the solar fraction. The high values of the rms result from a poor estimation of the critical radiation level. $I_{T,c}$ was defined in equation (3.17) as a constant during the day since the difference between the mains temperature (T_{mains}) and the monthly-average ambient temperature ($\bar{T}_{amb}$) is a constant. Erbs [29] developed a correlation to calculate the monthly-average temperature at any hour of the day, which could be used to define hourly values of the critical radiation level.

$$(\tilde{T}_{a,h} - \bar{T}_{amb}) / A_o = 0.4632 \cos(t^* - 3.805) + 0.0984 \cos(2t^* - 0.360) + 0.0168 \cos(3t^* - 0.822) + 0.0138 \cos(4t^* - 3.513) \quad (3.39)$$

$$A_o = 25.8 \bar{K}_T - 5.21 \quad (3.40)$$

where:

$\tilde{T}_{a,h}$ = monthly-average hourly ambient temperature

A_o = amplitude of the diurnal variation (peak to peak) in degrees Celsius

$\bar{K}_T$ = ratio of the monthly solar radiation on a horizontal surface to the monthly extraterrestrial radiation on a horizontal surface ($\bar{H} / \bar{H}_0$)

$$t^* = 2\pi (t - 1) / 24 \qquad (3.41)$$

where t^* is in hours with 1 corresponding to 1 am and 24 corresponding to midnight.

The calculation of the monthly-average daily utilizability is based on the knowledge of the monthly-average hourly utilizabilities (equation 3.38). The introduction of a variable ambient temperature does not therefore increase the complexity of the $\bar{\phi}$,f-chart method. The monthly-average hourly critical radiation level is defined by equation (3.42)

$$\tilde{I}_{T,c\,min} = \frac{F_R U_L}{F_R(\overline{\tau\alpha})} (T_{mains} - \tilde{T}_{a,h}) \qquad (3.42)$$

The comparison of monthly and yearly solar fractions obtained from TRNSYS and $\bar{\phi}$,f-chart has been made when hourly critical levels are used. The results are shown in the fourth column (rms final) of Table 3.3. It can be seen that the version of the $\bar{\phi}$,f-chart method using the correlations developed in Sections III.2 and III.3 still provides a good estimate for the systems simulated.

III.4.5 Final Recommended Procedure

The first step of the recommended design method is to evaluate the maximum value of the monthly-average useful energy gains Q_{max}(tot) as described in Section III.3.4.2. The value of $\bar{\phi}_{max}$, the maximum monthly-average daily utilizability is determined with the algorithm developed by Theilacker (Section III.4.3) using hourly critical radiation levels (equation 3.42).

The useful energy gains are then calculated from equation (3.35).

The monthly-average tank temperature is calculated using equation (3.13),which leads to the value of the monthly tank losses (equation 1.17)

The monthly solar fraction is determined using equations (3.11) and (3.12). The method is iterated until the solar fraction converges.

An example of estimating the performance of a stratified SDHW system with the

recommended procedure is presented in Appendix B.

The method developed in this chapter is restricted to open-loop systems using a low flow rate of 10 kg/hr-m^2 with the assumption of no mixing. The extension of the methods to other types of systems and other flow rates is investigated in Chapter IV.

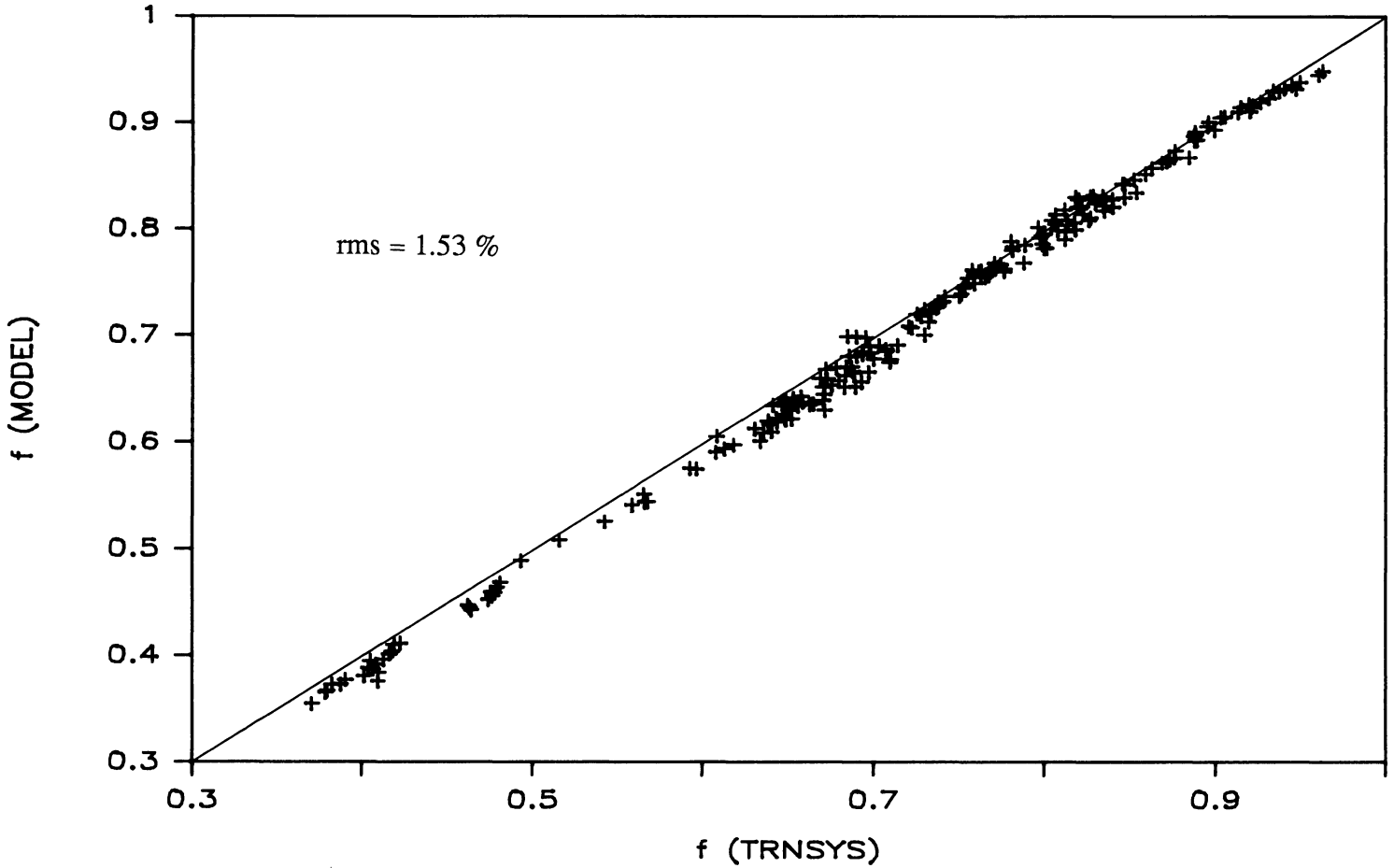

Figure 3.20 Comparison of the Yearly Solar Fraction predicted by TRNSYS and by the $\bar{\phi}$,f-chart Method in Madison

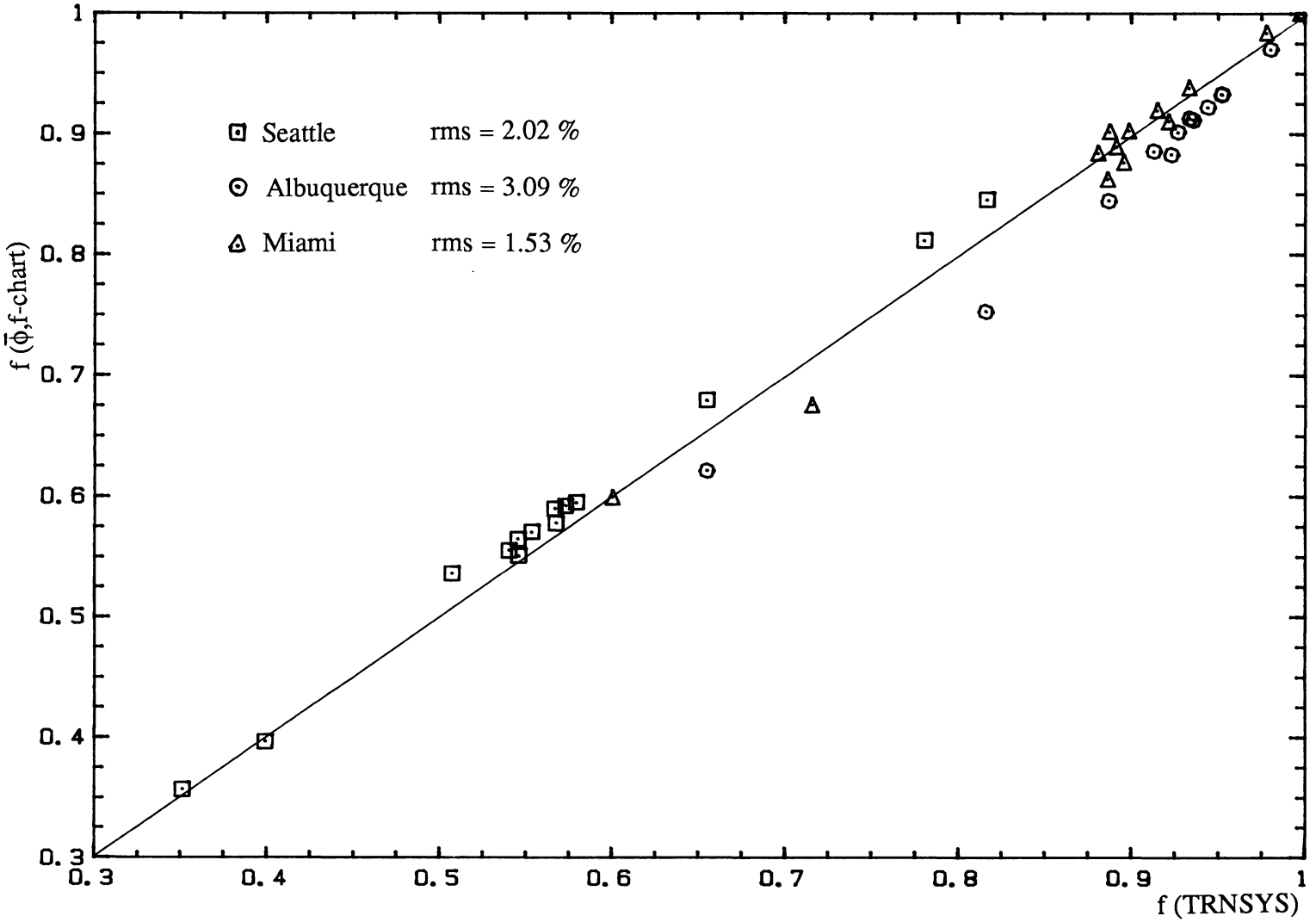

Figure 3.21 Comparison of the Yearly Solar Fraction predicted by TRNSYS and by the $\bar{\phi}$,f-chart Method for Different Locations

CHAPTER IV: LIMITATIONS OF THE METHOD

The procedure presented in Chapter III has been developed under certain restrictions. It is limited to open-loop systems and for a collector flow rate of 10 kg/hr-m^2. The purpose of this chapter is to check if the method developed could be extended to other types of systems. The estimate of the solar fraction by the design method developed in this paper is then compared to experimental results.

IV.1 Influence of a Radiation Controller

Some solar systems are equipped with radiation controllers and timers that prevent the system from running during the night. Various systems have been simulated with the radiation controller feature. One expected overestimates of the performance by the design method since nighttime gains are included in the design method although they are not allowed in the TRNSYS simulations. The solar fractions predicted by TRNSYS have therefore been compared with the estimates by the $\bar{\phi}$,f-chart method such as it was developed in Chapter III. The rms of 2.8 % for the monthly solar fraction shows the good agreement of the method for these systems. The reason is that the thermal gains are found to be small both in the simulations and in the design method.

The thermal gains of a particular system have been plotted in Figure 4.1 versus the time of the year to determine the effect of the radiation controller. It can be seen that the nighttime gains are small. Various types of collector have been studied and the importance of the nighttime gains remains small. The new design method was developed to give good estimates of the performance of the systems when there are nighttime gains. Since the nighttime gains are small, the solar fraction predicted by TRNSYS does not change significantly when the nighttime gains are suppressed and the estimate from the design method remains applicable.

In the design method, the determination of the maximum possible thermal gains through the term Q_{max}(therm) is made with the cooling degree-day method. It includes the fact that the temperature is lower during the night, which means nighttime gains are smaller than daytime gains. The design method does not therefore overestimate nighttime thermal gains.

As a result, no special modification of the design method has been introduced to

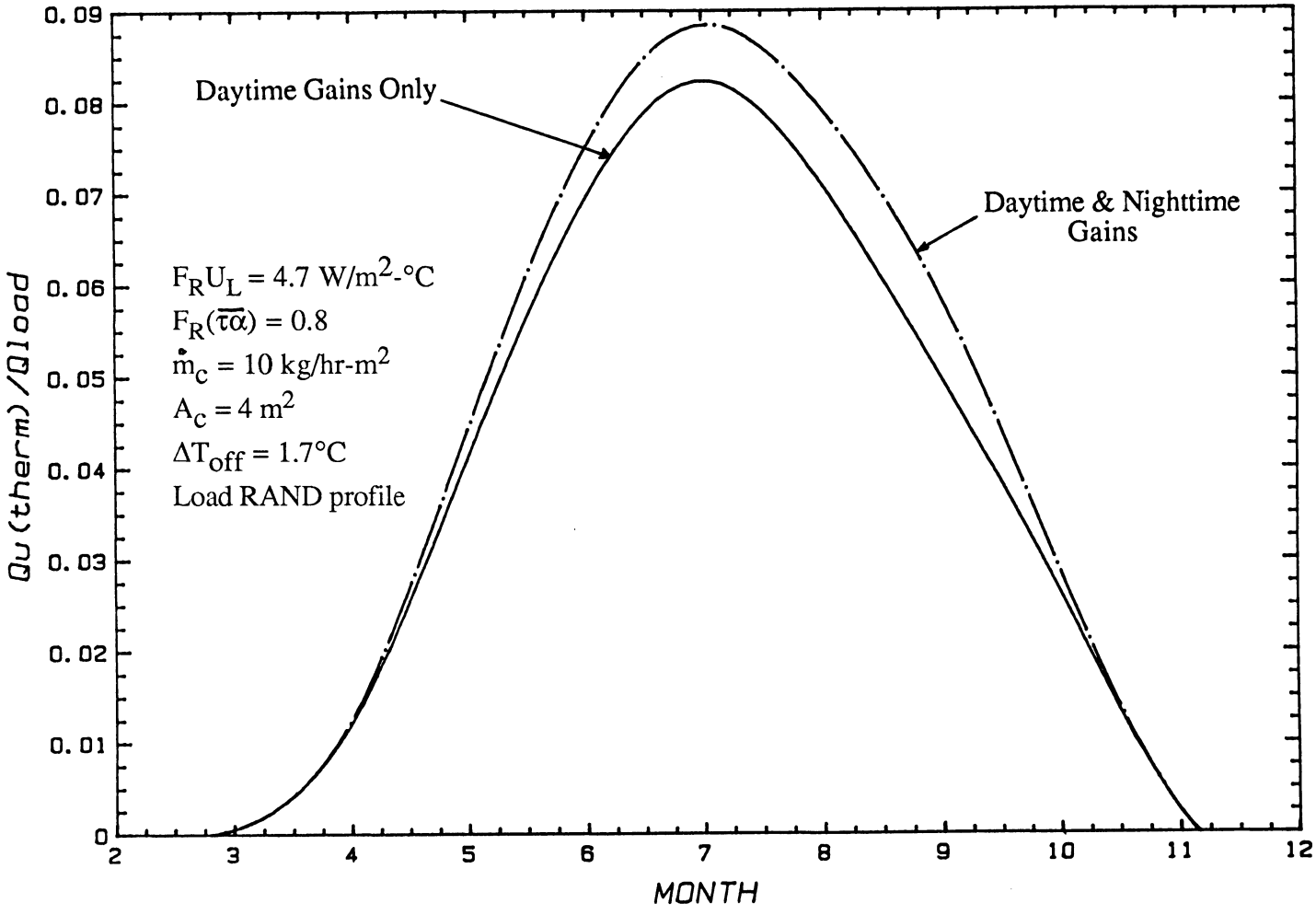

Figure 4.1 Influence of a Radiation Controller on the Thermal Gains to the Collector

account for the presence or absence of nighttime thermal gains.

It is possible to use a radiation controller without a differential controller. The controller is characterized by a radiation level $I_{t,off}$ below which the pump is turned off. In order to use the method developed in the previous chapter, a value of ΔT_{off} is defined by the temperature rise of the fluid passing through the collector when the solar radiation is $I_{t,off}$.

$$\Delta T_{off} = I_{t,off} / A_c \dot{m} C_p \qquad (4.1)$$

where

$\dot{m}$ = collector flow rate

A_c = collector area

IV.2 Closed-Loop Systems

The $\bar{\phi}$,f-chart method developed in Chapter III was based on simulations with an open-loop system. The extension of the method for closed-loop systems such as used for space and industrial process heating must be investigated. The term closed-loop implies that a heat exchanger exists between the solar system and the load. This type of systems is characterized by a smaller temperature difference between the delivery water and the makeup water. It is equivalent to simulate a closed-loop system and an open-loop system, with a set temperature close to the mains temperature (for a range of mains temperature) and a high daily load demand. The monthly solar fraction of different systems simulated in Madison (with a flow rate of 10 kg/hr-m^2) has been compared to the solar fraction estimated by the newly developed $\bar{\phi}$,f-chart method. The mains temperature is equal to 60°C and the set temperature is 65°C. The rms of the monthly value of the solar fraction is 19.4%.

The reason of the discrepancy is that the correlations in Chapter III have been established without accounting for the temperature of the environment of the tank (T_{env} around 20°C). T_{env} only appears in the definition of the tank losses. But the collector inlet temperature is sensitive to the influence of the temperature outside of the tank since thermal losses occur at the bottom of the tank. The collector inlet temperature might therefore be as low as T_{env} (i.e., 40°C below T_{mains}). Since the calculation of the maximum useful energy gains in the design method assumes that the lowest collector inlet temperature is T_{mains}, the useful energy gains are

underestimated as well as the solar fraction. The closer T_{mains} is to T_{env}, the smaller the error is.

The influence of T_{env} on the performance of the systems simulated in Chapter III is not as important since the mains temperatures is between 5°C and 20°C, i.e. close to T_{env}. The effect of T_{env} is also implicitly included in the correction term of the useful energy gains, Q_{corr}.

The design method is not applicable for closed-loop systems.

IV.3 Influence of the Flow Rate

The model developed in Chapter III assumed a low collector flow rate of 10 kg/hr-m^2. The effect of the collector flow rate of a system on the performance of a solar system when there is no mixing has to be investigated to define the range of flow rates where the method is applicable.

The performance of different SDHW systems has been determined when two collector flow rates, 10 kg/hr-m^2 (low flow rate) and 72 kg/hr-m^2 (high flow rate) are used. The plug-flow storage tank model is used with a simulation timestep of one minute to minimize mathematical mixing.

For each system, the difference Δf = f (Low Flow) - f (High Flow) = $f_{LF} - f_{HF}$ has been plotted in Figure 4.2 versus the solar fraction for the low collector flow rate, f_{LF}. Each system simulated is identified, for reference, by the coefficient C_L, ratio of the daily load to the mass of water in the tank (334 kg).

$$C_L = M_{load} / M_t \qquad (4.2)$$

It can be seen from Figure 4.2 that the difference $\Delta f = f_{LF} - f_{HF}$ reaches values up to 10 percent for these simulations. As a result, the proposed $\bar{\phi}$,f-chart method would overestimate the performance of a high flow rate system (72 kg/hr-m^2) with no mixing by up to 10 percent.

The large difference in solar fractions between the flow rates of 10 and 72 kg/hr-m^2 could stem either from the limitations built in the plug-flow model (i.e., an upper limit of 50 nodes and a mixing of adjacent nodes when the temperature difference is below 0.5°C) or from a too large value of the timestep (1 minute). The system that resulted in the higher difference $\Delta f = f_{LF} - f_{HF}$ among the systems previously simulated (e.g., the system with $C_L = 0.9$) has been studied further for the

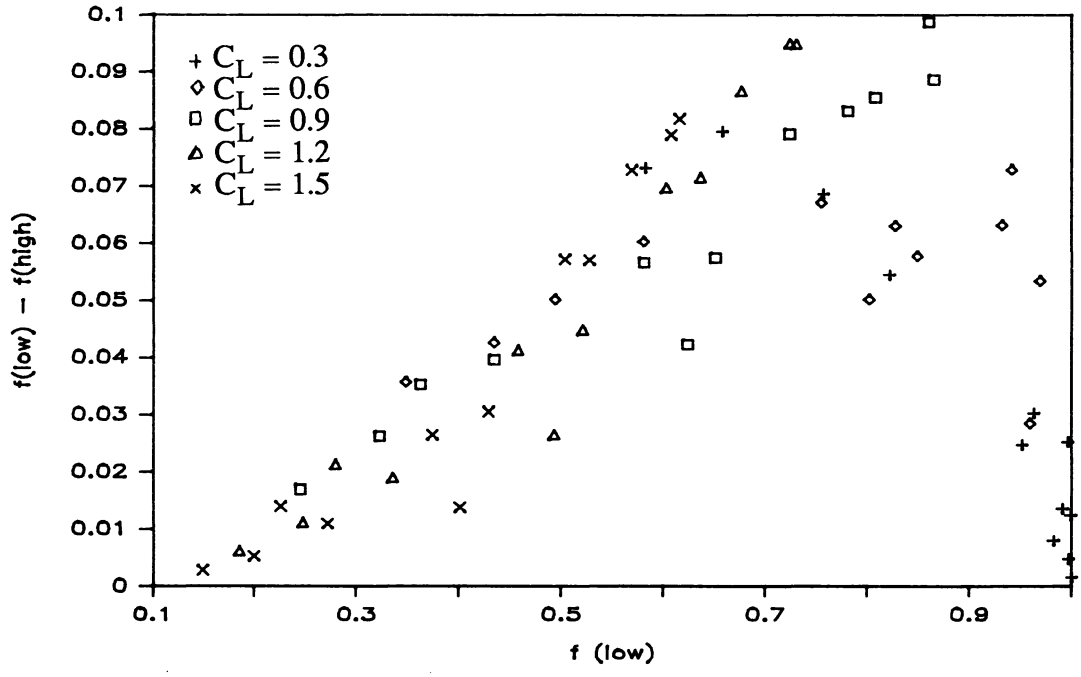

Figure 4.2 Difference in Solar Fraction between a Low Flow Rate and a High Flow Rate System for a Range of Load Requirements

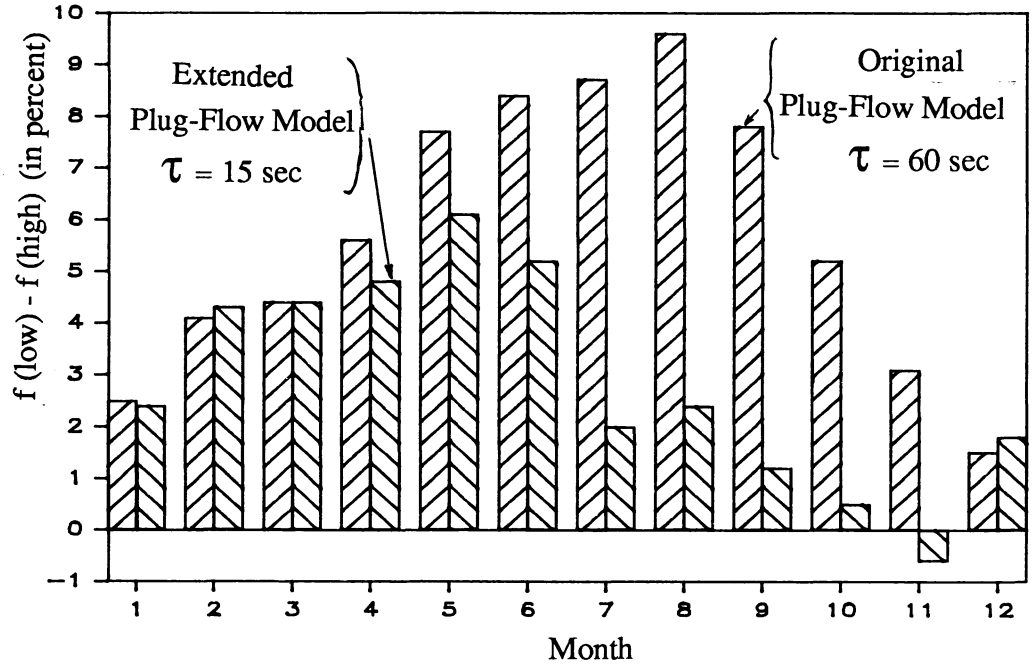

Figure 4.3 Difference in Solar Fraction between a Low Flow Rate and a High Flow Rate System for Different Amounts of Mixing in the Tank.

same two flow rates (10 kg/hr-m^2 and 72 kg/hr-m^2).

At first, the effect of the timestep on the solar fraction of the system has been investigated. The performance of the system (solar fraction in percent) with a low collector flow rate and a timestep of one minute is given in column 3 of Table 4.1. The performance of the system with the high flow rate and a one minute timestep is given in column 6 of Table 4.1. A smaller timestep (15 seconds) has then been chosen in the simulation of the system for the two flow rates. The monthly solar fractions of the low flow rate system do not change. The solar fractions (in percent) for the high flow rate system are indicated in column 5 of Table 4.1. It can be seen from Table 4.1 that the reduction of the timestep from 1 minute to 15 seconds may increase the solar fraction by up to 4.2 percent points (October), therefore reducing the difference in performance between the two flow rates.

TABLE 4.1

Month	Low Flow 500 Nodes τ = 1min	Low Flow 50 Nodes τ = 1min	High Flow 500 Nodes τ = 15 sec	High Flow 50 Nodes τ =15 sec	High Flow 50 Nodes τ = 1min
January	32.2	32.2	29.8	29.8	29.7
February	43.6	43.6	39.3	39.1	39.5
March	62.6	62.6	58.2	57.9	58.2
April	65.0	65.0	60.2	59.4	59.4
May	72.3	72.2	66.2	65.2	64.5
June	80.7	80.6	75.5	72.4	72.2
July	86.3	86.3	84.3	81.6	77.6
August	85.7	85.7	83.3	80.6	76.1
September	77.6	77.6	76.4	74.1	69.8
October	57.6	57.6	57.1	56.6	52.4
November	35.8	35.8	36.4	36.2	32.7
December	24.3	24.4	22.5	22.5	22.8
YEAR	60.4	60.4	57.5	56.4	54.6

Table 4.1 Influence of the Number of Nodes in the Storage Tank on the Solar Fraction

The solar fraction in February and March decreases with a decrease in the timestep. This paradox (the performance of the system should increase when mathematical mixing is reduced) is due to the transient aspect of the systems simulated. The effect of the energy stored in the tank had been assumed to be negligible. It is, however, found from the simulations that the energy stored in the storage tank during a month (ΔQ_{stor}) can be as high as 1.5% of Q_{load}. It is not therefore relevant to compare two values of the solar fraction when the difference is smaller.

The model has then been extended to 500 nodes and the temperature difference at which the mixing of adjacent nodes occurs has been reduced from 0.5°C to 0.05°C. A timestep of 15 seconds has been used. The results are given in column 2 of Table 4.1 for the low flow rate system and in column 4 of Table 4.1 for the high flow rate system. Table 4.1 shows a further increase in the solar fraction for the high flow rate system. A timestep of 5 seconds has been used for the month of January with the extended version of the plug-flow model. The solar fraction increases to 30.4 % when the high flow rate is used.

Using Table 4.1, the difference in solar fraction between the low flow rate system and the high flow rate system has been plotted for different months in Figure 4.3 for two cases:

- simulation timestep of 1 minute and original plug-flow model
- simulation timestep of 15 seconds and extended version of the plug-flow model

Figure 4.3 suggests that the performance of the system becomes independent of the flow rate when mathematical mixing decreases in the tank. The choice of a smaller timestep (and maybe a further increase in the allowance of the number of nodes in the plug-flow tank model) could result in further improvements in the solar fraction for the high flow rate system. However, the use of timesteps smaller than 1 minute requires considerable computational effort.

Figure 4.3 shows that the difference in solar fraction between the low flow rate system and the high flow rate system is dependent upon the time of the year. An increase in the number of the nodes in the tank does not change the performance of the high flow rate system for the first months of the year. The reason of the dependence might be related to the utilizability $\bar{\phi}$, calculated from the value of Q_u provided by TRNSYS (Figure 4.4) or to the cooling degree-days (Figure 4.5).

To avoid the problems related to the energy stored in the tank, the comparison of

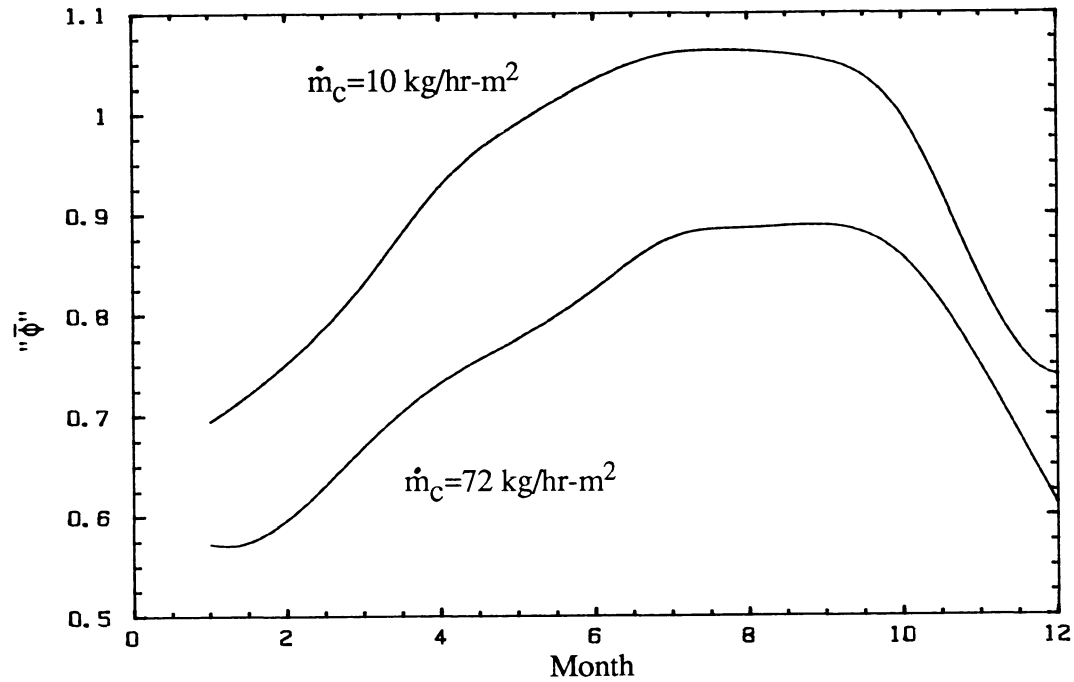

Figure 4.4 Value of "$\bar{\phi}$" determined from Equation (1.6) for the System studied in Figure 4.3 and for two Different Collector Flow Rates (Extended Plug-Flow Model)

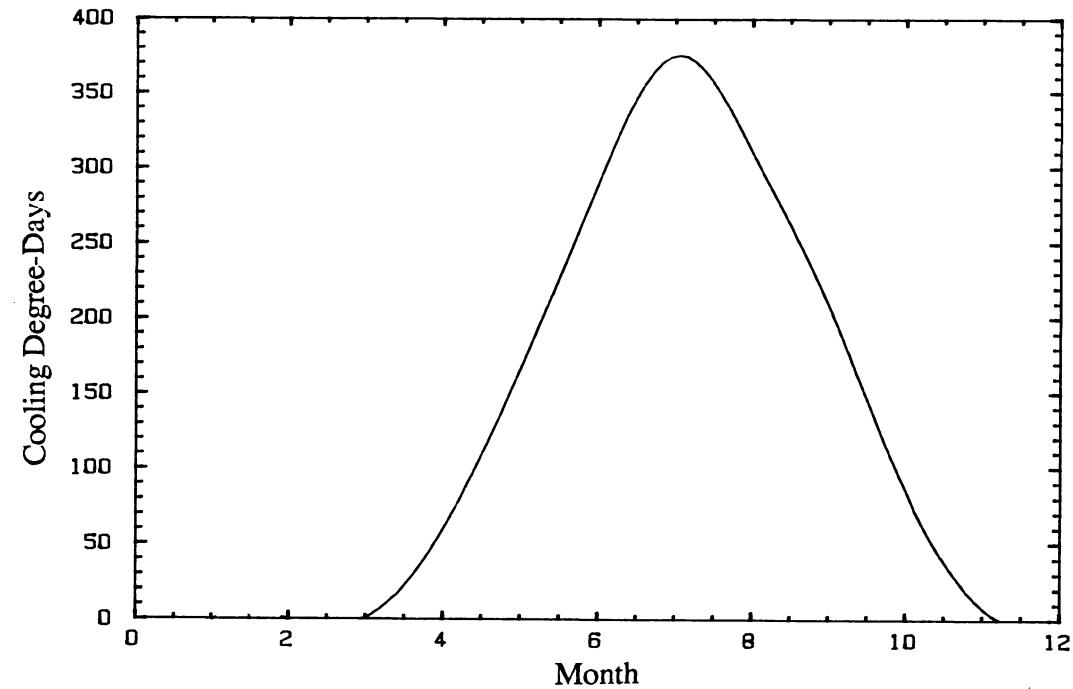

Figure 4.5 Cooling Degree-Days ($T_b = T_{mains}$) vs. the Time of the Year for the TMY in Madison

the solar fraction between the high flow rate system and the low flow rate system should be done on a yearly basis. As seen in Table 4.1, the difference in yearly solar fraction between the two flow rates decreases when the number of nodes in the tank increases (due to a smaller timestep or a larger node allowance in the storage tank).From this result, it is estimated that the performance of a system with no mixing is not very dependent of the collector flow rate. This means (Figure 4.6) that the gains due to a smaller recirculation would be approximately equal to the losses in collector efficiency due to a lower collector heat removal factor, F_R.

This result is limited to cases when the daily collector flow rate is greater than the daily load flow rate. When the flow rate is low enough so that no water recirculates through the collector, the advantage due to a smaller recirculation levels off (only water from the mains is used by the collector). The collector heat removal factor (F_R), however, keeps decreasing when the flow rate decreases (Figure 1.2). Therefore, the performance of the system drops dramatically when the flow rate is lowered further. The performance of the systems should be studied further for very low flow rates ($\overline{M}_C/M_L < 1$) to include this effect in a design method.

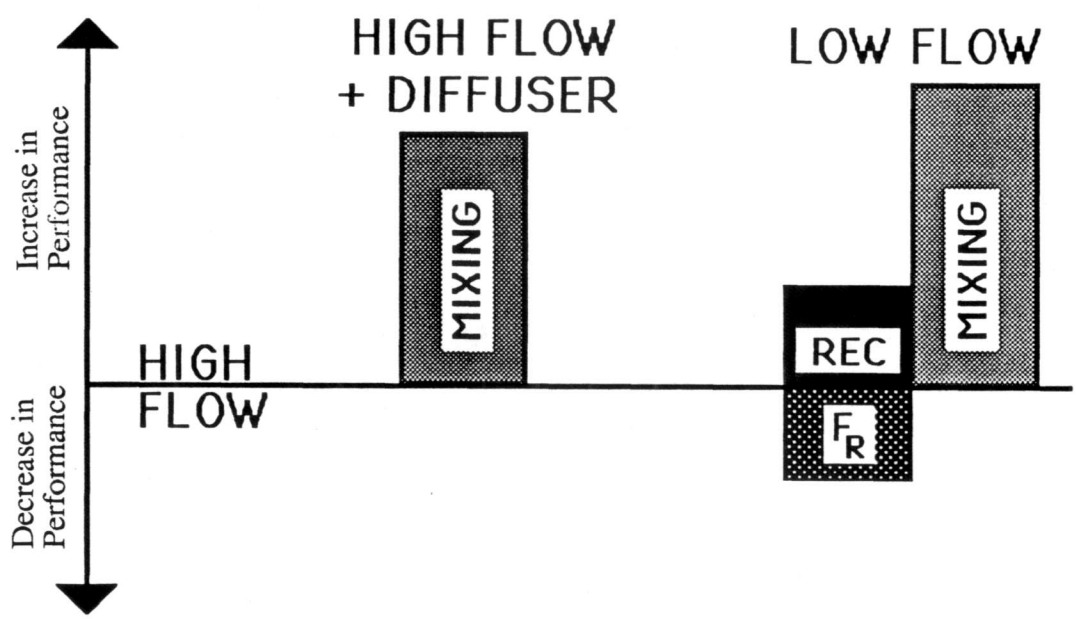

Figure 4.6 Different Effects Influencing the Performance of a SDHW System

As long as the daily collector flow is higher than the daily load flow ($\overline{M}_C/M_L > 1$), the result of the design method developed in Chapter III is applicable to any flow rate provided there is no internal mixing in the tank. Since the method has been developed for a flow rate of 10 kg/hr-m^2, the parameters dependent on the flow rate (e.g., $F_R U_L$ and $F_R(\overline{\tau\alpha})$) have to be converted to this reference flow rate before being used in the design method. The value of the actual flow rate is not needed in the method (except when a radiation controller is used).

IV.4 Comparisons of the $\bar{\phi}$,f-chart Method with Experiments

IV.4.1 Comparisons for a High Flow Rate System

The first set of experiments results from the study of the performance of different solar systems during one year by Fanney et al. [12]. The flowrate is 0.0833 liters/sec for a collector area of 4.2 m^2 (71.5 kg/hr m^2). The results from the new version of the $\bar{\phi}$,f-chart method should overestimate the actual performance of the system because this version has been developed when there is no mixing. Mixing is actually important since the collector flow rate is high and no stratification-enhancing device is used. The double-tank direct system has been chosen for the comparison of the experiments with the results from the two versions of $\bar{\phi}$,f-chart. The estimate by the f-chart method from Fanney et al. [12] is also shown as a comparison.

The results for each month are shown in Figure 4.7. It can be seen that the actual performance lies between both versions of $\bar{\phi}$,f-chart. The difference between the original method of $\bar{\phi}$,f-chart and the experimental result is due to the assumption of the fully-mixed tank in the method. The f-chart method provides good estimates of the solar fraction since the assumption of a fully-mixed tank is compensated by an underestimate of the preheat tank losses. For a low flow rate system, however, the assumption of a fully-mixed tank (like in the f-chart and in the original $\bar{\phi}$,f-chart method) will result in larger underestimates of the solar fraction (next section).

IV.4.2 Comparisons for Low Collector Flow Rate Systems

The influence of flow rate on the performance of a two-tank system and a single-tank system has been experimentally studied by Fanney [3] for short periods of time. The comparison with the design methods which gives monthly estimates of the solar fraction is possible if it is assumed that 15 days of data (for the double-tank system) and 24 days of data (single tank system) represent the long term average behavior of

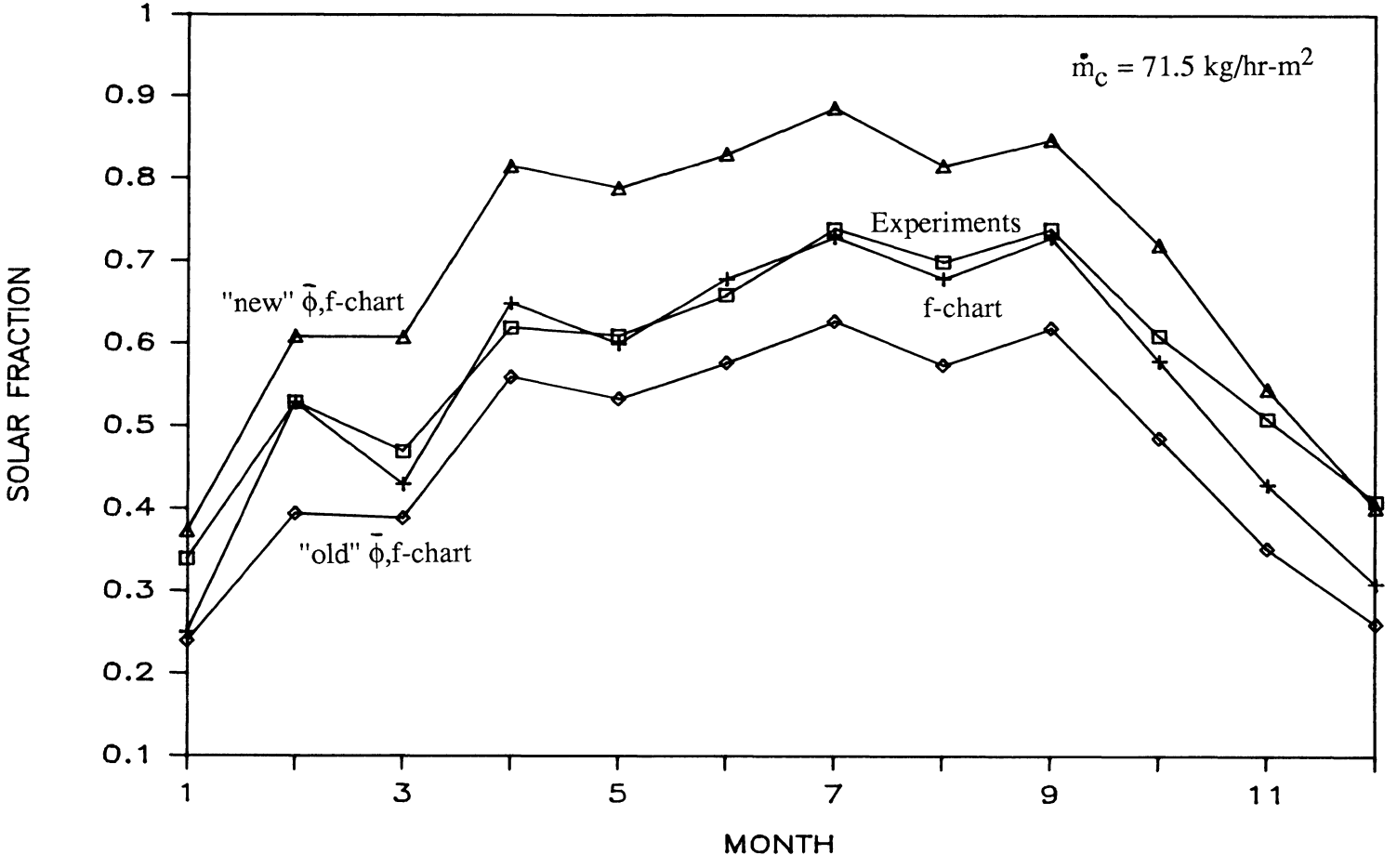

Figure 4.7 Comparison of the Estimates of the Monthly Solar Fraction provided by Different Design Methods with the Experimental Results

the system. Side-by-side experiments have been made by Fanney for each type of system to compare the effect of the flow rate on the performance of the system. The two flow rates for the double-tank system are 11.9 and 72 kg/hr-m^2. The two flow rates for the single-tank system are 9 and 72 kg/hr-m^2.

Estimates of the solar fraction have been made using the f-chart method (used in FCHART © [30]), the original version of the $\bar{\phi}$,f-chart method (used in FCHART 4.2 © [24]), the modification of the $\bar{\phi}$,f-chart method by Copsey [22] and the $\bar{\phi}$,f-chart method developed in this paper.

TABLE 4.2

SYSTEM	Experimental [12]	f-chart [30]	$\bar{\phi}$,f-chart(old) [24]	Copsey [22]	$\bar{\phi}$,f-chart(new)
Double-Tank					
- Low Flow (63°C)	0.61	0.46	0.43	0.59	0.67
- High Flow (63°C)	0.57	0.51	0.47	0.51	0.67
Single Tank					
- Low Flow (56°C)	0.86	0.63	0.60	0.85	0.88
- High Flow (56°C)	0.77	0.73	0.67	0.72	0.88

Table 4.2 Comparisons of the Solar Fraction Estimates by Different Design Methods with Experiments

The problem in the comparison of the design methods with the experiments is that there is no mixing valve used in the experiments. A fixed amount of water (265 liters) is drawn every day. When the temperature of the water delivered by the solar system is higher than the set temperature, more energy is delivered than it is needed by the load. On the other side, the thermostat has a large deadband. As noted by Fanney, the thermostat energizes the heating element at approximately 54°C and disconnects the element at 60°C. The consequence of these two features is that the water delivered to the load may have a temperature anywhere above 54°C instead of having a constant set temperature (60°C) as assumed in all the design methods. To allow a fair comparison,

the load has to be the same for all the design methods and for the experiments. An average temperature of the water delivered is calculated from the value of the load provided for each experiment. This value corresponds to the set temperature for a system having a mixing valve, a perfect thermostat and the same load as in the experiment.

Table 4.2 shows the estimates of the solar fraction by the design methods and the experimental result for each system, for each flow rate and for the set temperature equal to the average temperature of the water actually delivered. The proposed version of $\bar{\phi}$,f-chart still overestimates the solar fraction for a low flow rate system. Mixing exists in the experiments even at a low collector flow rate and mixing may also result from the conditions with which the load has been taken from the storage tank, a fast draw of a large amount of water may destroy some of the existing stratification in the tank.

It can be seen from Table 4.2 that Copsey's modification gives good estimates of the solar fraction because his method introduces some mixing in the storage tank. The agreement may be good for this example but remains uncertain for other systems. Moreover, Copsey's estimates are dependent on the value of $(\tau\alpha)$ assumed for the collector. In this example, a value of $(\tau\alpha)$ equal to 0.85 has been arbitrarly chosen. For a value of $(\tau\alpha)$ equal to 0.8, the solar fraction estimated by Copsey's method would be 80% for the single tank system (low flow rate) instead of 85%.

The comparison of the estimates of the solar fraction by different design methods with the experimental results leads to the following conclusions:

- the f-chart method and the $\bar{\phi}$,f-chart method developed by Braun can not be used to evaluate the performance of a low flow rate system since these methods may result in underestimates of the solar fraction by up to 26%.

- Copsey's modification of the $\bar{\phi}$,f-chart method gives good estimates of the solar fraction at low flow rates for the systems studied and might be used as long as stratification-enhancing devices are not used for high flow rate systems.

- The $\bar{\phi}$,f-chart method developed in this thesis assumed no mixing and gives overestimates of the solar fraction in all cases studied. As long as the degree of mixing in the tank is not known, only an upper bound of the solar fraction is provided.

CHAPTER V: CONCLUSIONS AND RECOMMENDATIONS

V.1 Conclusions

The goal of this research was to develop a design method that could be used to estimate the performance of a SDHW system in which stratification is present. It is possible to enhance stratification in the storage tank in different manners:

- to decrease the collector flow rate (the optimum performance occurs when the daily collector flow is slightly greater than the daily load flow)
- to introduce stratification-enhancing devices in conventional systems (collector flow rate between 50 and 70 kg/hr-m^2)

A reduction in the collector flow rate results in higher performance because the gains from smaller internal mixing in the tank and from less recirculation of the water through the collector overwhelm the decrease in the collector heat removal factor. When a stratification-enhancing device is used in a high flow rate system, only mixing is reduced.

It is not possible to account explicitly for mixing with the actual storage tank models in TRNSYS. Some mathematical mixing is, however, implicitly introduced in the simulations depending on the number of nodes specified in the tank (or on the simulation timestep when the plug-flow model is used). The influence of mathematical mixing on the performance of a system might be considerable for some systems (particularly for high collector flow rates). In these cases, reliable results cannot be obtained from simulations if the degree of mixing occurring in the tank is not known. Simulations can accurately predict the performance of a solar system only in the ideal situations when there is no mixing in the tank or when the tank is continuously fully-mixed.

It has been shown that the performance of a system when there is no mixing in the tank has little dependence on the collector flow rate. This result is true for the flow rates resulting in some recirculation through the collector during one day, i.e. , $(\overline{M}_c/M_{load} > 1)$.

A design method to estimate the performance of SDHW systems with no mixing in the storage tank has been developed. This method is structurally similar to the $\bar{\phi}$,f-chart method proposed by Braun et al [15]. But instead of using the assumption of a fully-mixed tank, the method accounts for the characteristics resulting from the

stratification in the tank (e.g., lower collector inlet temperature). A comparison of the solar fraction predicted by the modified $\bar{\phi}$,f-chart design method and by TRNSYS gives good results for systems with no mixing since the rms error is 1.5% for the yearly solar fraction and 3.4% for the monthly solar fraction in Madison.

The method developed in this thesis estimates the performance of the system if there were no mixing and provides therefore an upper bound for the solar fraction of an actual system. The method developed by Braun gives the performance of the system if the tank were fully-mixed, which is a lower bound for the solar fraction of the actual system. The actual performance of the system studied is confined between the estimates of the two design methods. The exact position is not known but the study of different procedures will be recommended in the next section.

Experimental results have been compared with the estimates by different design methods. It has been seen that the original $\bar{\phi}$,f-chart method and the f-chart method underpredict the solar fraction of low flow rate systems by about twenty percentage points. The modified $\bar{\phi}$,f-chart method, as expected, provides an upper bound for the performance of the system.

A method has been proposed by Copsey [22] to estimate the performance of a system for any flow rate. He implicitly assumed some mixing in the tank depending on the flow rate. Copsey's modification also requires the knowledge of the parameter $(\tau\alpha)$, which is not usually available. The arbitrary amount of mixing he assumed, however, leads to good estimates of the solar fraction when compared to a limited set of experimental values. As long as there is no accurate method to define the degree of mixing in the tank, this method might be used to give an estimate of the actual solar fraction between the upper and lower bound.

V.2 Recommendations

Mixing reduces the performance of the system depending to an extent on the system characteristics. The $\bar{\phi}$,f-chart method proposed in this paper assumed no internal mixing in the storage tank. There is a standard test method for SDHW systems, called ASHRAE 95-1981 [27], that could possibly be used to characterize the degree of mixing in the tank. The ASHRAE 95-1981 test procedure measures the daily performance under prescribed meteorological and load conditions until the steady periodic one-day performance is achieved. The result of the test could be compared with predicted results for the same system if the tank were fully-mixed ($f_{FM}^{\#}$) and

predicted results if the tank had no internal mixing ($f_{NM}^{\#}$), under the same conditions as in the test. This comparison would give an indication of the degree of mixing in the tank.

The first problem is to find, for each system studied, a general way to estimate $f_{FM}^{\#}$ and $f_{NM}^{\#}$ for the test conditions. A solution is to introduce a "fictitious" month in the $\bar{\phi}$,f-chart weather data file. The use of this month in the original $\bar{\phi}$,f-chart method (developed for a fully-mixed tank) would give the value of $f_{FM}^{\#}$ and the use of the new version of the $\bar{\phi}$,f-chart method would give $f_{NM}^{\#}$. This "fictitious" month might be characterized simply by the values of H and T_{amb} used during the test. The value of the utilizability during the test could also be used if the knowledge of H and T_{amb} is not sufficient to accurately describe the test conditions.

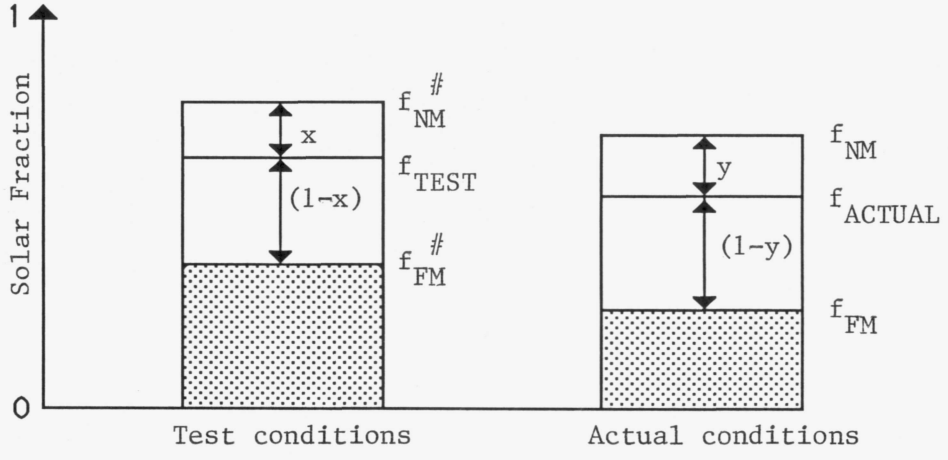

Figure 4.4 Schematic of the Solar Fraction under Test and Actual Conditions

Once the position of the solar fraction for the test is known to lie somewhere between $f_{FM}^{\#}$ and $f_{NM}^{\#}$ (under the test conditions), the position of the solar fraction under actual conditions could be estimated from the values of f_{FM} and f_{NM} (from the weather data available). In the simplest case, the relative position of the test results ($f_{TEST}^{\#}$) between $f_{FM}^{\#}$ and $f_{NM}^{\#}$ would be the same as the relative position of the actual performance between f_{FM} and f_{NM} (Figure 4.4). Otherwise, a correlation has to be found to relate the actual position of the solar fraction of the system between f_{FM} and f_{NM} from the relative position of $f_{TEST}^{\#}$ between $f_{FM}^{\#}$ and $f_{NM}^{\#}$.

If results from experiments are not available for this analysis, simulations on

TRNSYS could be used under the assumption that the degree of mixing during the test is the same as during actual conditions. In this case, comparisons between results from the test and results from simulations on TRNSYS would give the simulation timestep that provides the best agreement with the test result. The same timestep could be used for the long term simulations representing actual conditions (with TMY weather data). The use of the results of the test ASHRAE 95-1981 in the $\bar{\phi}$,f-chart method requires the detailed knowledge of the weather conditions used in the test to simulate the system on TRNSYS and to compare the test performance with the $\bar{\phi}$,f-chart results. This approach should also be validated with actual experiments.

A same approach could also be used to determine which amount of mixing should be used in the simulations in TRNSYS. For a given SDHW system, the timestep to use could be found from the ASHRAE test results while running the simulation for the test conditions. The drawbacks of this procedure are its complexity and the fact that the results of the ASHRAE test are not known for all types of systems.

The degree of mixing in the tank is an important variable and its influence should be introduced in the tank models. Comparisons between the performance of the plug-flow tank model with experimental data are therefore needed to improve the TRNSYS simulations.

Oppel et al [31] have developed a model for mixing that requires a constant inlet temperature. Some results of this study might be used to extend the prediction of the design method developed in this thesis to systems with some mixing. The constant inlet temperature needed could be approximated by the monthly-average collector inlet temperature deduced for a system with no mixing. A correction of TRNSYS is not possible unless Oppel's method is extended to fluctuating inlet temperatures.

APPENDIX A

```
**********************************************************************
                TRNSYS DECK FOR A SINGLE-TANK SYSTEM
                      PLUGFLOW  TANK MODEL
                MIXING VALVE + PERFECT AUXILIARY TANK
                TESTFLOW=FLW => NO CORRECTIONS ON F_R
**********************************************************************

CONSTANTS 32
NUMBER = 1001. , STEP = 5. / 60. , TSTART = 1. , TEND = 8760. ,
TSIM = TEN - TST , DAYSTART = 1. , TBEGIN = 1. , FLWATER = 10. * AC ,
TOTALLOADPERDAY = 300. , VT = .3341 TSET = 60. , UAT = 9. , AC= 4. ,
TMAINS = 10  , CPW = 4.19  ,  ROWATER = 1000. ,  ENV = 20.
FRTANTEST = .805 , FRULTEST = 17.03 , TESTFLOW = FLW / AC , B0 = 0.
ATDEADBAND = 0. , TUDEADBAND = 8.9 , TLDEADBAND = 1.7 , TINI = 18. ,
HT = 1.6 ,  UAAUX = 0. ,  SOLARCONST = 4871. ,  LATITUDE = 43.13 ,
ROGROUND = 0.2 ,  AZIMUTH = 0.0 , BETA = LATITUDE
**********************************************************************
SIMULATION
TST TEN STE
TOL -.01 -.01
LIMITS 50 9 45
WIDTH 132
**********************************************************************
UNIT 9 TYPE 9     TMY Data Reader (Formatted)
PAR 10
 2 1 -1 1 0 -2 1 0 10 1
(T15,F4.0,T20,F4.1)
*
UNIT 16 TYPE 16  Solar Radiation Processor (with Erbs' Correlation)
PAR 7
3   1   DAY   LAT   SOL    0.0    -1
INPUTS 6
9,1  9,19  9,20  0,0    0,0   0,0
0.0   0.0   1.0   ROG  BET  AZI
**********************************************************************
UNIT 1 TYPE 1     Solar Collector
PAR 12
1  1  AC  CPW  1  TES  FRTA  FRUL  -1  CPW  1  B0
INPUTS 10
3,1  3,2  3,2  9,2  16,6  16,4  16,5  0,0  16,9  0,0
25.  0.0  0.0  20.  0.0   0.0   0.0   ROG  0.0   BET
*
UNIT 2 TYPE 2     Pump Controller
PAR 3
3  TUD  TLD
INPUTS 3
1,1      5,1      2,1
```

```
TMA  TMA   0.0
*
UNIT 3 TYPE 3    Pump
PAR 1
FLW
INPUTS 3
5,1    5,2    2,1
TMA  0.0    0.0
*
UNIT 13 TYPE 13 Pressure Relief Valve (to check the influence of Boiling)
PAR 2
100.   CPW
INPUTS 3
1,1    1,2    1,1
15.  0.0    15.
 *
UNIT 14 TYPE 14 Hourly Fractions of the Load
PAR 82
 0,0 5,0 5,.125 6,.125 6,.391 7,.391 7,.625 8,.625 8,.703 9,.703 9,.549 10,.549
10,.391 11,.391 11,.297 12,.297 12,.422 13,.422 13,.242 14,.242 14,.203 15,.203
15,.156 16,.156 16,.297 17,.297 17,.549 18,.549 18,1.0 19,1.0 19,.786 20,.786
20,.549 21,.549 21,.422 22,.422 22,.391 23,.391 23,.156 24,.156 24,0.0
*
UNIT 15 TYPE 15 RAND-Load Synthesizer
PAR 8
-1  TOT  -1   8.254  2  0  1  -4
INPUTS  1
14,1
0.0
*
UNIT 5 TYPE 38   Preheat Tank (Plug-Flow Model)
PAR  11
2  VT  HT  HT  CPW  ROW   0   1  UAT  1  TIN
INPUTS  5
 1,1  1,2  11,1  11,2  0,0
15.  0.0  TMA  0.0   ENV
*
UNIT 11              Temperature Controlled Flow Diverter
PAR 2
4   4.
INPUTS 4
0,0     15,1   5,3      0,0
TMA  0.0    TSET   TSET
*
UNIT 12 TYPE 11 Tee-Piece
PAR 1
1
INPUTS 4
5,3     5,4    11,3     11,4
TMA   0.0    TMA    0.0
```

```
*
UNIT 27 TYPE 14 Hour Number for each Month (for TYPE 49)
PAR 48
 0,1 744,1 744,2 1416,2 1416,3 2160,3 2160,4 2880,4 2880,5 3624,5 3624,6 4344,6
4344,7 5088,7 5088,8 5832,8 5832,9 6552,9 6552,10 7296,10 7296,11 8016,11
8016,12 8760,12
*
UNIT 49 TYPE 49 Perfect Auxiliary Tank (Instantaneous Heater)
PAR 5
TBE TSET TMA CPW DAY
INPUTS 9
27,1 12,1  12,2  5,8  5,6  5,10  5,1  5,5  1,3
1.    0.    0.   0.   0.   1.    1.   1.   1.
*
UNIT 48 TYPE 48 Solar Fraction by the Original φ̄,f-chart Method
PAR 9
TSET TMA ENV AC VT TOT UAT UAAUX DAY
INPUTS 8
0,0  27,1  16,6  16,4  16,1  9,2  0,0  0,0
1   1    1.0  1.0  1.0  1.0 FRUL FRTA
*
UNIT 29 TYPE 15 Transforms Parameters in Variables for the Output Files
PAR 27
-1 TSET -4  -1 TMA -4  -1 UAT -4 -1 ENV -4 -1 AC -4 -1 FRUL -4 -1 FRTA -4 -1
NUMBER -4 -1 VT -4 INPUT 1 1,6 0.0
*
UNIT 28 TYPE 28 Simulation Summary (First Output File)  "PHIMAD.TOT"
PAR 28
 -1  TBE  TEN  15  2  4 -1 NUM -4 0 -4 0 -4 0 -4  0 -4  -1  TOT -4  0 -4 0 -4 0  -4 0
-4  INPUTS 8
48,1    49,1    49,8    5,7    13,3    2,1    1,8    1,9
LABELS 10
 N° f_Braun   f_sol   T_inc  Q_stor  TOT  Q_boil  P.R.T  Q_u(gains) Q_u(loss)
*
UNIT 30 TYPE 25 Second Output File (Tank Temperatures)  "TTANK.TOT"
PAR 4
-1  744.  TEN  16
INPUTS 9
29,8  49,7  49,11  49,12  29,1  29,2  29,3  29,4  49,9
N°   T_tank Q_aux  Q_load  T_set T_mains UA_t  T_env  Q_los
*
UNIT 31 TYPE 25 Third Output File  "CORRELAT.TOT"
PAR 4
-1    744.   TEN   17
INPUTS 10
29,8   49,11   49,12   29,1  29,2    29,5   29,6   49,10  48,2   29,9
N°     Q_aux    Q_load  T_set  T_mains A_C    F_RU_L  Q_u     T_amb  VOL
*
END
```

APPENDIX B

EXAMPLE OF THE USE OF THE MODIFIED $\bar{\phi}$,f-chart METHOD

The performance for a system having the following parameters is to be estimated for the month of April in Madison.

WEATHER DATA

$\overline{\overline{H}}$ = 15.87 MJ / m^2

$\overline{T}_{amb}$ = 7.4°C

$\overline{T}_{amb}$(year) = 7.2°C and σ_{yr} = 10.92

COLLECTOR

Area = 4.2 m^2

$F_R U_L$ = 4.73 W/m^2-°C for a test flow rate of 71.5 kg/hr-m^2

$F_R(\tau\alpha)_n$ = 0.805 "

$(\tau\alpha)_n / (\overline{\tau\alpha})$ = 0.925

$\dot{m}_c$ (use) = 10 kg/hr-m^2

slope = latitude = 43.13°

ΔT_{off} = 1.7°C

PREHEAT TANK

Volume = 300 liters

UA_t = 2.75 W/ °C

Tenv = 20°C

AUXILIARY TANK

No tank losses assumed

HOT WATER LOAD

Daily demand = 300 liters

Tmains = 10°C

Tset = 60°C

Q_{load}(month) = 300 30 4.19 (60 - 10) = 1,886 MJ

From reference [6], $\overline{R}$ = 1.01 and F_R(use) / F_R(test) = 0.841

The values of $F_R U_L$ and $F_R(\tau\alpha)_n$ have to be determined for the reference flow rate, i.e., 10 kg/hr-m^2. In this example, the reference flow rate happens to be equal to the actual flow rate.

$F_R U_L$ = 3.98 W/m^2°C for a flow rate of 10 kg / hr m^2

$F_R(\tau\alpha)_n$ = 0.677 "

Determination of the solar fraction

Step 1: A good initial guess for the solar fraction would be the solar fraction from the previous month. In this example, we assume f = 0.60

Step 2: Determination of $Q_{max}(tot)=Q_{max}(rad)+Q_{max}(therm)$

a) $Q_{max}(rad)$

Determination of $\tilde{T}_{a,h}$ and $\bar{\phi}$.

A (amplitude) = 25.8 * 0.475 - 5.21 = 7.045

$\tilde{T}_{a,h}$ is calculated with equation (3.40)

The monthly-average hourly utilizabilities $\tilde{\phi}$ are calculated with equation (3.35)

hour	$\tilde{T}_{a,h}$ (°C)	$\tilde{\phi}$	G_T (kJ/m^2)	$\tilde{\phi}\ G_T$
9	6.5	0.63	49.9	31.4
10	7.8	0.95	244.5	232.3
11	8.9	0.986	452.8	446.5
12	9.8	0.998	587.8	586.6
13	10.5	1.0	587.6	587.6
14	10.9	1.0	452.3	452.3
15	11.1	1.0	243.9	243.9
16	11.0	1.0	49.5	49.5
			$\bar{H}_T$ = 15.88 MJ/m^2	15.63

$\bar{\phi}_{max}$ = 15.63 / 15.88 = 0.984

$Q_{max}(rad) = A_c\ F_R(\overline{\tau\alpha})\ \bar{\phi}_{max}\ \bar{H}_T\ N_m = 4.2\ 0.984\ 15.88\ 30\ 0.677$

= 1332.5 MJ

b) Q_{max}(therm)

$\sigma_m = 1.45 - 0.0290\,\overline{T}_{amb} + 0.0664\,\sigma_{yr} = 1.96$

$T_b = T_{mains} + \Delta T_{off} = 11.7°C$

$h^* = (T_{amb} - T_b) / \sqrt{N_m}\,\sigma_m = -0.40$

CDD_b (equation (3.17)) = 21.7 °C-day

and $N^0 = N_m\,[1 + \exp(-3.396\,h^*)]^{-1} = 6.13$ days

thus $Q_{max}(therm) = 24\ A_c\ F_R U_L\ (CDD_b + \Delta T_{off}\,N^0) = 46.3$ MJ

Step 3: Calculation of Q_u:

$C_s^* = 4.19\ 300 / 350\ 4.22 = 0.85$

$Z = (60 - 10) / 100 = 0.5$

$X = 4.2\ 100\ 3.98\ 3.6\ 30\ 24\ /\ 1886000 = 2.30$

$T_{amb}^* = Q_{max}(therm) / Q_{load}\,X = 0.011$

$Q_u = Q_{max}(tot) - \alpha\,(Cs^*)^{\beta}\,[\exp(\chi\,f) - 1]\,\exp(\delta\,Z)\ X\ [1 + (\varepsilon\,X\,T_{amb}^*)^{\gamma}]$

$= 1300.8$ MJ

Step 4: Evaluation of the tank losses

$Y = N_m\,\overline{H}_T\,F_R(\overline{\tau\alpha})\,A_c\,/\,Q_{load} = 0.718$

$T_t^* = (C_s^*)^{-.27}\,\{0.542\,f^2 + 1.263\,10^{-2}\,f\,[\exp(3.4\,f) - 1]\,[1 - \exp(-.922\,Y/f)]^2\,/\,Z\}$

$\Rightarrow\ T_t = 22.54°C$

$Q_{los} = 2.75\ 3.6\ (22.54 - 20)\ 24\ 30 = 18.1$ MJ

Step 5: Evaluation of a new solar fraction

$f = (Q_u - Q_{los}) / Q_{load} = (1300.8 - 18.1) / 1886 = 68.0\ \%$

The process has to be iterated with this new value as an initial guess. The solar fraction obtained after convergence is 65.7 %

REFERENCES

[1] Veltkamp, W.B., van Koppen, C.W.J., "Optimization of the flows in a solar energy system", Report Eindhoven University of Tehnology, WPS3-82.09 R335, (1982).

[2] Cole, R.L. and Bellinger, F.O., "Natural Thermal Stratification in Tanks", Argonne National Lab, 82-7, (February 1982).

[3] Fanney, A.H.and Klein, S.A., Thermal Performance Comparisons for Solar Hot Water Systems Subjected to Various Collector Array Flow Rates. Proceedings ISES Congress Montreal, Pergamon (pp538-543) (1985).

[4] Wuestling, M.D., "Investigation of Promising Control Alternatives for Solar Water Heating Systems", M.S. Thesis in Mechanical Engineering, University of Wisconsin-Madison, (1983).

[5] Turner, J.S., Buoyancy Effects in Fluids, Internal Mixing Processes, Cambridge University Press, pp. 313-337 (1973).

[6] Duffie, J.A. and Beckman, W.A., Solar Engineering of Thermal Processes, Wiley, New York, (1980).

[7] Klein, S.A., Beckman, W.A., "Review of Solar Radiation Utilizability", Journal of Solar Energy Engineering 106, pp. 393-401, (1984).

[8] Clark, D.R., Klein, S.A. and Beckman W.A., "Algorithm for Evaluating the Hourly Radiation Utilizability Function", Journal of Solar Energy Engineering 105, pp. 281-287, (1983).

[9] Klein, S.A., "Calculation of Flat-Plate Collector Utilizability", Solar Energy 21, pp. 393-402, (1978).

[10] Lunde, P.J., Solar Thermal Engineering, Wiley, New York, (1980).

[11] Beckman, W.A., Klein, S.A. and Duffie, J.A., Solar Heating Design by the f-chart method, Wiley, New York, (1977).

[12] Fanney, A.H., Klein, S.A., "Performance of Solar Domestic Hot Water Systems at the National Bureau of Standards - Measurements and Predictions", ASME Fifth Annual Solar Energy Conference, Orlando (1982).

[13] Klein, S.A., Beckman W.A., "A General Design Method for Closed-Loop Solar Energy Systems", Solar Energy 22, pp 269-282, (1979).

[14] Buckles, W.E., Klein, S.A., "Analysis of Solar Domestic Hot Water Heaters", Solar Energy 25, pp. 417-424, (1980).

[15] Braun, J.E., Klein, S.A. and Pearson, K.A., "An Improved Design Method for Solar Water Heating Systems", Solar Energy 31, pp. 597-604, (1983).

[16] Solar Energy Laboratory, "TRNSYS - A Transient System Simulation Program", Version 12.1, University of Wisconsin - Madison, (1983).

[17] Hirsch, U.T., "Control Strategies for Solar Water Heating Systems", M.S. Thesis in Chemical Engineering, University of Wisconsin-Madison, (1985).

[18] Veltkamp, W.B., "Thermal Stratification in Heat Storage", In C. den Houden, Thermal Storage of Solar Energy, Martinus Nijhoff, The Hague, 2, p.6 (1980).

[19] Fanney, A.H., Thomas, W.C., Scarbrough, C.A., and Terlizzi, C.P., "Analytical and Experimental Analysis of Procedures for Testing Solar Domestic Hot Water Systems", National Bureau of Standards Building Science Series Publication, No. 140, (February 1982).

[20] Lavan, Z., and Thompson J., "Experimental study of Thermally Stratified Hot Water Storage Tanks", Solar Energy 19, pp.519-524, (1977).

[21] McGrath P., "Preliminary Tests Performed on an Experimental Stratification Tank Used in Solar Domestic Hot Water Systems", Solar Energy Program (Coop Work Term Report), (January 1985).

[22] Copsey, A.B., "A Modification to the f-chart and ϕ,f-chart Method for Solar Domestic Hot Water Systems with Stratified Storage", M.S. Thesis in Mechanical Engineering, University of Wisconsin-Madison, (1984).

[23] Solar Products Specifications Guide, SolarVision, Inc. ©, (June 1983).

[24] Mitchell, J.C., et al.,"FCHART 4.2, A Design Program for Solar Heating Systems", Solar Energy Laboratory, University of Wisconsin-Madison, (1985).

[25] Klein, S.A. and Theilacker, J.C., "An Algorithm for Calculating Monthly -Average Radiation on Inclined Surfaces", Journal of Solar Energy Engineering 103, pp. 29-33, (February 1981).

[26] Erbs, D.G., Klein, S.A., and Beckman, W.A., "Estimation of the Diffuse Radiation Fraction for Hourly, Daily and Monthly-Average Global Radiation", Solar Energy 28, pp. 293-302, (1982).

[27] Klein, S.A., "Calculation of the Monthly-Average Transmittance-Absorptance Product", Solar Energy 23, pp.547-551, (1979)

[28] Klein, S.A., " Loss-of-Load Probabilities for Stand-Alone Photovoltaic Systems", to be published, (1986).

[29] Erbs, D.G., Klein, S.A., and Beckman, W.A., "Estimation of Degree-Days and Ambient Temperature Bin Data from Monthly-Average Temeratures", ASHRAE Journal, pp.60-65, (June 1983).

[30] Klein, S.A., and Beckman, W.A., "F-CHART SOFTWARE ©", (1985)

[31] ANSI/ASHRAE Standard 95-1981, "Methods of Testing to Determine the Thermal Performance of Solar Domestic Water Heating Systems", ASHRAE, Atlanta, Ga. 30329, Dec.17, 1981.

[32] Oppel, F.J., Ghajar, A.J., and Moretti, P.M., "A Numerical and Experimental Study of Stratified Thermal Storage", ASHRAE Transactions 92, (1986).